Virgo interferometer calibration and h(t) strain reconstruction uncertainty during the O4 observing run

Cervane Grimaud - CEA - Saclay / Irfu / DPhP

Summary

- I. Gravitational waves theory
- II. Gravitational waves detection
- III. Advanced Virgo interferometer calibration
- IV. Photon Calibrators calibration
- V. Electromagnetic actuators calibration
- VI. h(t) strain reconstruction and uncertainty computation

Summary

Einstein's equation and radiative solution

General relativity (Einstein 1915) :
Gravitation is a manifestation of the space time curvature induced by the presence of matter and Energy in our Universe

Einstein's equation:

$$G_{\mu\nu} = \frac{8\pi G}{c^4} T_{\mu\nu}$$

Einstein's tensor — Energy-momentum tensor

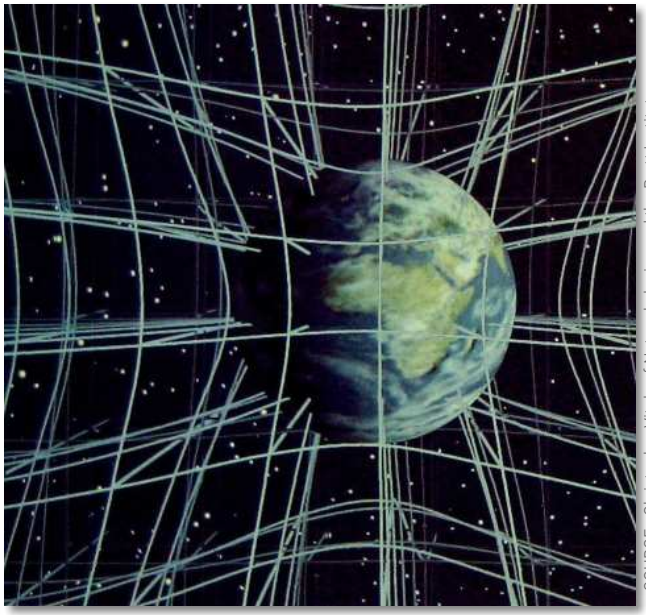

SOURCE - Christopher Vitale of Networkologies and the Pratt Institute

Einstein's equation and radiative solution

General relativity (Einstein 1915) :
Gravitation is a manifestation of the space time curvature induced by the presence of matter and Energy in our Universe

Einstein's equation:

$$G_{\mu\nu} = \frac{8\pi G}{c^4} T_{\mu\nu}$$

Einstein's tensor — Energy-momentum tensor

Gravitational wave:
Radiative solution of Einstein's equation
Dynamical deformation of space-time propagating at the speed of light

A gravitational wave amplitude has two polarizations:

h_+ and $h_\times$

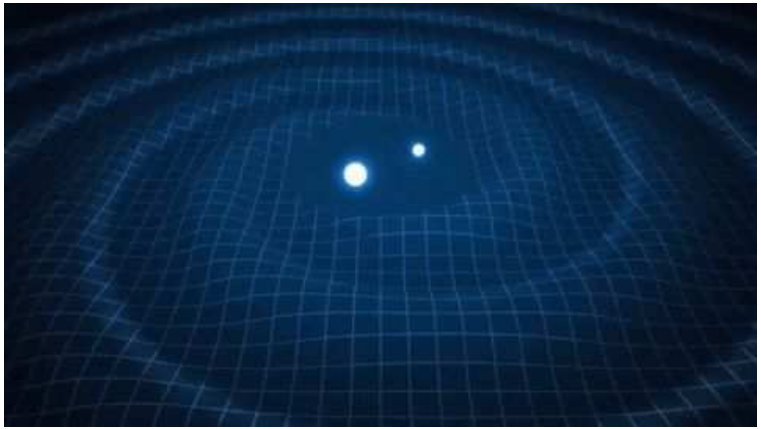

Einstein's equation and radiative solution

Detectable effect of a gravitational waves:

→ Space-time deformation

→ Length modification

$$h(t) \propto \frac{\Delta L}{L_0}$$

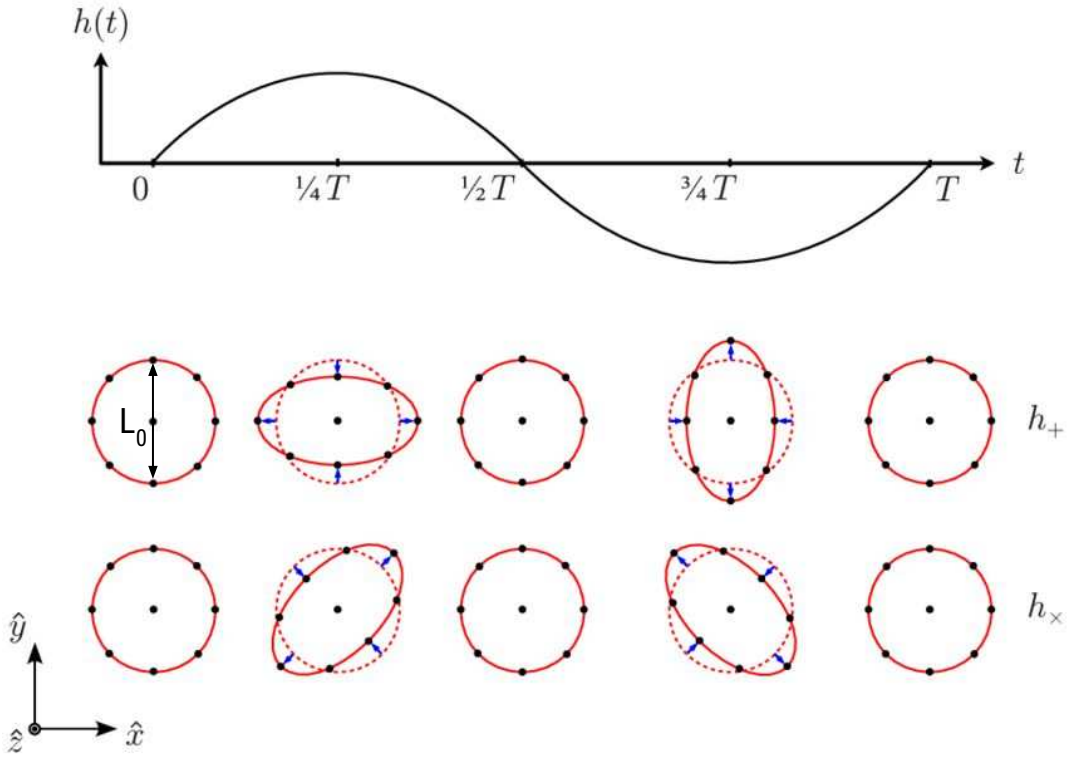

SOURCE - A. Le Tiec & J. Novak

Gravitational waves sources

A gravitational wave can only be produced by **asymmetrical systems**

Compact Binaries Coalescences (CBCs)

Neutron stars and black holes created after stars end of life (mostly)

<u>Three coalescence phases :</u>

- Inspiral
- Merger
- Ring-down

Corresponds to three distinct phases in the gravitational wave signal

Only detected sources for now

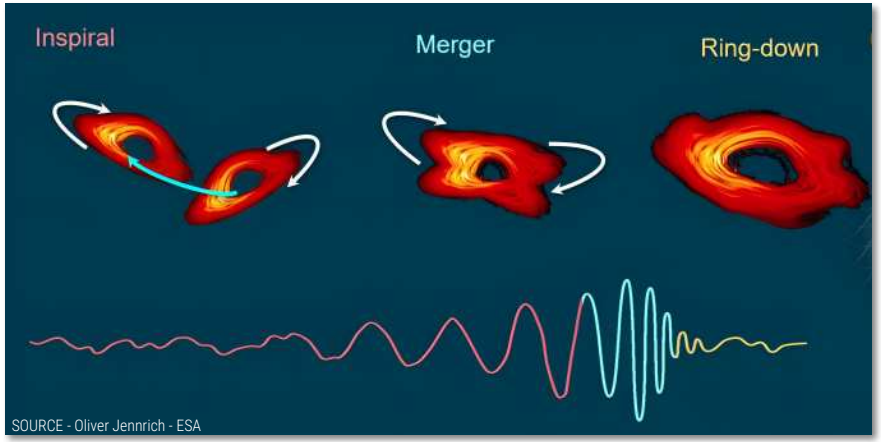

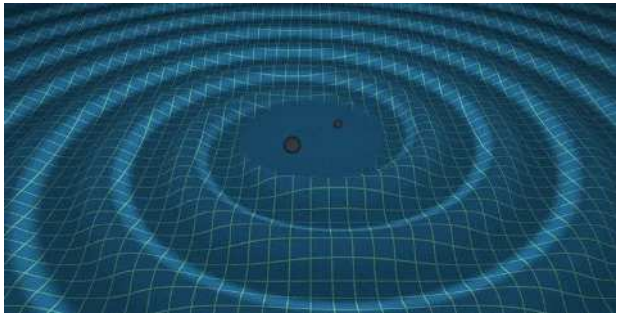

LIGO-Virgo-KAGRA collaboration

International collaboration between 3 collaborations and 4 interferometers

First detection during the O1 run, three additional runs since

More than 400 signals detected since 2015

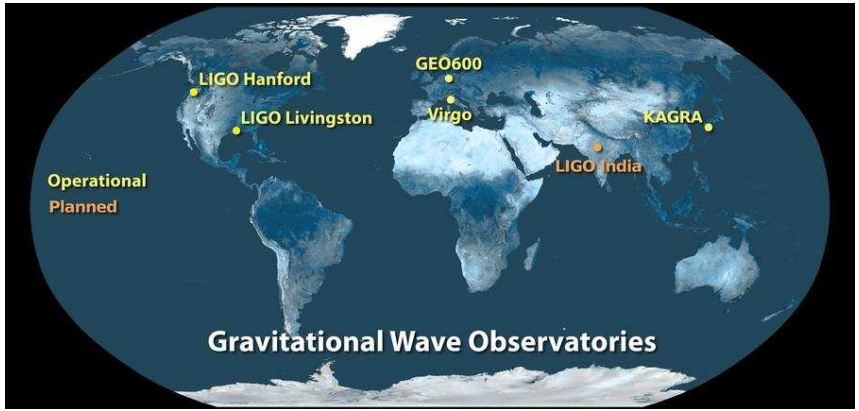

SOURCE - Caltech/MIT/LIGO Lab

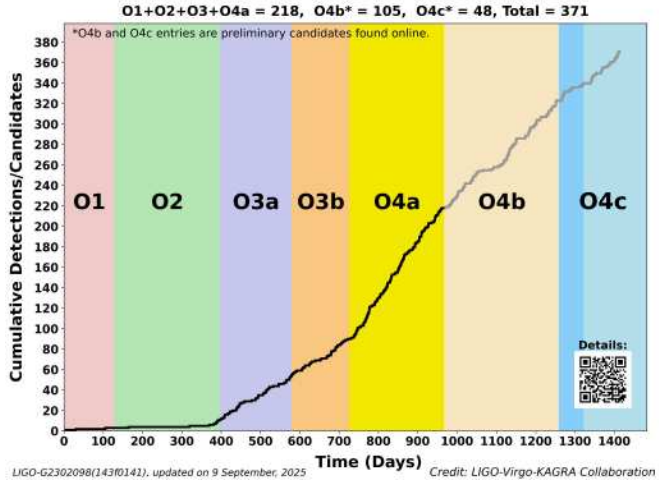

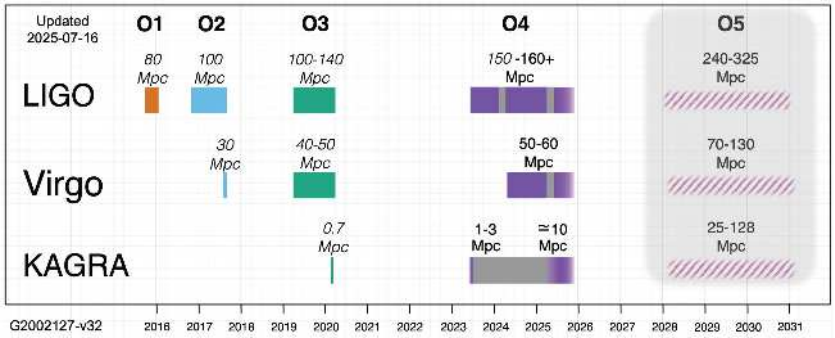

SOURCE - LVK collaboration

LIGO-Virgo-KAGRA collaboration

LIGO

Virgo

KAGRA

Observation band
10 Hz - 2 kHz

h(t) strain signal

Bias

Uncertainty

CALIBRATION

Analysis

Gravitational waves detection

Parameter estimation

Calibration impact

First detection - GW150914

- Binary Black Hole coalescence
- 36 $M_\odot$ and 29 $M_\odot$
- Distance ⟶ 410 Mpc
- Signal over Noise Ratio (SNR) ⟶ 24

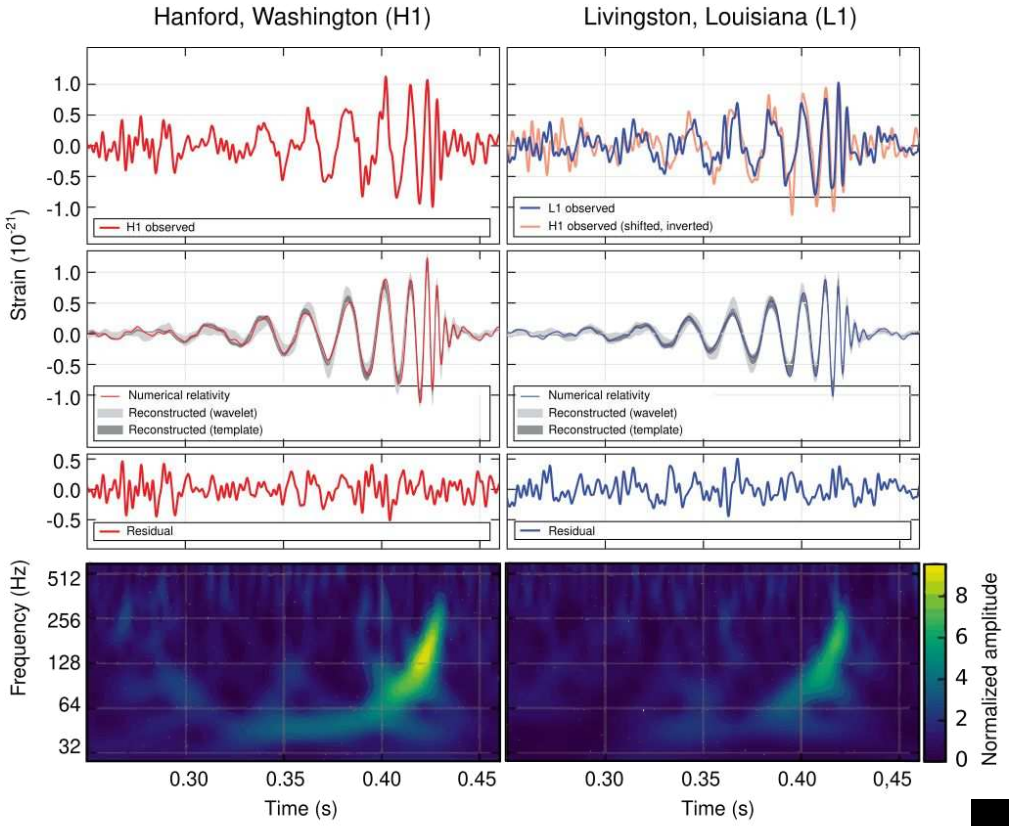

Calibration impact

First detection - GW150914

- Binary Black Hole coalescence
- 36 $M_\odot$ and 29 $M_\odot$
- Distance ⟶ 410 Mpc
- Signal over Noise Ratio (SNR) ⟶ 24

Stronger detection - GW250114

- Binary Black Hole coalescence
- 33 $M_\odot$ and 32 $M_\odot$
- Distance ⟶403 Mpc
- SNR ⟶ 80

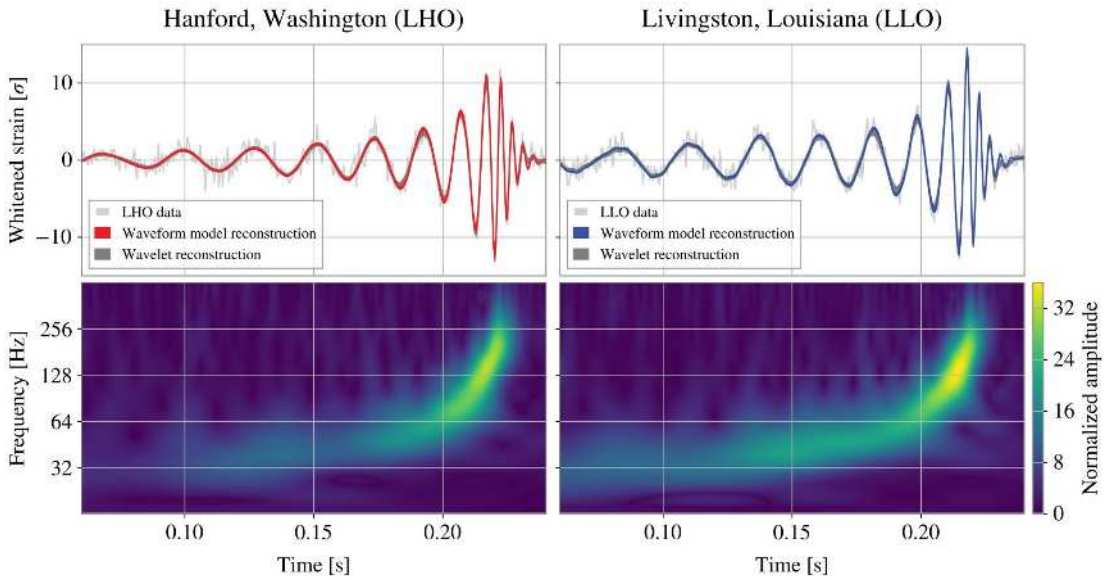

Calibration

Uncertainty on h(t) strain amplitude
⟶ precision on the GW waveform shape
⟶ precision on the parameter estimation

⟶ Necessary to improve the calibration at the same time as the detectors

Calibration impact

First Multi Messenger detection - GW170817

- GW detected by LIGO and Virgo
  Gamma Ray Burst (GRB) detected 1.7 s later by INTEGRAL et Fermi

- Importance of the gravitational wave detectors network → Precise localisation

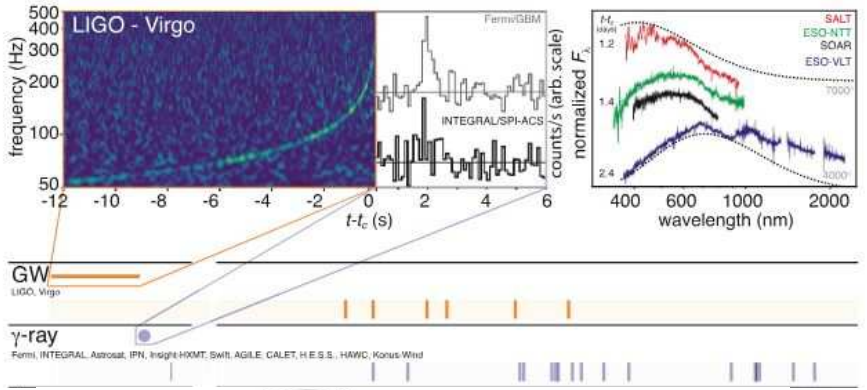

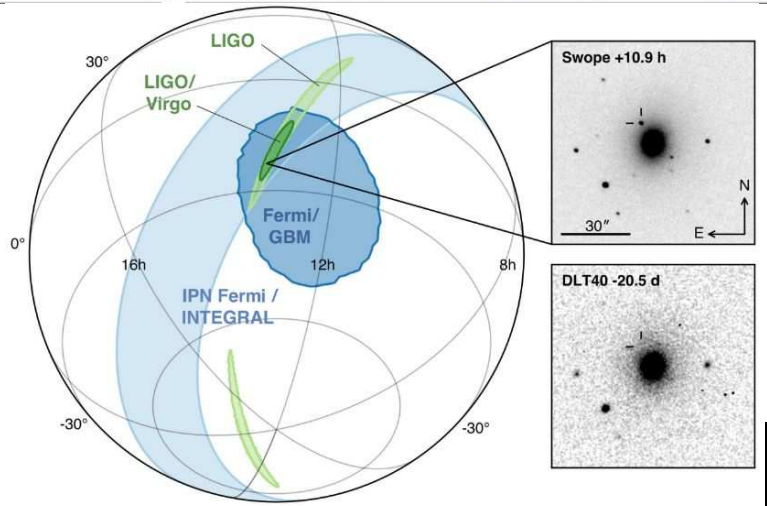

Calibration

Uncertainty on the h(t) strain phase
→ precision on the time of detection
→ precision on the localisation

Summary

Advanced Virgo detection method

Ground interferometer with 3 km long arms:

- Laser source, near-IR (1064 nm)
- Beam splitter
- End mirrors
- **3 km long resonant Fabry-Perot cavities**
  → Increases the effective distance traveled by the laser beam inside the arms
  → Increases the laser power variation on the detection photodiode

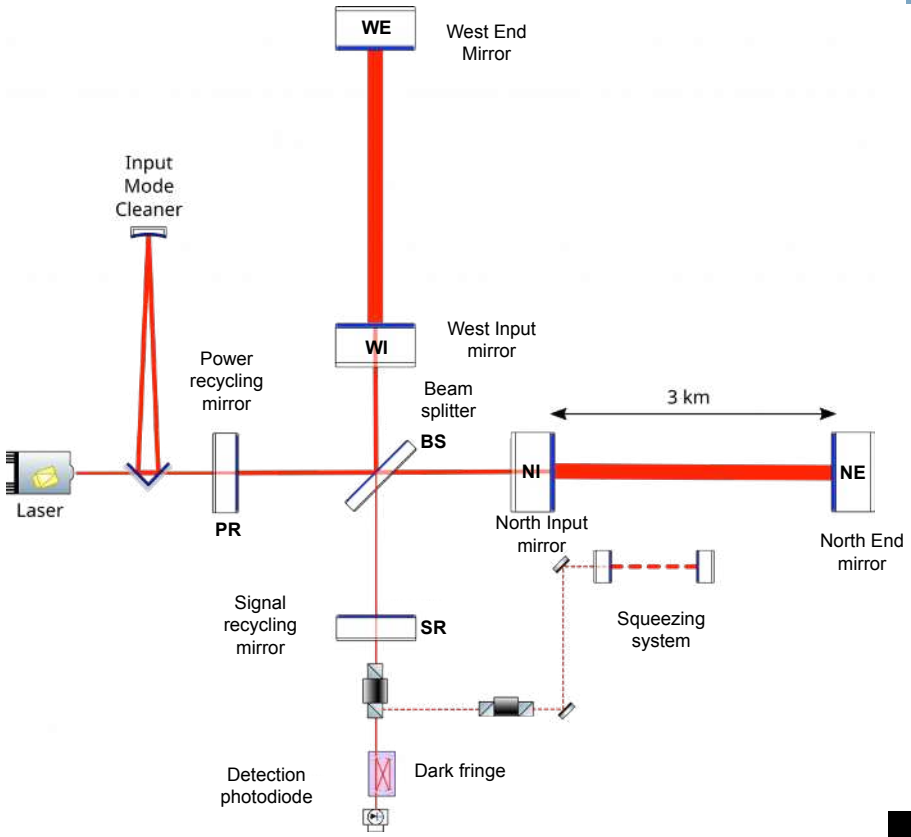

Advanced Virgo detection method

Ground interferometer with 3 km long arms:

- Laser source, near-IR (1064 nm)
- Beam splitter
- End mirrors
- 3 km long resonant Fabry-Perot cavities
  → Increases the effective distance traveled by the laser beam inside the arms
  → Increases the laser power variation on the detection photodiode
- **Mirrors are suspended with a passive attenuation system in vacuum**

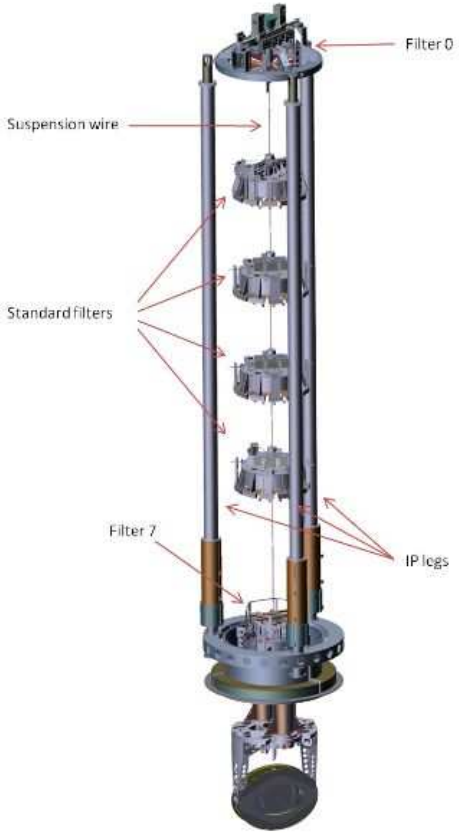

Advanced Virgo detection method

Gravitational wave effect on an interferometer:

- Alternatively modifying the arm length L_W et L_N
  ⟶ Changes in the interference pattern
  ⟶ Changes in the measured power

- We measure the differential arm length variations

$$\Delta L = L_N - L_W$$

- The gravitational wave signal is given by

$$h(t) = \frac{\Delta L}{L_0}$$

Where L_0 = 3 km

$\Delta L \sim 10^{-19}$ m

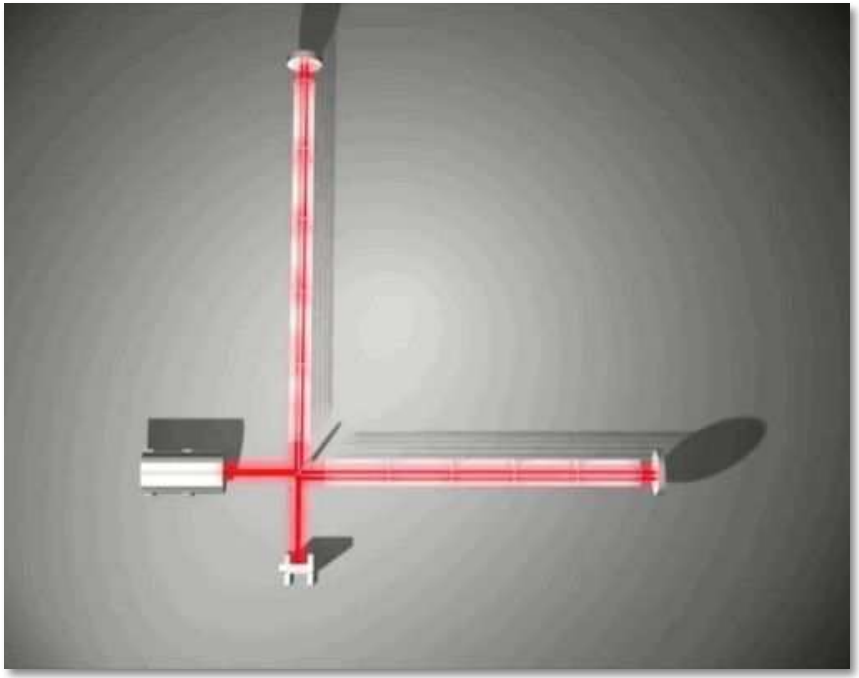

SOURCE - IUCAA

Interferometer controls

Mirror displacement at low frequency caused by different “noise” (seismic, quantum, etc.)

Necessary to very precisely control the mirror position and the resonant cavities length to allow for GW detection

Use **control loops**

Allow to control the different parameters of the interferometer

Example : DARM → allow to keep the interferometer on the same position on the interference pattern → counteract the ΔL variations

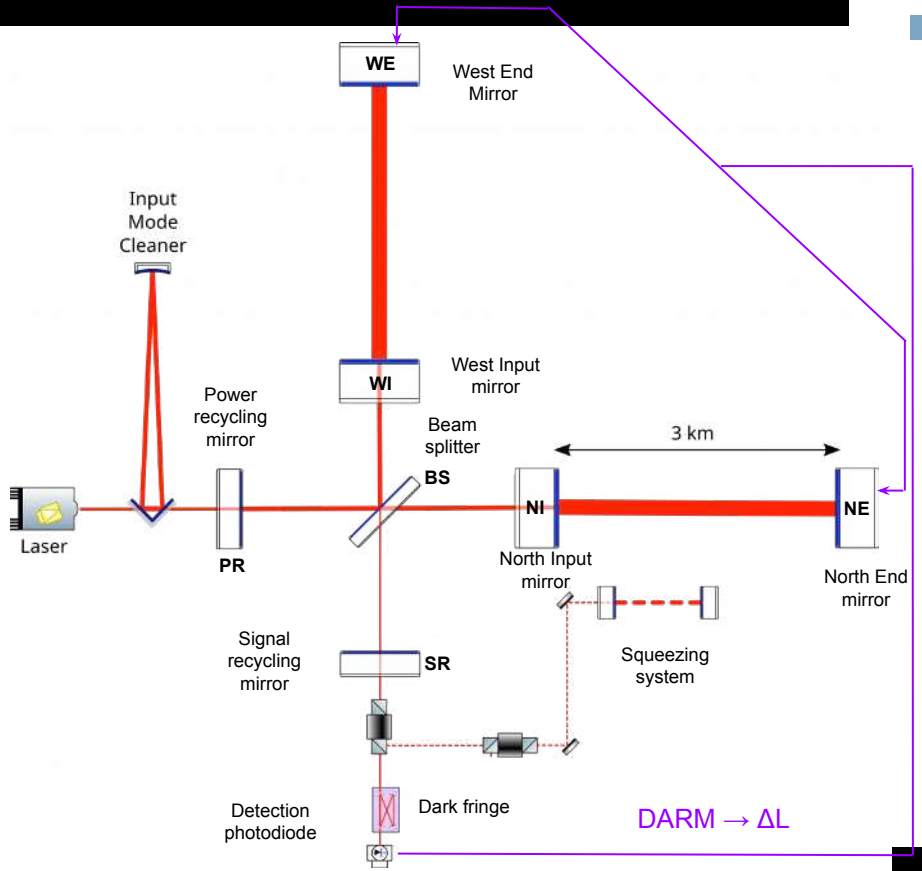

Electromagnetic actuators

E.M. actuators are composed of:

- Magnets placed at the back of the Virgo mirrors
- Coil placed in front of these magnets in the actuation cage

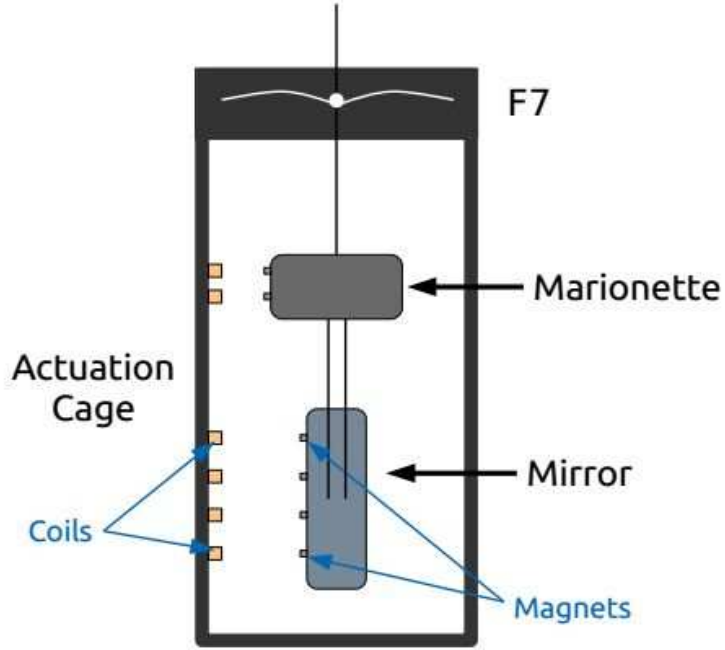

With $A_{E.M.}(f)$ the actuator response function in $[m/V]$ composed of:

- The electronic response in $[N/V]$
- The mechanical response in $[m/N]$

Summary

- I. Gravitational waves theory
- II. Gravitational waves detection

- III. Advanced Virgo calibration
  - Calibration principle
  - Newtonian Calibrator
  - Photon Calibrator

- IV. Photon Calibrators calibration
- V. Electromagnetic actuators calibration
- VI. h(t) strain reconstruction and uncertainty computation

Calibration principle

Interferometer operated thanks to control loops and electromagnetic actuators

CONSEQUENCE: A part of the gravitational wave signal is "diluted" in the control signal
→ **Need to reconstruct the h(t) strain signal**

Hrec algorithm:
GW signal reconstruction by subtracting from the dark fringe signal the contribution of the different control loop signal

Need to have:
- Electromagnetic actuator response models
- Optical responses

→ Calibration measurements

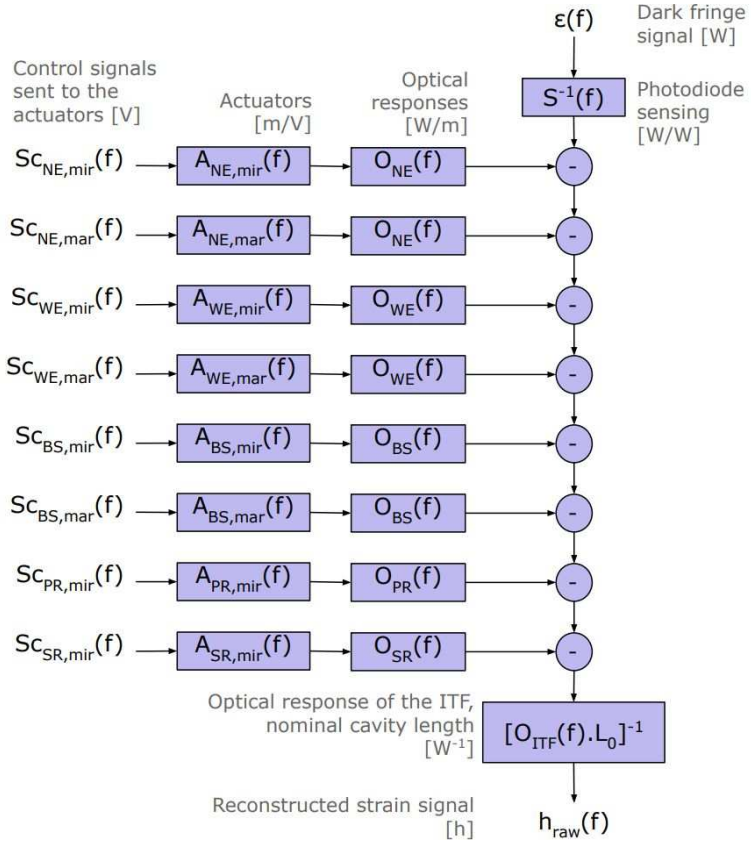

Calibration transfers principle

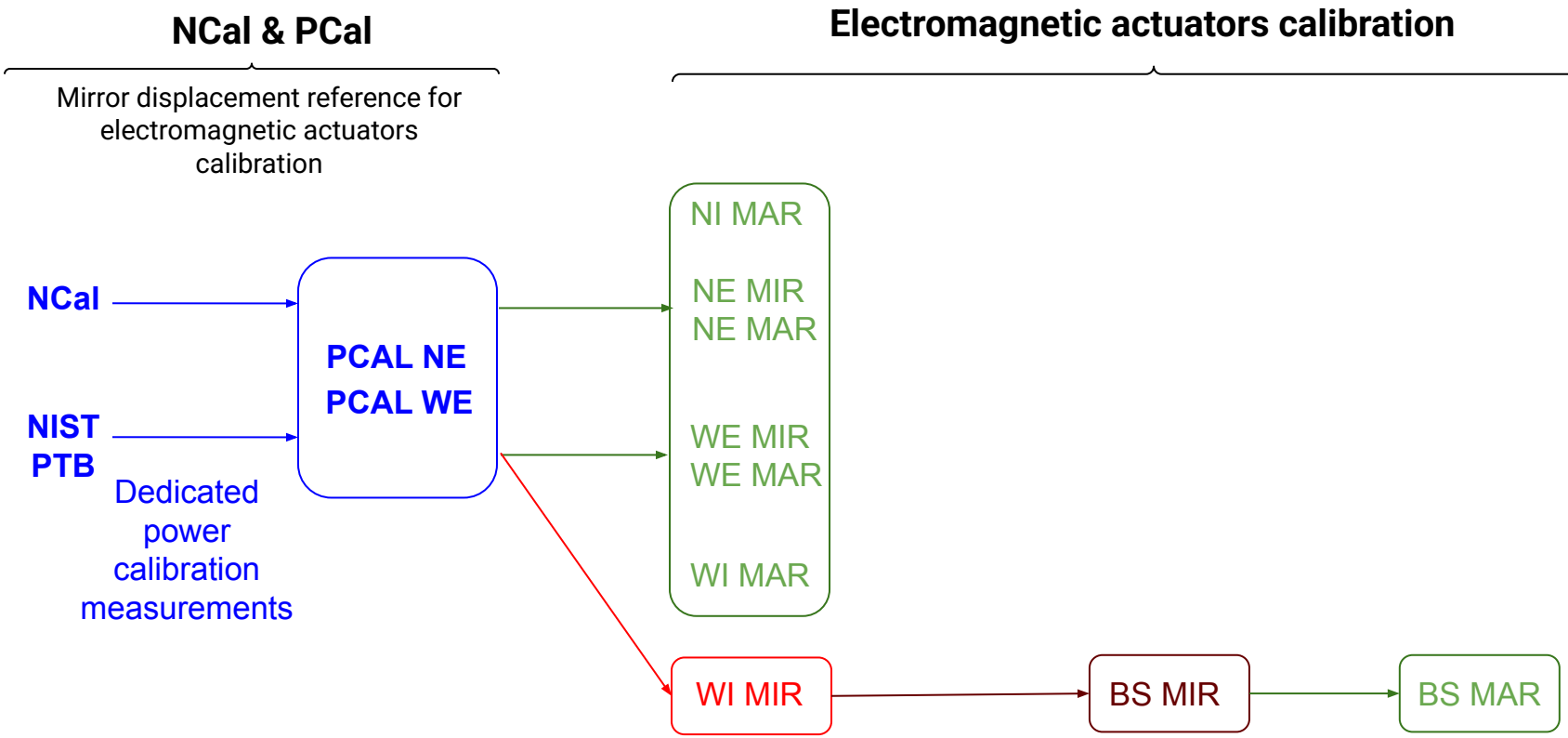

Newtonian Calibrator

Uses a **variable gravitational field** created by rotating masses to induce a miroir displacement with an uncertainty of ± 0.12 %

NCal composed of several rotors ⟶ with each 2 rotating masses

NCal ⟶ Absolute displacement reference during O4

NCal can induce displacement up to 150 Hz

SOURCE - VIR-08551-25

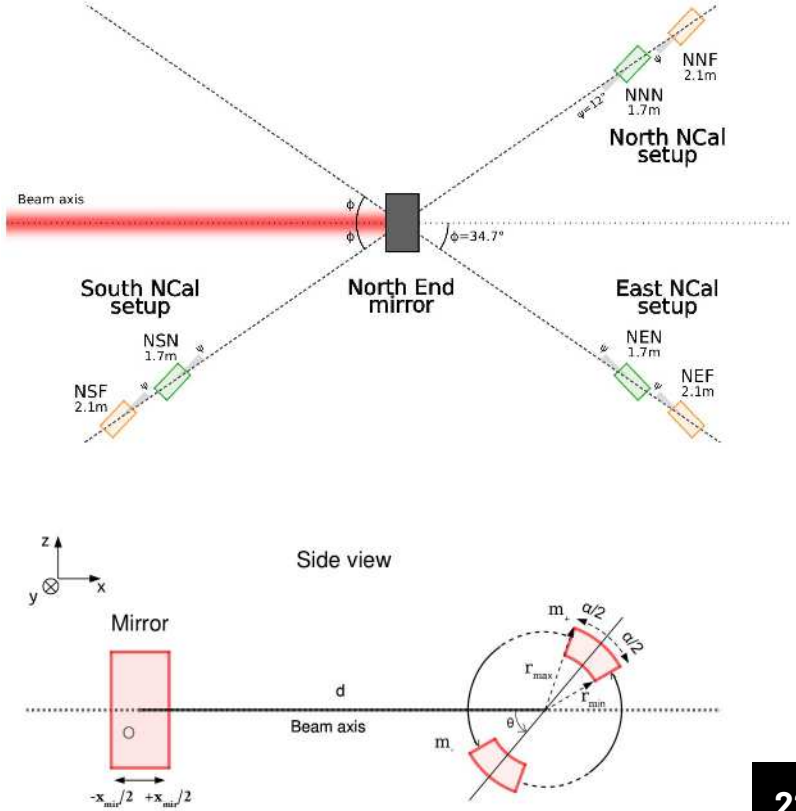

Photon Calibrator

Uses **radiation pressure** of an auxiliary beam send toward an end mirror with an angle θ to induce a displacement **Δx**

$$\Delta x_{PCal(f)} = (A_{pend} + A_{drum}) \frac{2\ \cos(\theta)}{c} \Delta P_{ref}(f)$$

To get **Δx** we need to measure **ΔP$_{ref}$**

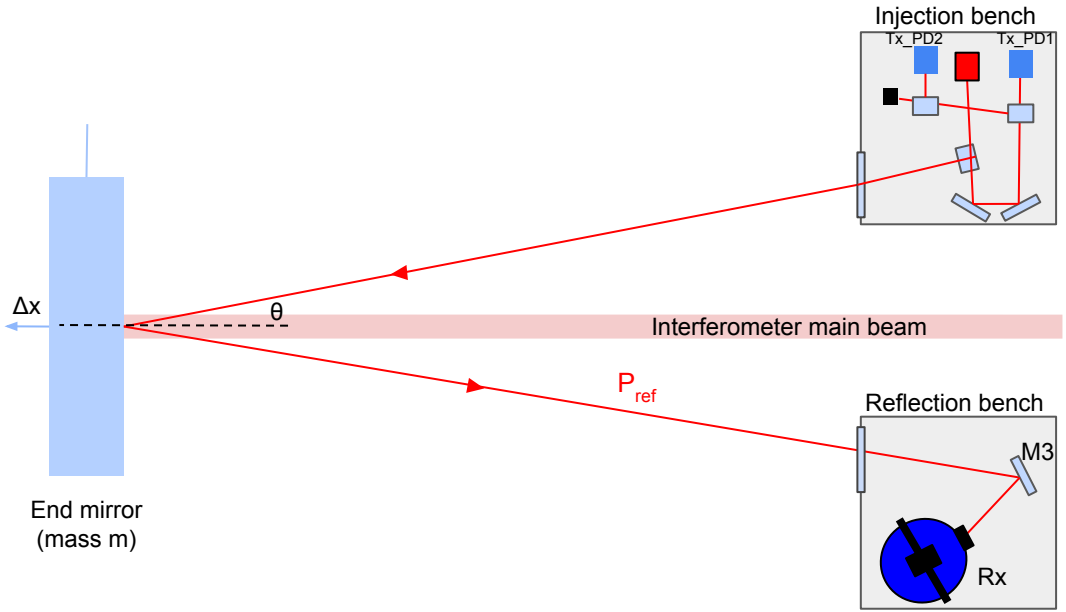

Injection bench:
- Laser collimator (1047 nm)
- 2 photodiodes (Tx_PD1 et Tx_PD2)

Reflection bench:
- Director mirror M3
- Integrating sphere **Rx** to measure the reflected beam power

The PCal can induce a Δx displacement from 10 Hz up to ~8 kHz

Photon Calibrator

Power measurement devices → Integrating spheres

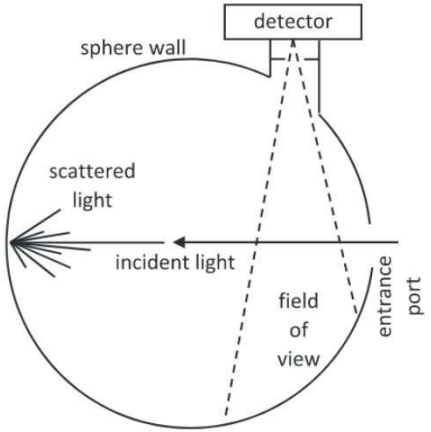

- Measure a voltage V → need to convert this voltage in power W
- Conversion factor → **responsivity ρ** → unique for each sphere

Virgo → 4 integrating spheres
- 2 **Rx spheres**, one on each PCal benches (NE et WE)
- **WSV** (Working Standard Virgo): Reference sphere for Rx calibration at Virgo
- **GSV** (Gold Standard Virgo): Monitoring sphere, always staying at LAPP

2 **Transfer Standard spheres** used to intercalibrate within the LVK collaboration

- **TSA** (Transfer Standard A)
- **TSB** (Transfer Standard B)

Summary

PCals calibration

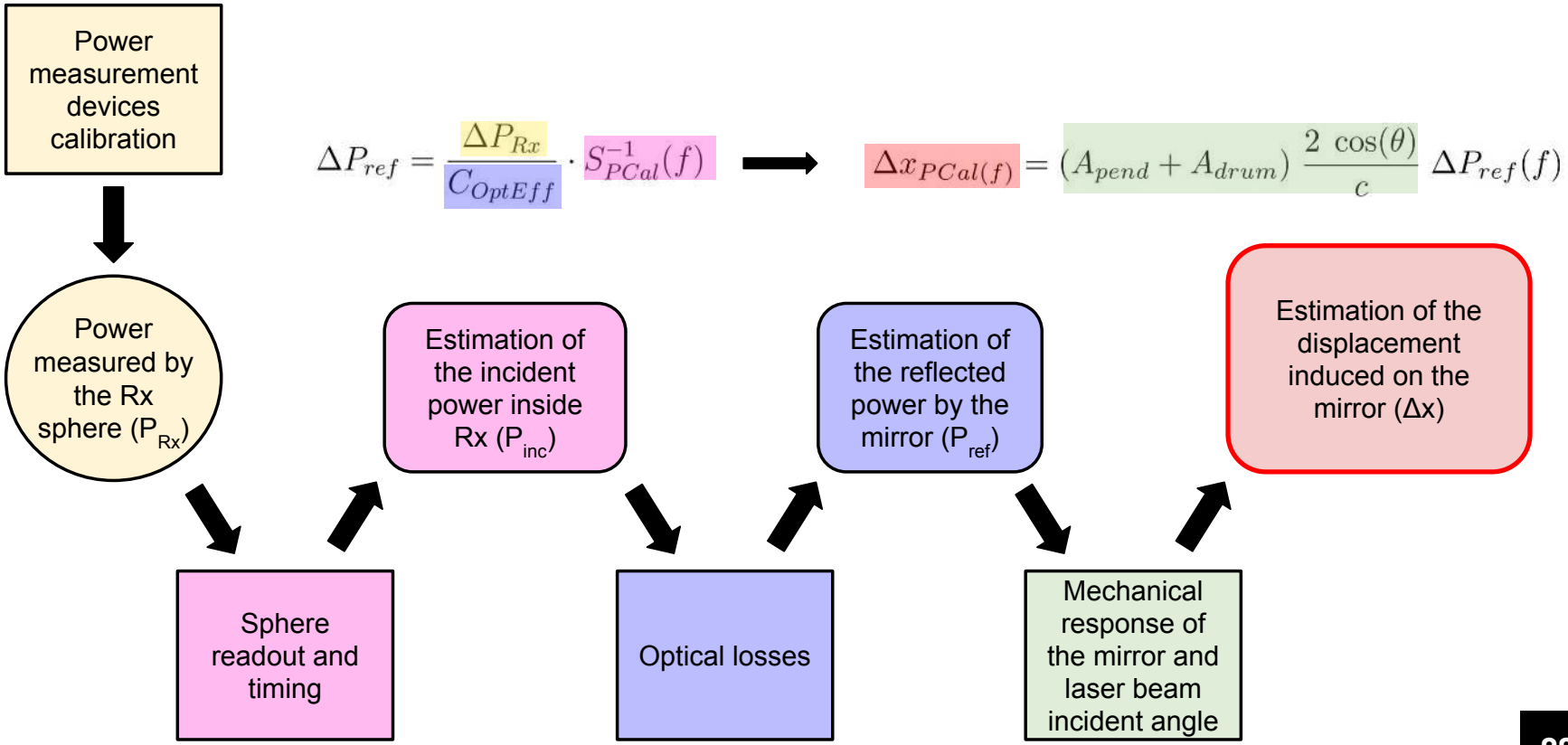

Integrating spheres intercalibration

Power measurement devices calibration

Power measured by the Rx sphere (P_{Rx})

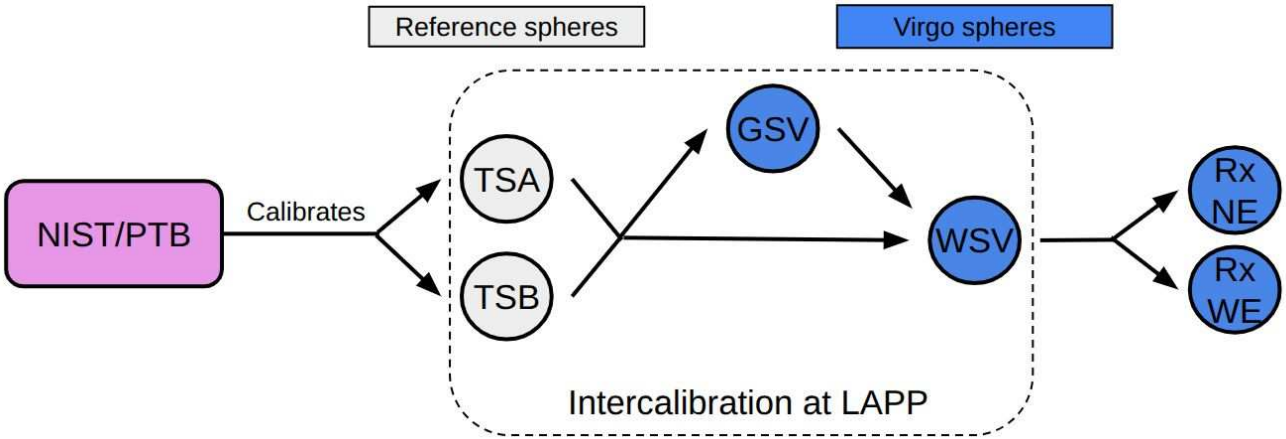

Intercalibration : TSA et TSB

GOAL : Measure the responsivity ρ for WSV and GSV sphere using TSA and TSB as references

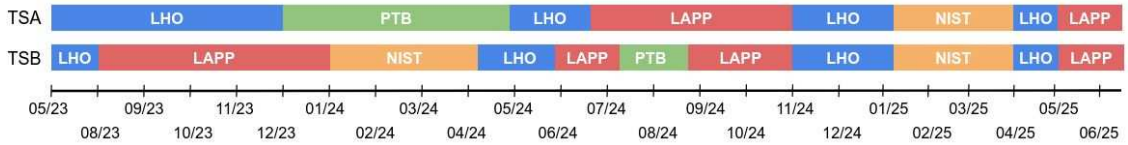

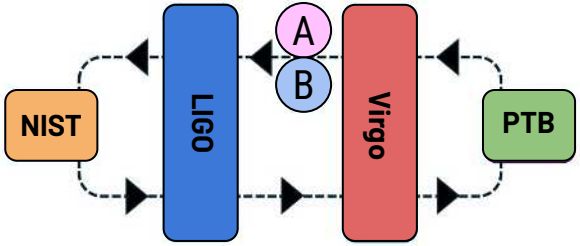

TSA

→ 3 measurements at NIST and 2 at PTB
→ 2 measurements at LAPP

TSB

→ 4 measurements at NIST and 2 at PTB
→ 4 measurements at LAPP

	CR [V/W]	u(CR) [%]	DoE [%]	u(DoE) ($\sigma = 2$) [%]
TSA	-4.35988	0.08	-0.21	0.32
TSB	-4.27856	0.08	-0.23	

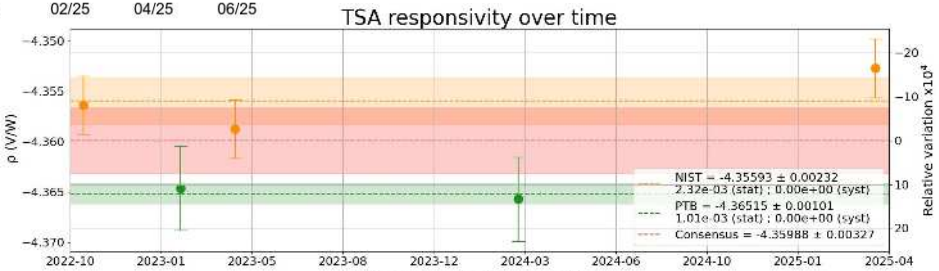

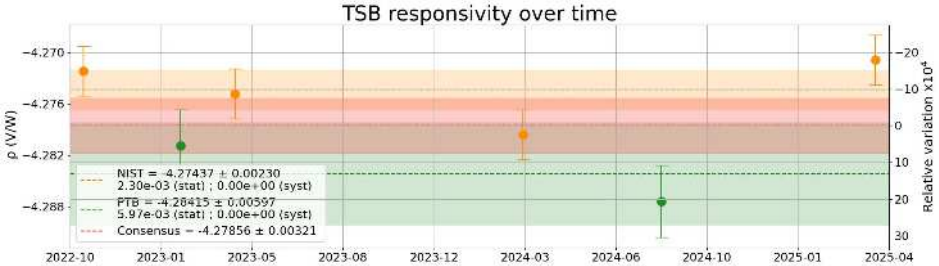

Intercalibration : Measurement protocol

Protocol (example for TSA) :

- TSA and WSV are placed on pneumatic rails in LAPP clean room

- A laser beam is sent towards the two spheres (0.3 W on each sphere)

- 1h long measurement with change in sphere position every 15 s
  - Data acquired for 10 s

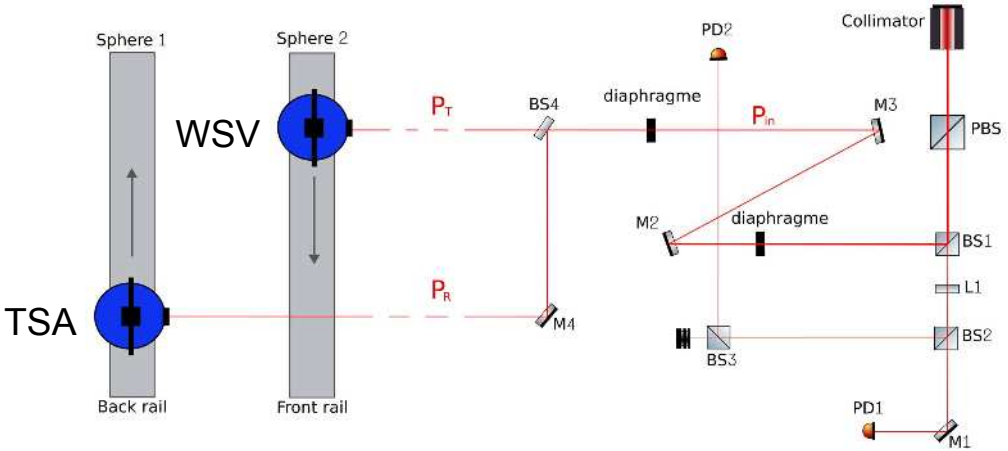

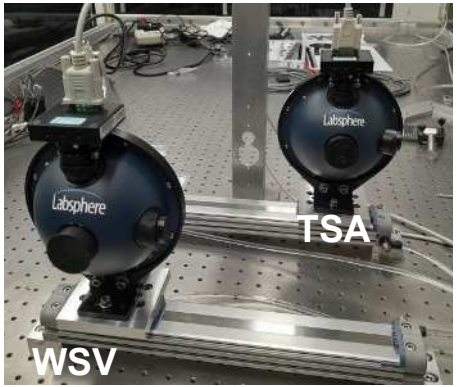

Intercalibration : α’ ratio computation

α’ ratio computation at 300.15 K

Correcting from the spheres temperature dependencies, we can compute the **α’** coefficient which corresponds to the **responsivity ratio**

$$\alpha' = \sqrt{\frac{V_{WSV}^{corr}(T \cdot P_{in})}{V_{TSA}^{corr}(R \cdot P_{in})} \cdot \frac{V_{WSV}^{corr}(R \cdot P_{in})}{V_{TSA}^{corr}(T \cdot P_{in})}} = \frac{\rho'_{WSV}}{\rho'_{TSA}}$$

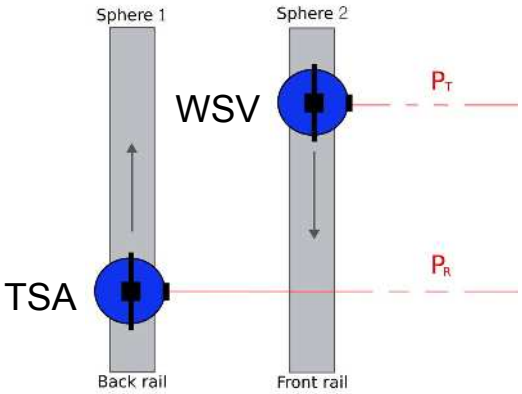

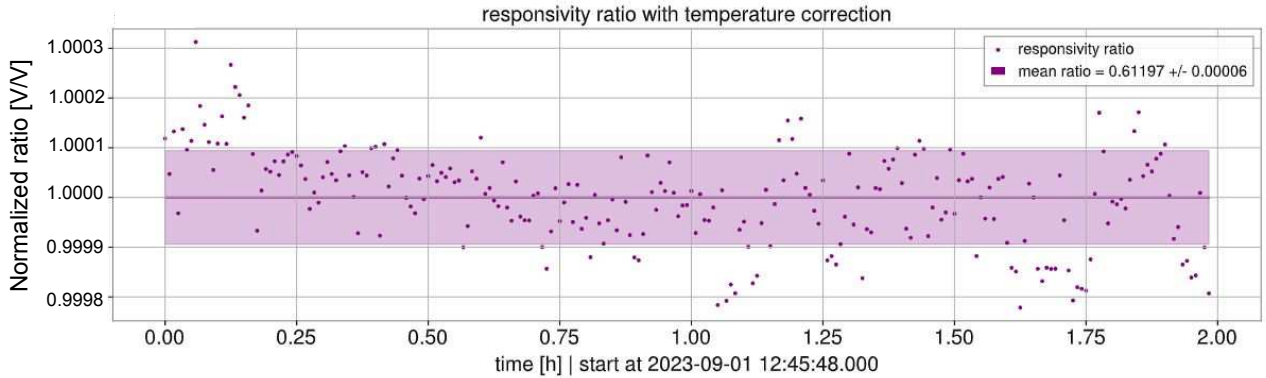

Intercalibration : α' ratio evolution

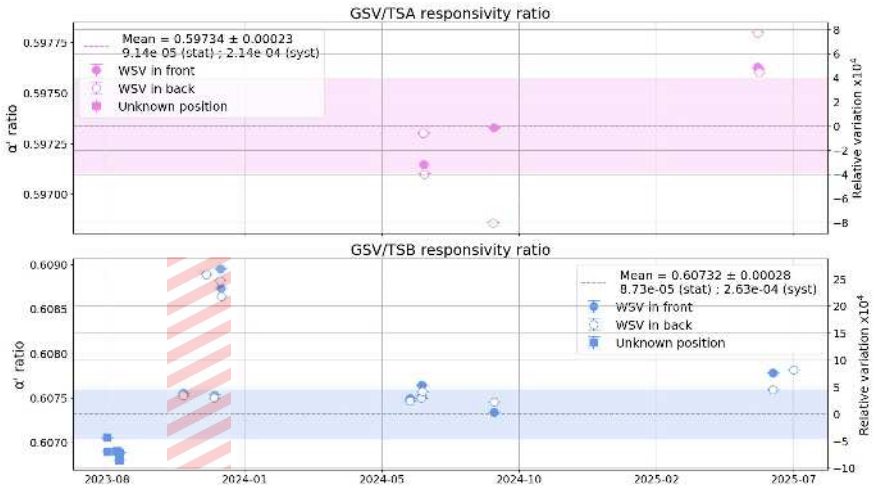

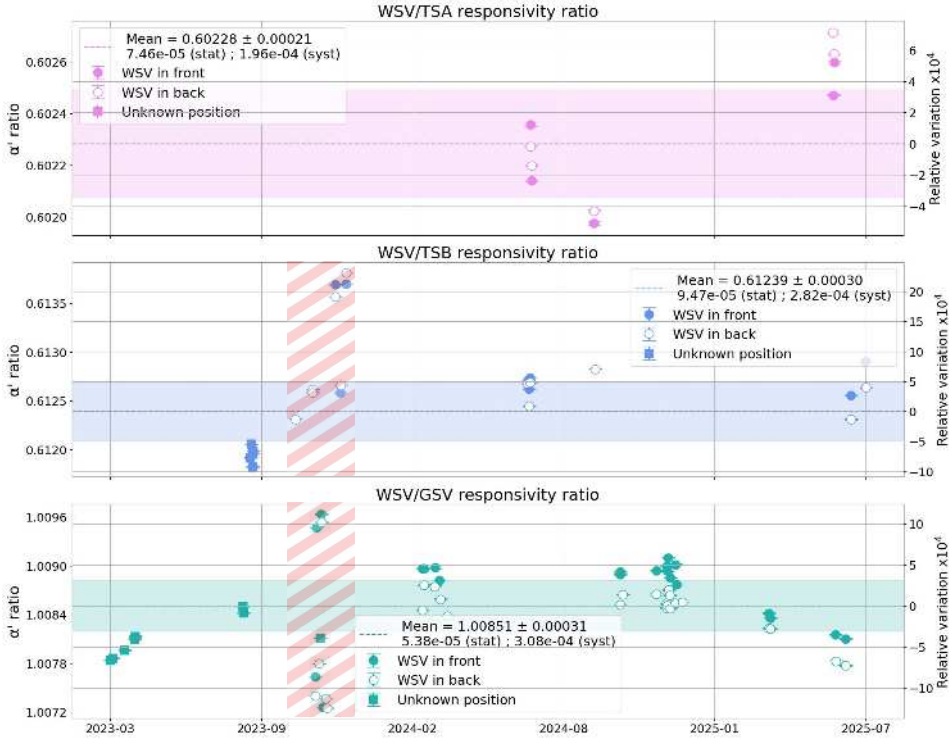

α' ratio evolution during O4:

GSV → ±0.05 % variations within 2 years

WSV → ±0.05 % variations within 2 years

Increased variations caused by the misadjustment of diaphragm opening on the setup

Intercalibration : Responsivity computation

$$\alpha' = \sqrt{\frac{V_{WSV}^{corr}(T \cdot P_{in})}{V_{TSA}^{corr}(R \cdot P_{in})} \cdot \frac{V_{WSV}^{corr}(R \cdot P_{in})}{V_{TSA}^{corr}(T \cdot P_{in})}} = \frac{\rho'_{WSV}}{\rho'_{TSA}}$$

Responsivity computation at 300.15 K

$$\rho'_{WSV} = \rho'_{TSA} \cdot \alpha'$$

	CR [V/W]
TSA	-4.35988
TSB	-4.27856

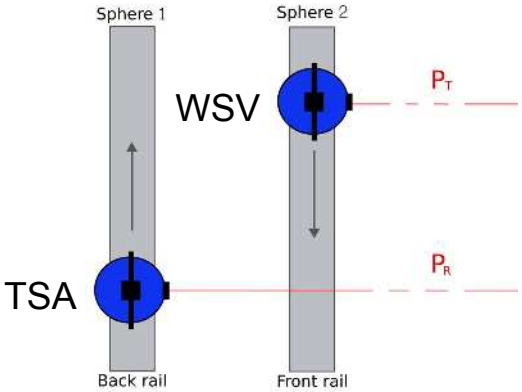

Intercalibration : Responsivity evolution

Highlighting of a **~0.2%** discrepancy between the responsivity computed with TSA and TSB

This difference is seen with both WSV and GSV

Similar difference seen at LIGO starting in July 2024 →Need to confirm with further measurements

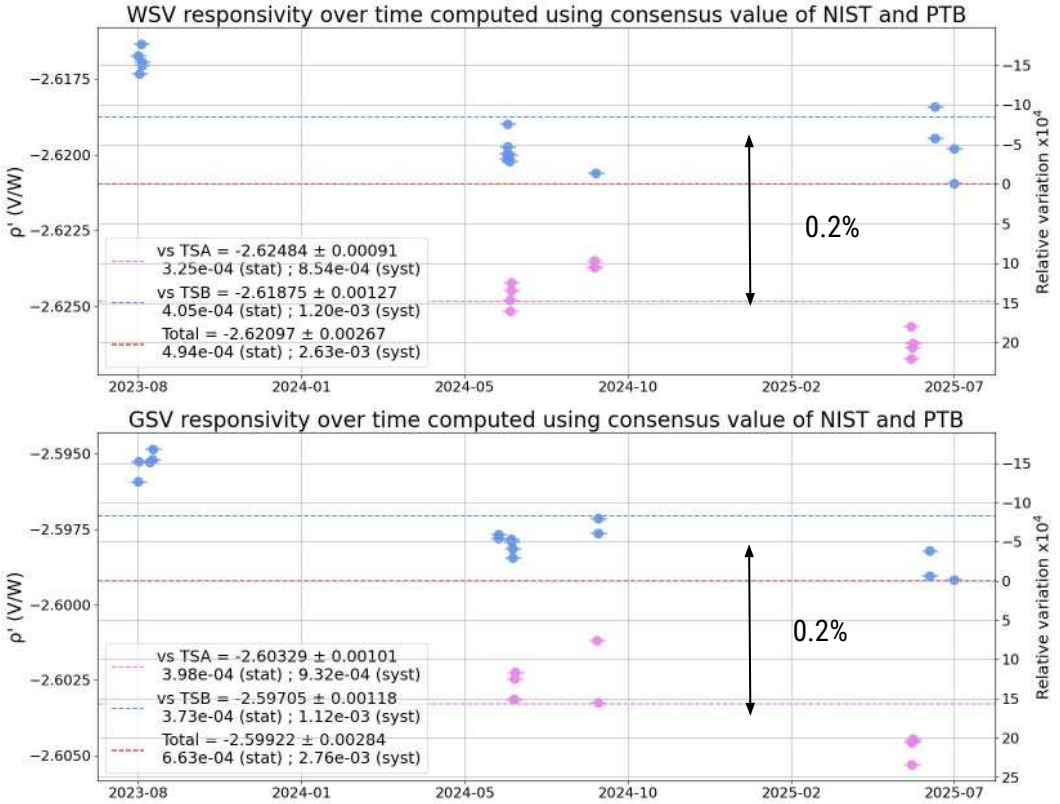

Intercalibration : Responsivity evolution

WSV responsivity computed using 2 years of intercalibration measurement compared to the initial value used for O4

$$\rho'_{WSV} = -2.61787 \pm 0.00288 \text{ V/W}$$

$$\rho'_{u} = -2.62097 \pm 0.00267 \text{ V/W}$$

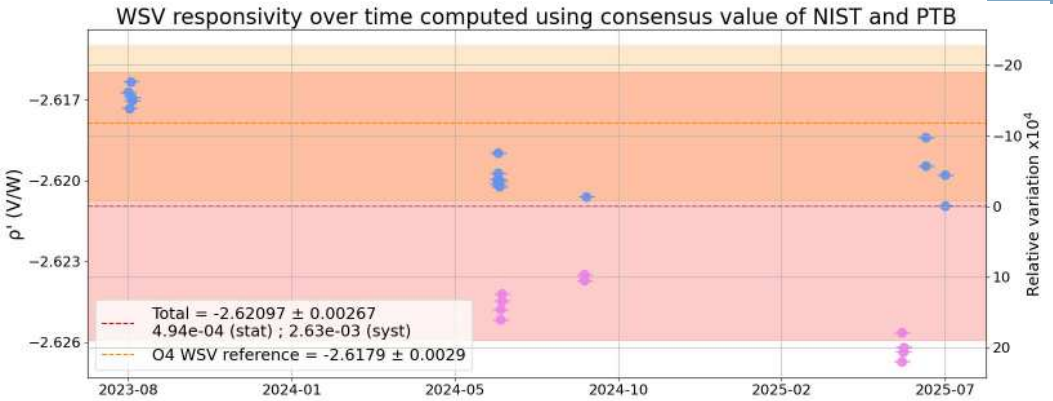

Source	Relative uncertainty [%]	
TS responsivity	0.08	
TSA/TSB discrepancy	0.16	
α' ratio WSV/TS	0.05	
ρ_{WSV} temperature dependence	0.04	
Output voltage	ADC conversion	0.03
	Background voltage	0.03
	Total	0.04
Total	**0.19**	

Power measurement devices calibration

Power measurement devices calibration

Power measured by the Rx sphere (P_{Rx})

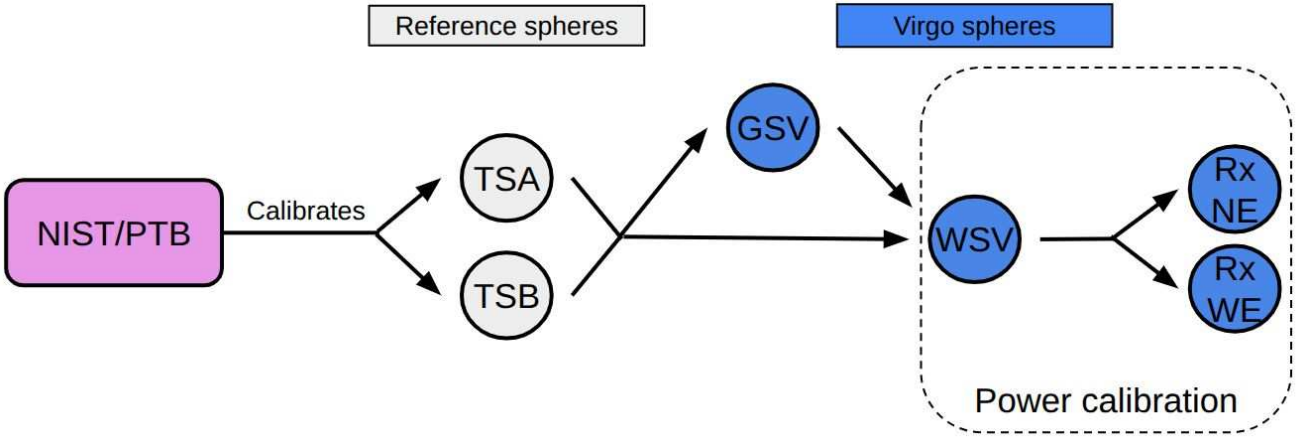

Power measurement devices calibration

GOAL : Measuring the **Rx** sphere responsivity ρ pusing **WSV** as reference

Protocole :

- Placing WSV in Rx's place
- Calibrating the photodiodes with WSV as reference → ~6h measurement with laser at 1.3W

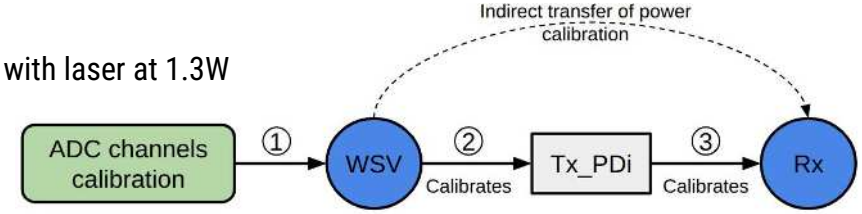

- Putting Rx back at its place
- Calibrating Rx using a photodiode as reference→ ~6h measurement with laser at 1.3W

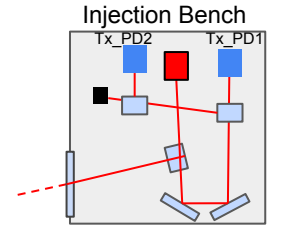

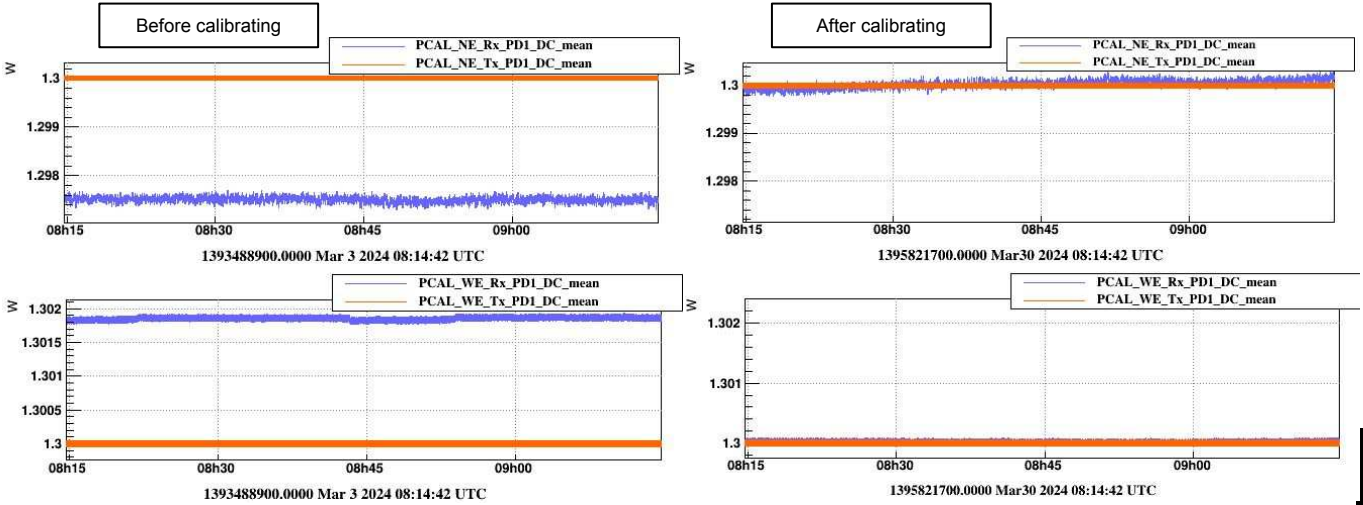

Power measurement devices calibration

Calibration measurement made before and during O4:

- December 2022
- June 2023
- March 2024 (just before O4b)
- April 2025 (juste before WE replacement)

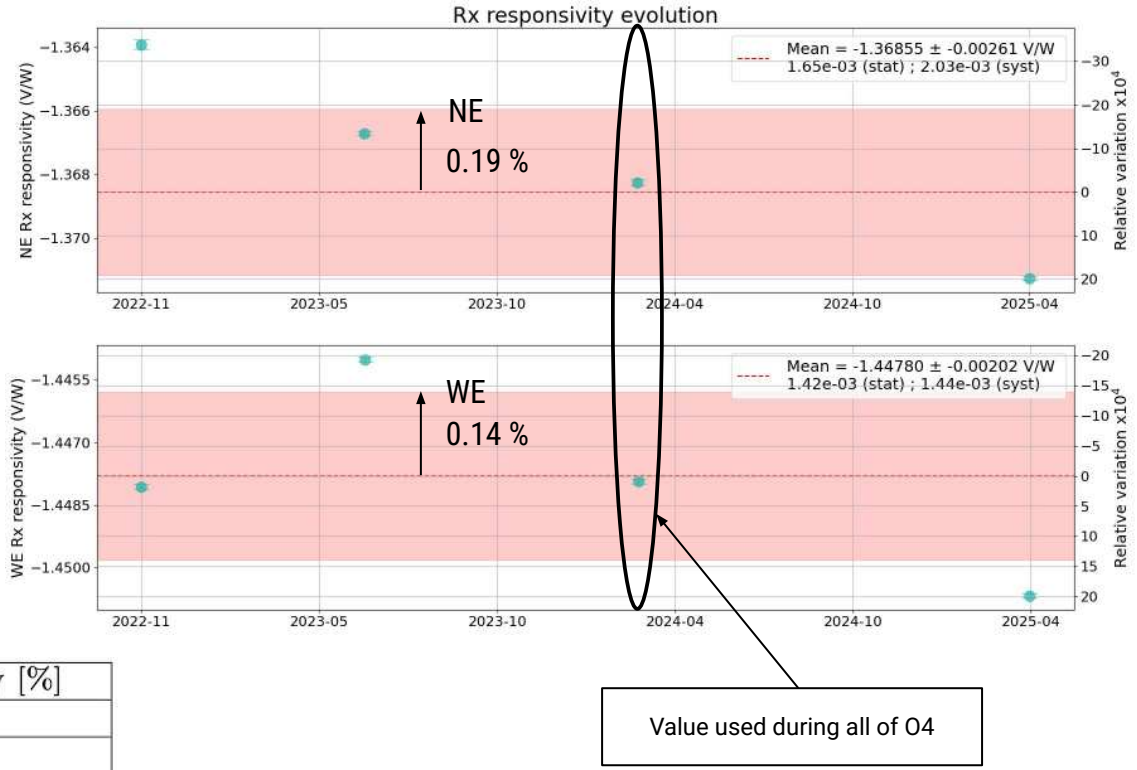

Source	Relative uncertainty [%]
WSV responsivity	0.19
Rx calibration	0.19
Total	**0.27**

Detection electronic calibration

Power measurement devices calibration

$$\Delta P_{ref} = \frac{\Delta P_{Rx}}{C_{OptEff}} \cdot S^{-1}_{PCal}(f) \longrightarrow \Delta x_{PCal(f)} = (A_{pend} + A_{drum}) \frac{2\ \cos(\theta)}{c} \Delta P_{ref}(f)$$

Power measured by the Rx sphere (P_{Rx})

Estimation of the incident power inside Rx (P_{inc})

Sphere readout and timing

Detection electronic calibration

PCal readout chain:

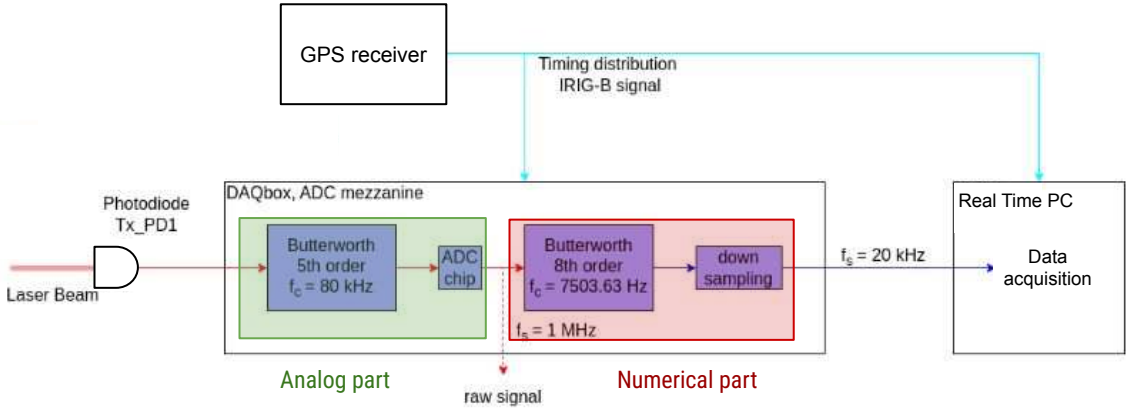

Frequency response measurement of the readout chain:

Nominal model	PCal	NE			WE		
	Sensor	Tx_PD1	Tx_PD2	Rx	Tx_PD1	Tx_PD2	Rx
	Analog filter	5^{th} order Butterworth filter f_c= 80 kHz					
	Digital filter	8^{th} order Butterworth filter f_c= 7503.65 kHz					
	Down sampling delay	-49 μs					
	Fitted residual delay	0.62 μs	0.54 μs	1.45 μs	0.72 μs	0.66 μs	1.38 μs

CRÉDIT - Paul Lagabbe

Optical losses

Power measurement devices calibration

$$\Delta P_{ref} = \frac{\Delta P_{Rx}}{C_{OptEff}} \cdot S^{-1}_{PCal}(f) \longrightarrow \Delta x_{PCal(f)} = (A_{pend} + A_{drum}) \frac{2\ \cos(\theta)}{c} \Delta P_{ref}(f)$$

Power measured by the Rx sphere (P_{Rx})

Sphere readout and timing

Estimation of the incident power inside Rx (P_{inc})

Optical losses

Estimation of the reflected power by the mirror (P_{ref})

Optical losses

Optical losses:

$$P_{ref}(f) = \frac{P_{Rx}}{(1 - l_{vp})(1 - l_M)} \cdot S^{-1}_{PCal}(f)$$

$$l_{vp} = 0.57 \pm 0.096\%$$

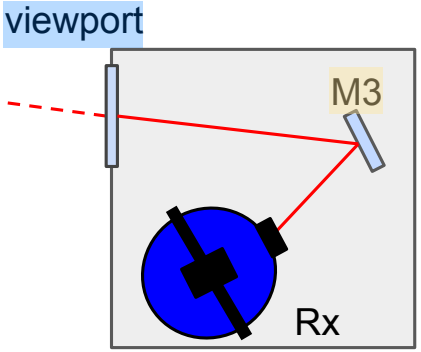

$$l_M = 0.107 \pm 0.012\%$$

Measurement made with samples at LAPP

Then, estimation on site in June 2023

→ Confirming optical losses for WE

→ Higher losses for NE

Uncertainty on optical losses → 0.1%

CRÉDIT - Paul Lagabbe

Mechanical response measurement

Power measurement devices calibration

$$\Delta P_{ref} = \frac{\Delta P_{Rx}}{C_{OptEff}} \cdot S^{-1}_{PCal}(f) \longrightarrow \Delta x_{PCal(f)} = (A_{pend} + A_{drum}) \frac{2\ \cos(\theta)}{c} \Delta P_{ref}(f)$$

Power measured by the Rx sphere (P_{Rx})

Sphere readout and timing

Estimation of the incident power inside Rx (P_{inc})

Optical losses

Estimation of the reflected power by the mirror (P_{ref})

Mechanical response of the mirror and laser beam incident angle

Mechanical response measurement

Model composed of:

- Pendulum response (fp = 0.6 Hz)
- First drum vibration mode (fd = ~7900 Hz)
- Higher order modes approximated with a static gain

$$A^{O4}_{PCal}(f) = A_{pend} + A_{drum,1} + G_{hod}$$
$$= \frac{G_p}{1 + \frac{i}{Q_p}\frac{f}{f_p} - (\frac{f}{f_p})^2} + \frac{G_d}{1 + \frac{i}{Q_d}\frac{f}{f_d} - (\frac{f}{f_d})^2} + G_{hod}$$

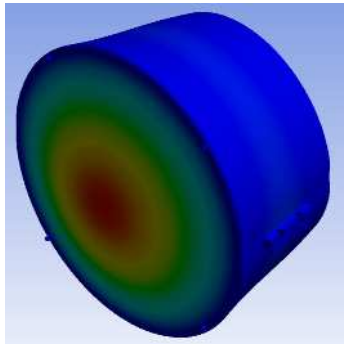

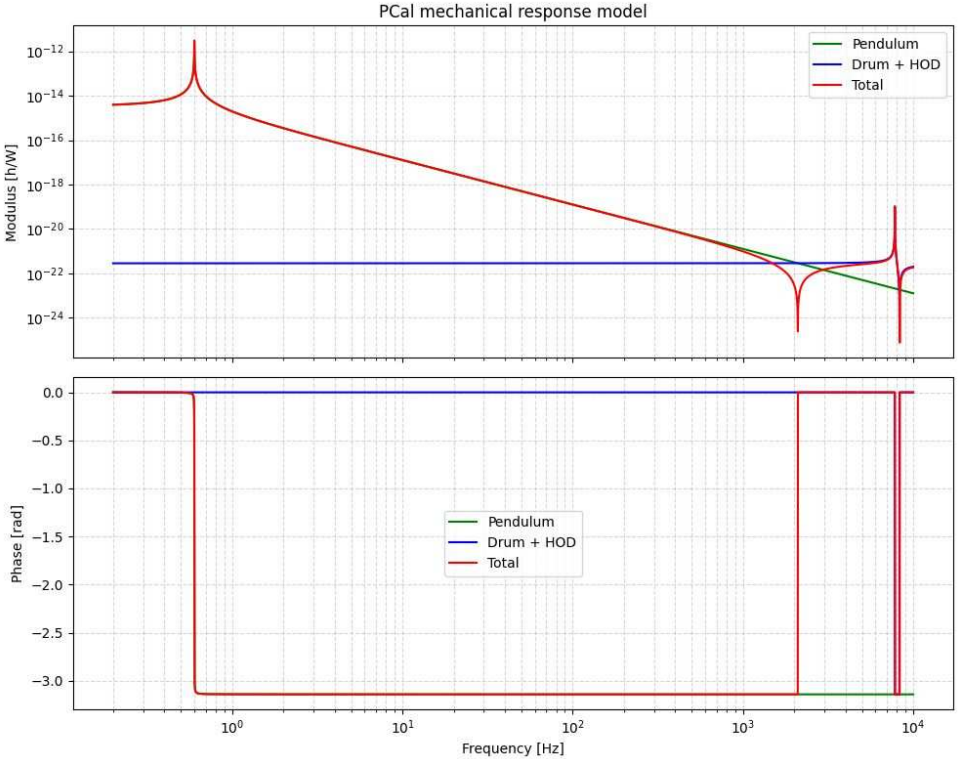

Mechanical response measurement

Protocol:

High frequency lines injection (1 kHz à 8 kHz)with the PCals

Computing the transfer function between the power measured by Rx and the power measured by the dark fringe photodiode of the ITF → Fit of the TF with the mechanical response model

NE

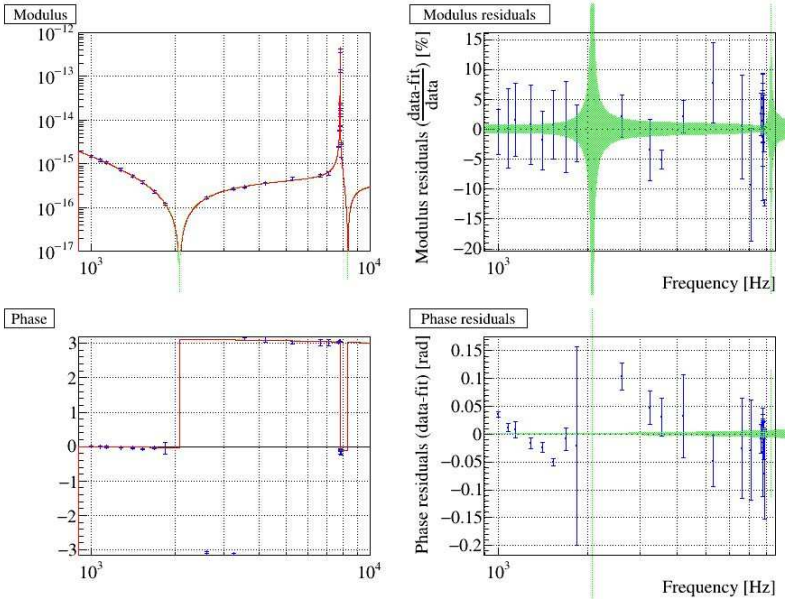

WE

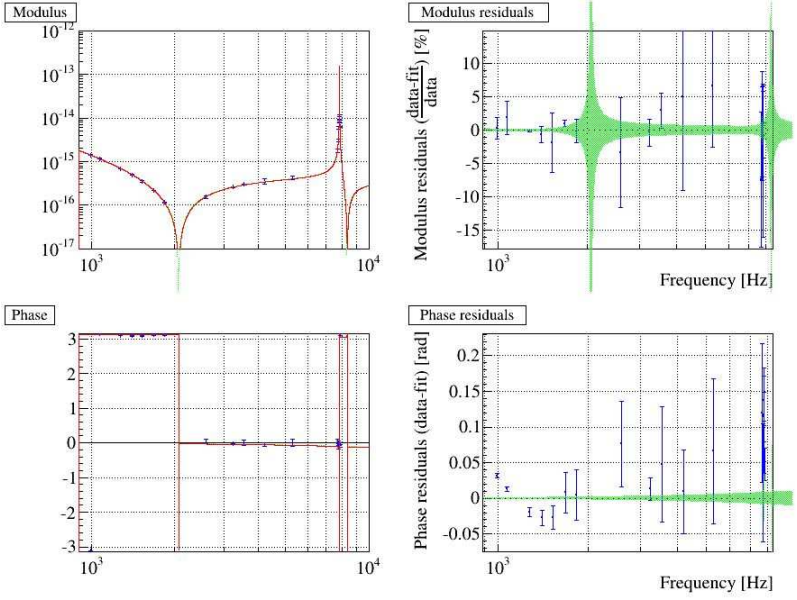

Final PCal displacement model

Power measurement devices calibration

$$\Delta P_{ref} = \frac{\Delta P_{Rx}}{C_{OptEff}} \cdot S^{-1}_{PCal}(f) \longrightarrow \Delta x_{PCal(f)} = (A_{pend} + A_{drum}) \frac{2\ \cos(\theta)}{c} \Delta P_{ref}(f)$$

Power measured by the Rx sphere (P_{Rx})

Sphere readout and timing

Estimation of the incident power inside Rx (P_{inc})

Optical losses

Estimation of the reflected power by the mirror (P_{ref})

Mechanical response of the mirror and laser beam incident angle

Estimation of the displacement induced on the mirror (Δx)

Final PCal displacement model

Source	Relative uncertainty [%]
WSV responsivity	0.19
Rx calibration	0.19
Total	**0.27**

Source		Relative uncertainty [%]
TS responsivity		0.08
TSA/TSB discrepancy		0.16
α' ratio WSV/TS		0.05
ρ_{WSV} temperature dependence		0.04
Output voltage	ADC conversion	0.03
	Background voltage	0.03
	Total	0.04
Total		**0.19**

Source		Relative uncertainty [%]
Rx responsivity		0.27
Deformation model		0.15
Optical efficiency		0.10
Pendulum model	Incident angle, $\cos(\theta)$	0.16
	ETM mass, M	0.05
	ETM rotation	0.09
	Total	0.19
Total		**0.48**

Uncertainty on the displacement induced by the PCal:

- Great progress compared to O3 (1.36%)

Summary

Calibration principle

Electromagnetic actuators response:

- Mirror mechanical response
- Actuators electronic response

$$A^{mir}(f) = \frac{G^{mir}_{mech}}{1 + \frac{i}{Q_p}\frac{f}{f_p} - (\frac{f}{f_p})^2} \times \frac{G_{elec}}{1 + i\frac{f}{f_{elec}}} e^{-i2\pi f \tau_{elec}}$$

We want to characterise the electronic response

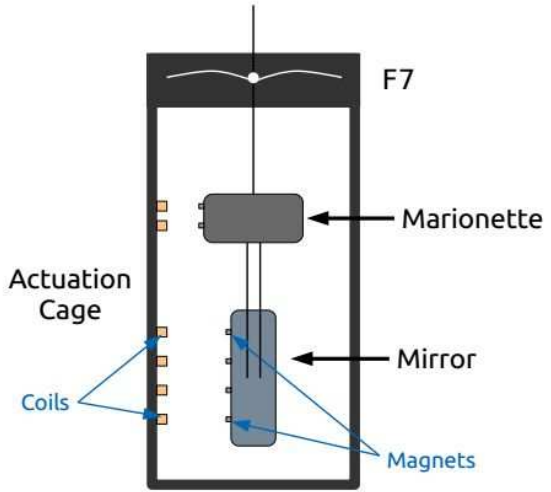

Calibration principle

Electromagnetic actuators response:

- Mirror mechanical response
- Actuators electronic response

$$A^{mir}(f) = \frac{G^{mir}_{mech}}{1 + \frac{i}{Q_p}\frac{f}{f_p} - (\frac{f}{f_p})^2} \times \frac{G_{elec}}{1 + i\frac{f}{f_{elec}}} e^{-i2\pi f \tau_{elec}}$$

We want to characterise the electronic response

Protocol:

- Series of calibration transferts
- Comparing an actuator of reference *(ref)* to an actuator to calibrate *(new)*

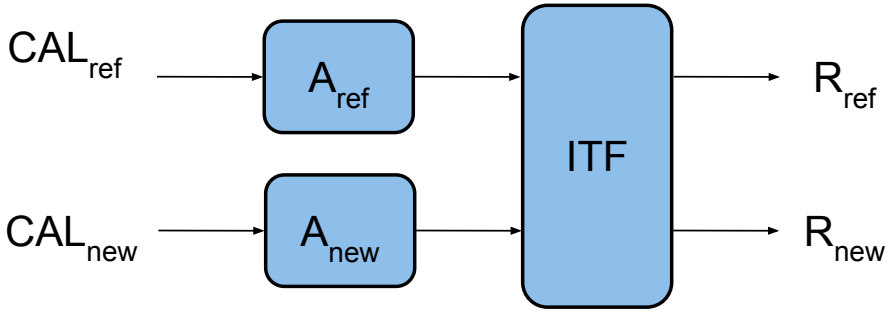

$$R_{ref} = CAL_{ref} \times A_{ref} \times ITF$$
$$R_{new} = CAL_{new} \times A_{new} \times ITF$$

$$A_{new} = (R_{new}/CAL_{new}) \times (R_{ref}/CAL_{ref})^{-1} \times A_{ref}$$

Results for NE and WE actuators

The electromagnetic actuators models for O4 have been computed using the average of all calibration measurement made between August 2023 and April 2024

NE model

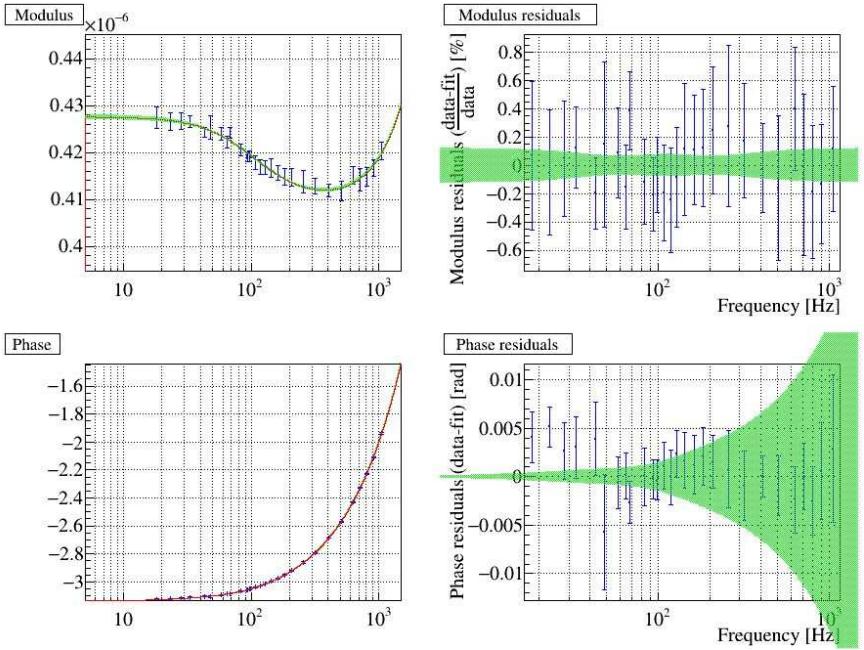

WE model

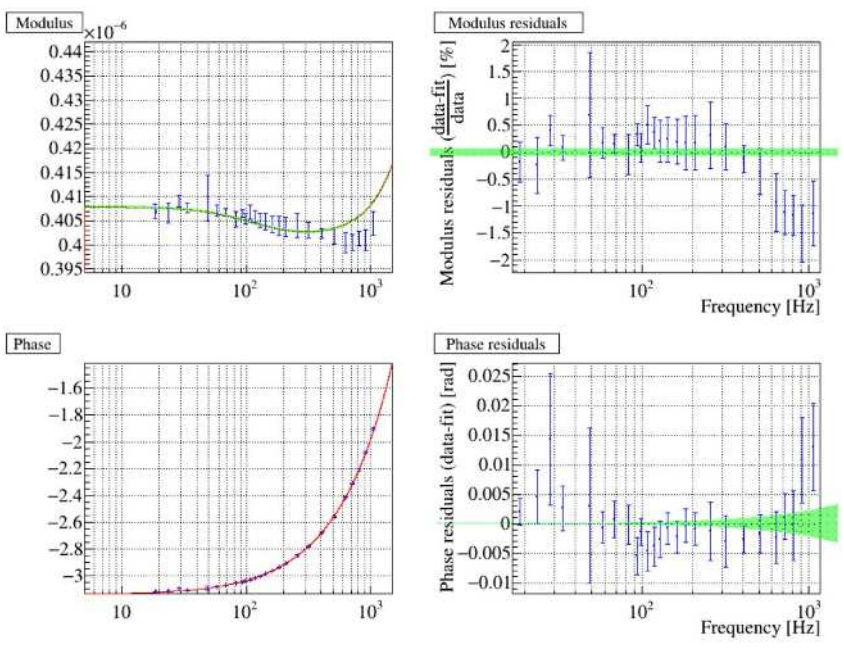

Results for NE and WE actuators

The electromagnetic actuators models for O4 have been computed using the average of all calibration measurement made between August 2023 and April 2024

Additional calibration measurement are performed once a week during the run to monitor potential calibration variations → **Stable within 0.5% for NE and WE**

NE model

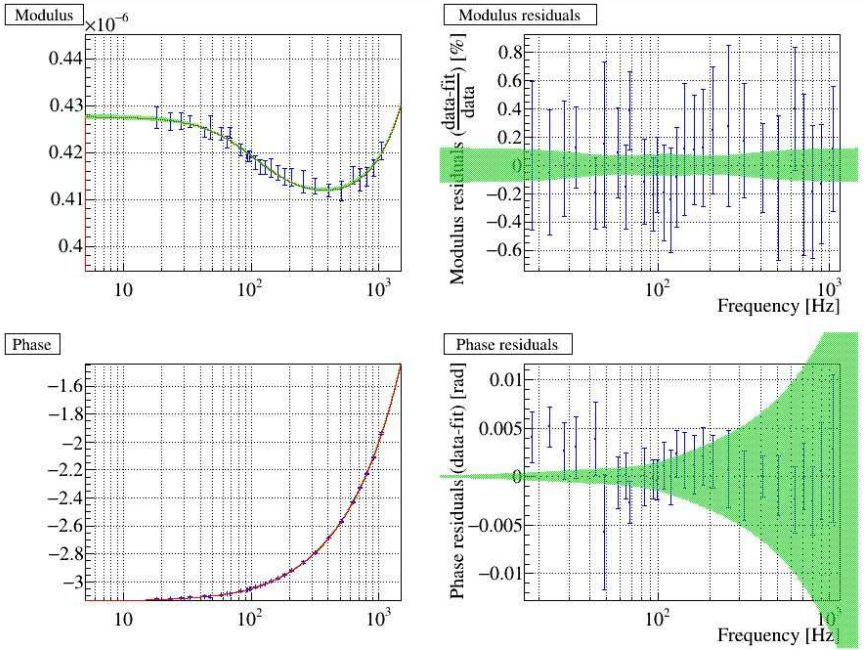

WE model

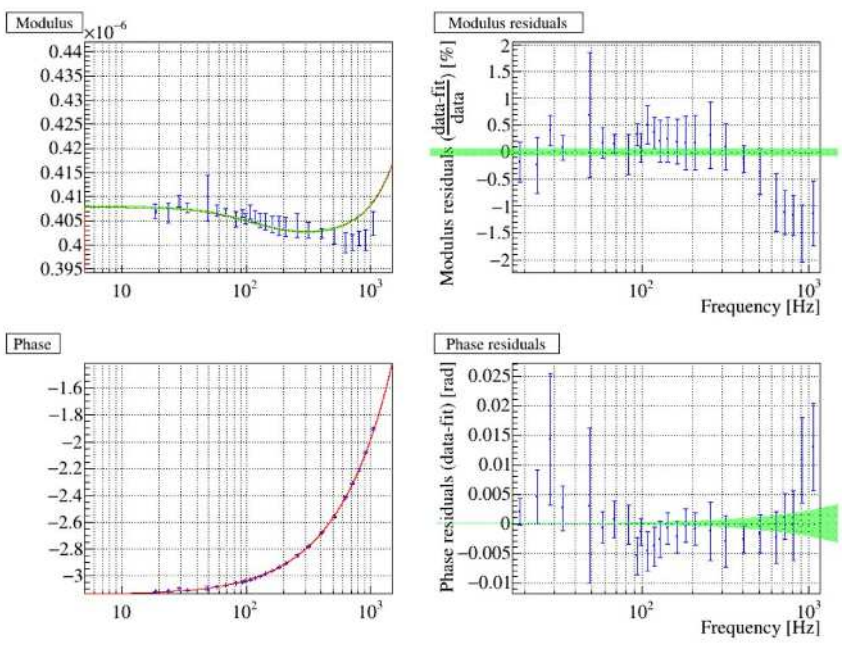

Summary

- I. Gravitational waves theory
- II. Gravitational waves detection
- III. Advanced Virgo interferometer calibration
- IV. Photon Calibrators calibration
- V. Electromagnetic actuators calibration

- VI. h(t) strain reconstruction and uncertainty computation
  - Reconstruction principle
  - Reconstruction monitoring
  - Bias and uncertainty computation methods
  - Results and stability during the run

Reconstruction principle

Hrec Algorithm:

GW signal is reconstructed by subtracting the contributions of the different control loop signal from the dark fringe signal → $h_{raw}(f)$

Unbiasing of the "raw" signal → $h_{unbias}(f)$

Subtracting the calibration lines → $h_{clean}(f)$

Subtracting noises → $h_{rec}(f)$

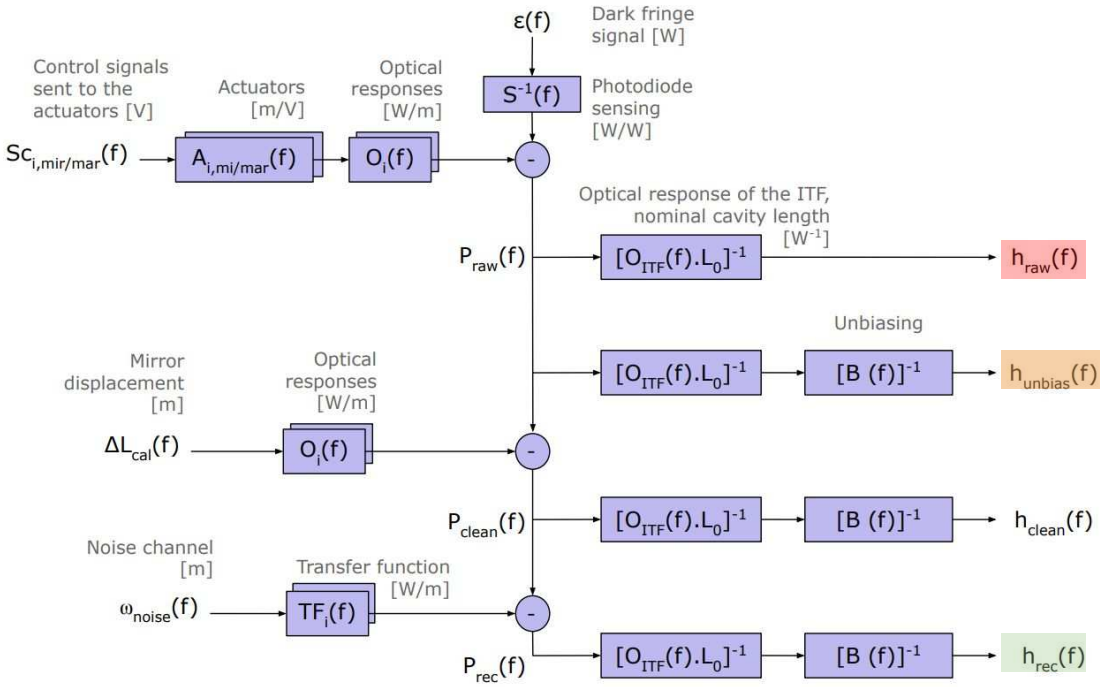

Reconstruction principle

Hrec Algorithm:

GW signal is reconstructed by subtracting the contributions of the different control loop signal from the dark fringe signal → $h_{raw}(f)$

Unbiasing of the "raw" signal → $h_{unbias}(f)$

Subtracting the calibration lines → $h_{clean}(f)$

Subtracting noises → $h_{rec}(f)$

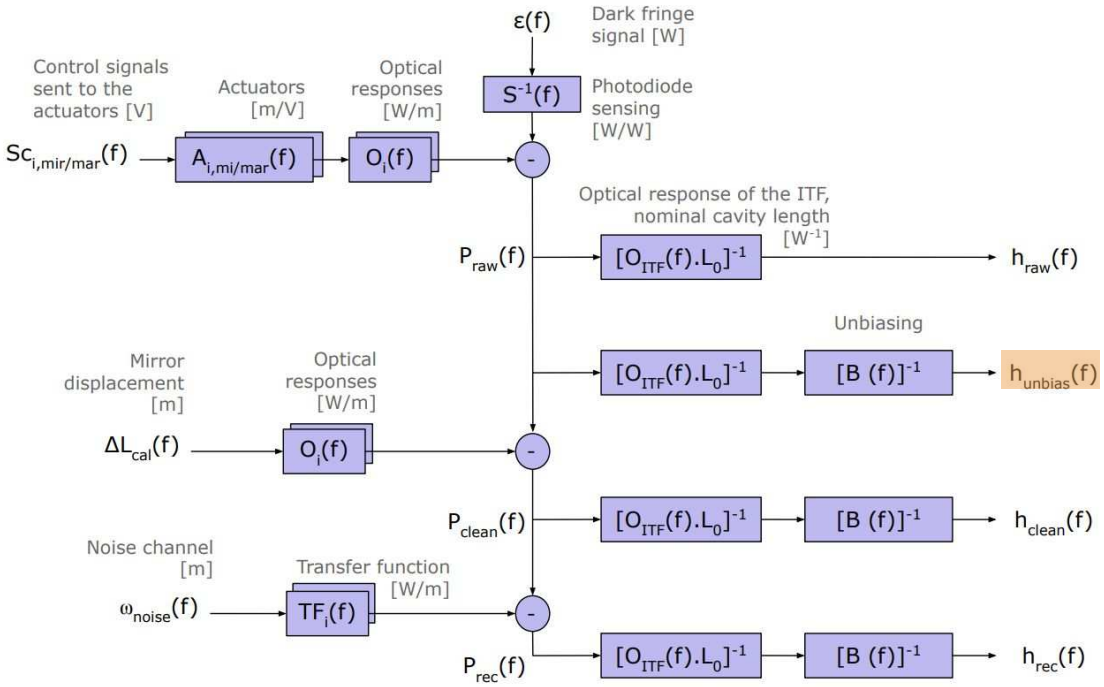

Reconstruction monitoring

Monitoring principle:

Calibration injections → Sinusoidal excitation of the mirror induced with the actuators (PCal or electromagnetic)

Comparing the reconstructed h(t) with Hrec ⟹ h_{rec}

To the h(t) reconstructed using the actuator calibration model directly ⟹ $\frac{h_{rec}}{h_{inj}}$

Allows to monitor the **reconstruction bias** → needs to be close to 1 (modulus) and close to 0 (phase)

Reconstruction monitoring

Monitoring principle:

Calibration injections → Sinusoidal excitation of the mirror induced with the actuators (PCal or electromagnetic)

Comparing the reconstructed h(t) with Hrec → $\frac{h_{rec}}{h_{inj}}$

To the h(t) reconstructed using the actuator calibration model directly →

Allows to monitor the **reconstruction bias** → needs to be close to 1 (modulus) and close to 0 (phase)

Two injection types:

Permanent lines

- 16 lines distributed between NE and WE
- Injected with the PCal and E.M. actuators
- Injected permanently to monitor h_{rec} / h_{inj}
- Injections frequency limited but allows to check on the bias shape and its evolution

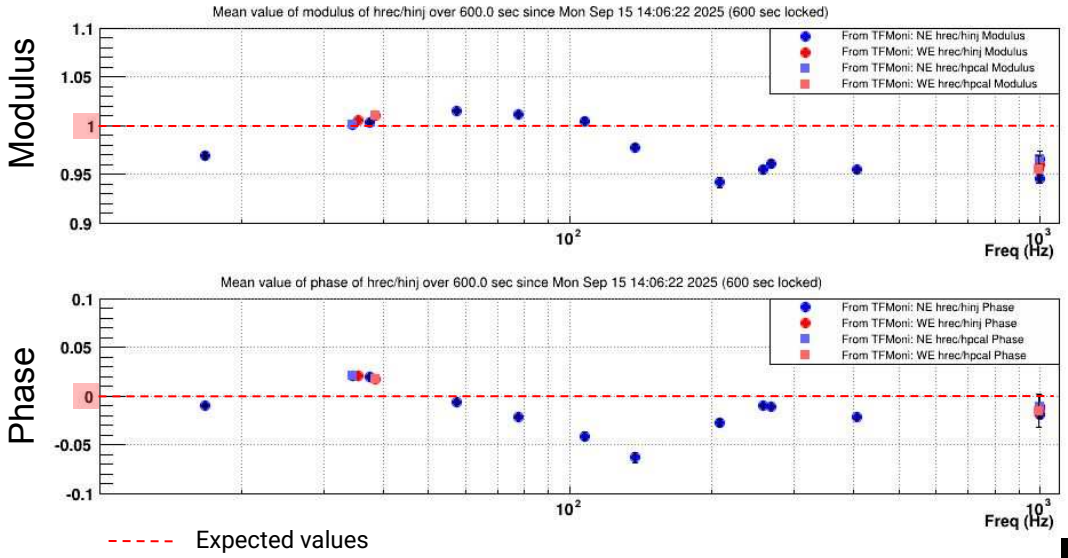

Reconstruction monitoring

Monitoring principle:

Calibration injections → Sinusoidal excitation of the mirror induced with the actuators (PCal or electromagnetic)

Comparing the reconstructed h(t) with Hrec ⟹ h_{rec}

To the h(t) reconstructed using the actuator calibration model directly ⟹ $\frac{h_{rec}}{h_{inj}}$

Allows to monitor the **reconstruction bias** → needs to be close to 1 (modulus) and close to 0 (phase)

Two injection types:

Weekly lines

- 32 lines injected between 18 Hz and 1238 Hz
- Injected for a few minutes every week with the NE and WE PCal and E.M. actuators
- Allows to monitor the reconstruction bias more precisely
- Allows to check the agreement between the 4 different actuators

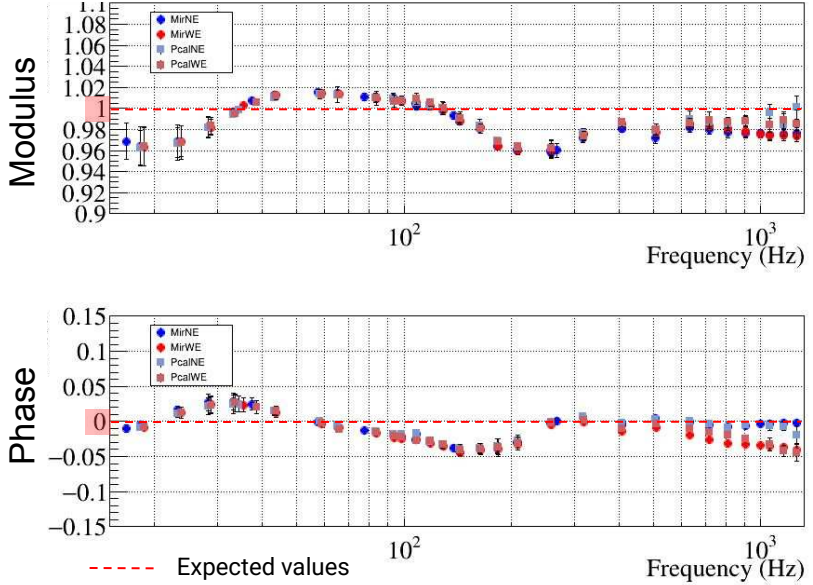

Bias and uncertainty computation method

GOAL: To develop a method for estimating the h(t) reconstruction bias and uncertainty on the full frequency band

Method:

1. Bias estimation to correct online the h(t) reconstruction→ **Weekly lines**

   - Precise bias estimation with the 32 lines
   - Monitor the stability for only a few minutes

Results and stability during the run

GOAL: To develop a method for estimating the h(t) reconstruction bias and uncertainty on the full frequency band

Weekly lines→ **BIAIS**

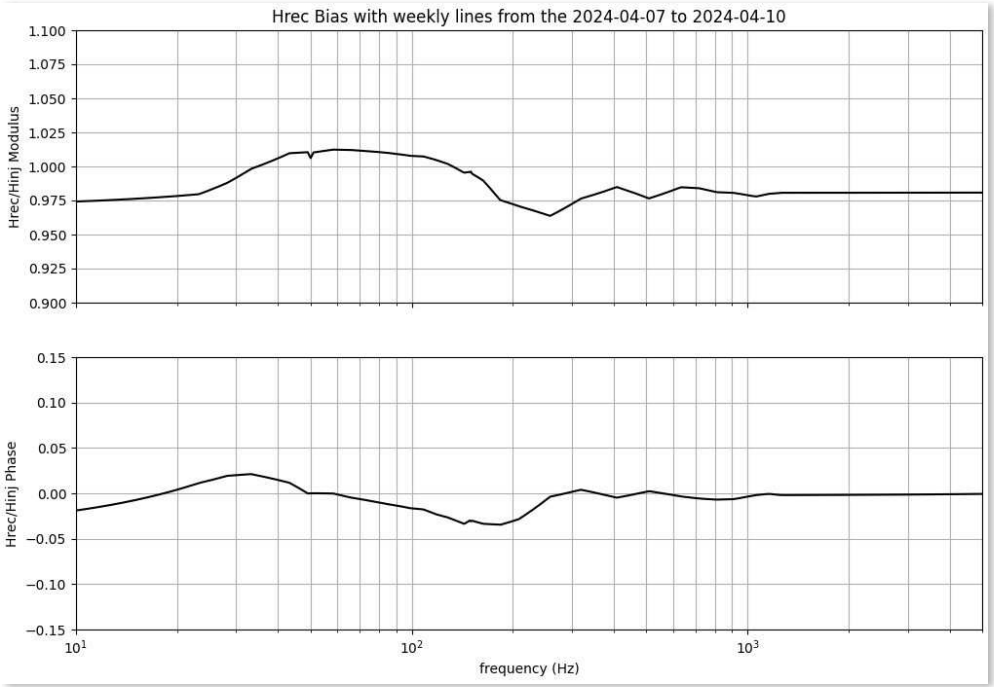

Results and stability during the run

Send to analysis pipelines

Residual bias negligible compared to the calibration uncertainties

Weekly lines

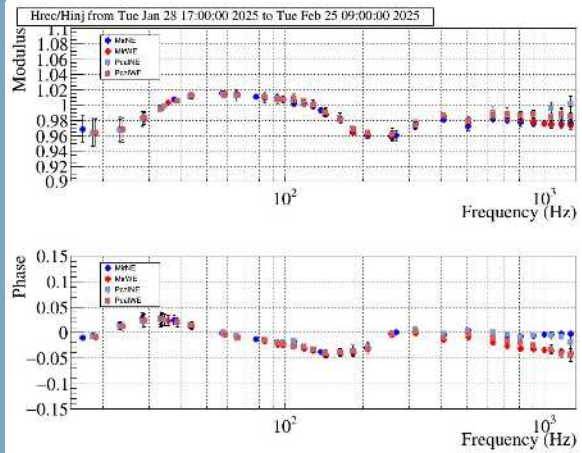

Hrec bias

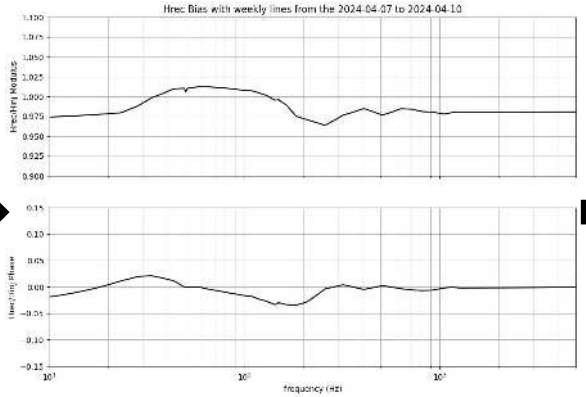

After unbiasing

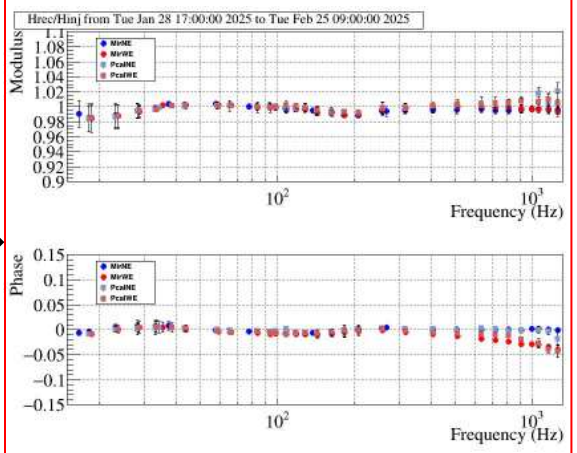

Bias and uncertainty computation method

GOAL: To develop a method for estimating the h(t) reconstruction bias and uncertainty on the full frequency band

Method:

1. Bias estimation to correct online the h(t) reconstruction→ **Weekly lines**

   - Precise bias estimation with the 32 lines
   - Monitor the stability for only a few minutes

2. Uncertainty estimation on the unbiased h(t) → **Permanent Lines**

   - Permanently injected lines
   - Monitor the stability on a longer timescale

Results and stability during the run

GOAL: To develop a method for estimating the h(t) reconstruction bias and uncertainty on the full frequency band

Permanent lines → **INCERTITUDE**

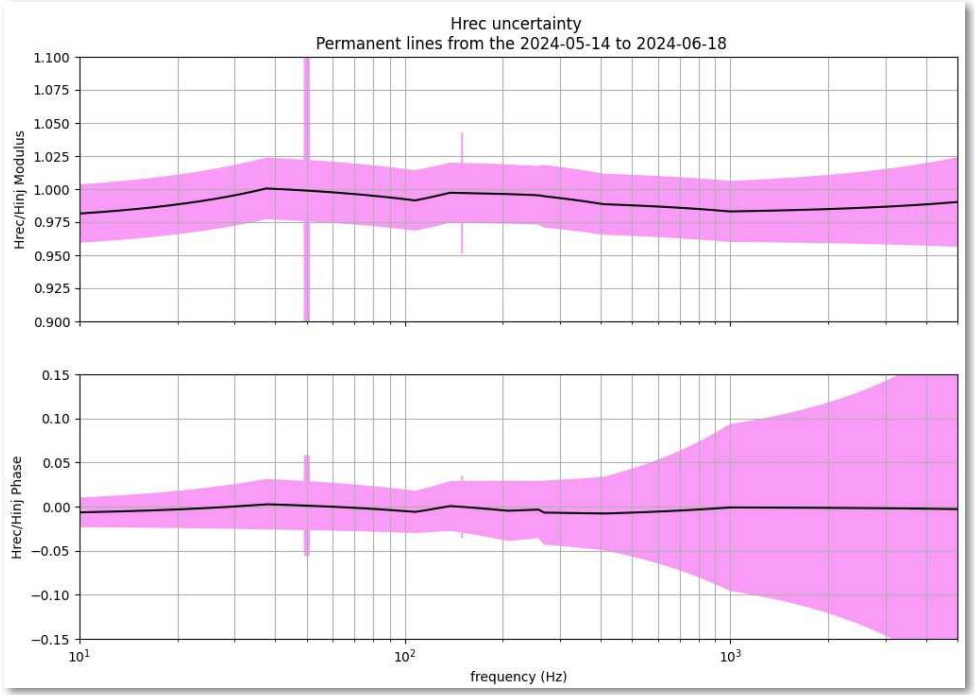

Results and stability during the run

Hrec residual bias is below **1%** and **10 mrad** on the full frequency band

The uncertainty is ± **2.5%** on the modulus

And for the phase, inferior to ± **70 mrad** up to 500 Hz and ± **10 µs** at higher frequency

The data distributed to analysis pipeline corresponds to:

- h(t) (unbiased)
- + frequency dependent uncertainties
- + residual bias

NOUVEAU pour O4

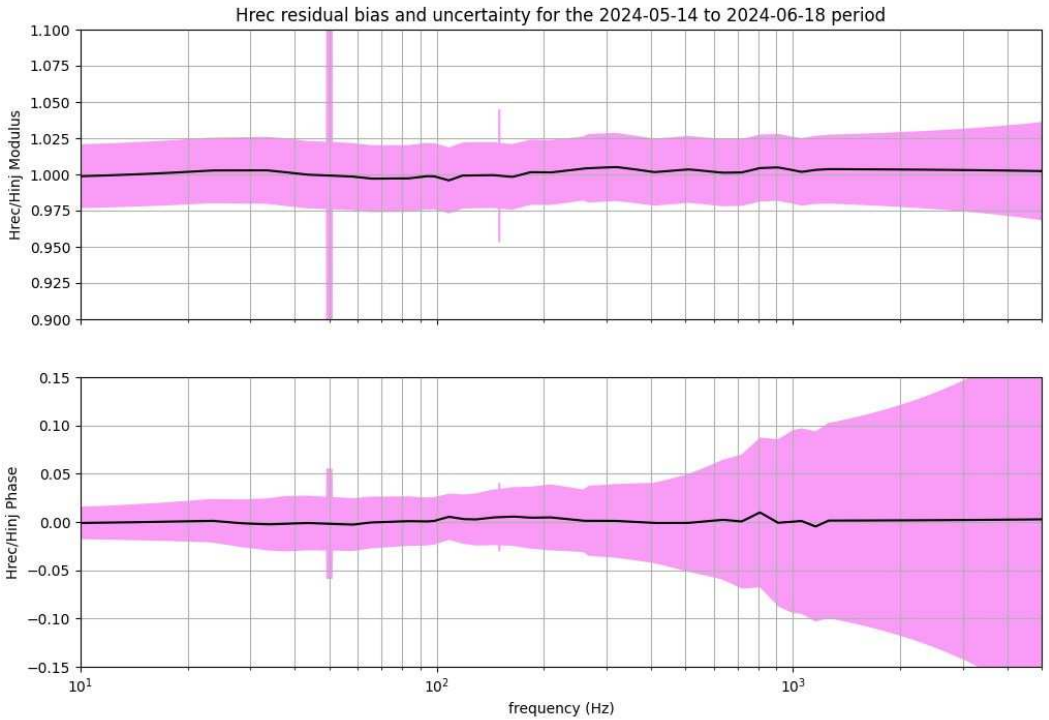

Conclusion

- **Success of the intercalibration scheme between the LVK observatories**
  Regular measurement during the entire run
- **PCal used as permanent reference for the Virgo calibration**
  Uncertainty of 0.48 % compared to 1.36% during O3
  Stability of 0.15 % during the run
- **H(t) reconstruction uncertainty improved**
  2.5% compared to 5% in O3
  Frequency dependent uncertainty
- **Calibration is crucial in order to get a precise h(t) strain signal**

Thank you !

Sources d’ondes gravitationnelles

Un onde gravitationnelle ne peut être produite que par des systèmes asymétriques.

- **Autres signaux attendus**

Explosions

CRÉDIT - SNR 0519-69.0 - Chandra X ray telescope - NASA

Ondes continues

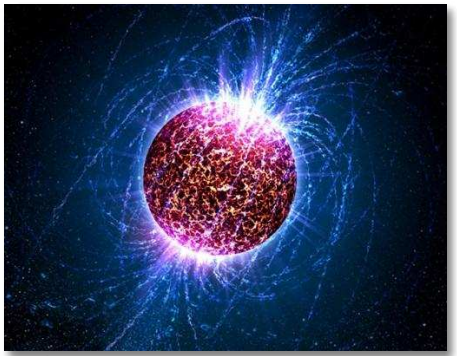

CRÉDIT - Casey Reed - Penn State University

Fond stochastique

CRÉDIT - Olena Shmahalo

h(t) émis par coalescences binaire compact

Signal d'OG émis par coalescences système binaire

$$h_+ \equiv 2\frac{\mathcal{M}}{d_L}(1+\cos^2 i)(\pi\mathcal{M}f)^{\frac{2}{3}}\cos(\Phi+\Psi)$$
$$h_\times \equiv 4\frac{\mathcal{M}}{d_L}\cos i(\pi\mathcal{M}f)^{\frac{2}{3}}\sin(\Phi+\Psi)$$

Masse Chirp :

$$\mathcal{M} = \frac{(m_1 m_2)^{\frac{3}{5}}}{(m_1+m_2)^{\frac{1}{5}}}$$

$$\Phi \equiv -2\left(\frac{t_0-t}{5\mathcal{M}}\right)^{\frac{5}{8}}$$

Radiation frequency :

$$f \equiv \frac{1}{\pi\mathcal{M}}\left[\frac{5}{256}\frac{\mathcal{M}}{t_0-t}\right]^{\frac{3}{8}}$$

Phase : Ψ

Temps de la fusion : t_0

Physique des ondes gravitationnelles

- **Mesures de la constante de Hubble**
  Mesure de la constante de Hubble avec GW170817
  → plus de détections multimessagers permettront de discriminer entre résultats des mesures “locales” (SHOES) et des mesures CMB (Planck)

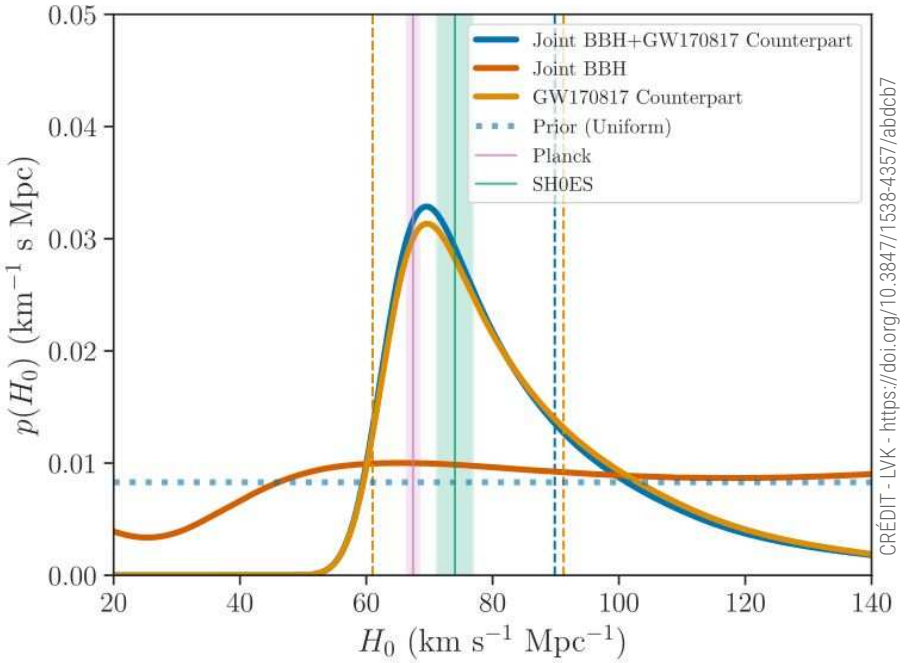

CRÉDIT - LVK - https://doi.org/10.3847/1538-4357/abdcb7

BNS – NSBH population

Taux volumétrique de coalescences en fonction de la masse de l'objet 1

Pic autour de 2 masses solaires → masse maximale des étoiles à neutrons postulée ~ 2.5 $M_\odot$
Déficit de masse en dessous de 5 $M_\odot$ → masse minimale des trous noirs postulée à ~ 5 $M_\odot$
Cependant, la courbe ne tombe pas complètement à zéros → quelques trous noir créés en dessous de 5 $M_\odot$ → Supernova peuvent créer des trous noires à ces masses → change notre compréhension des supernova

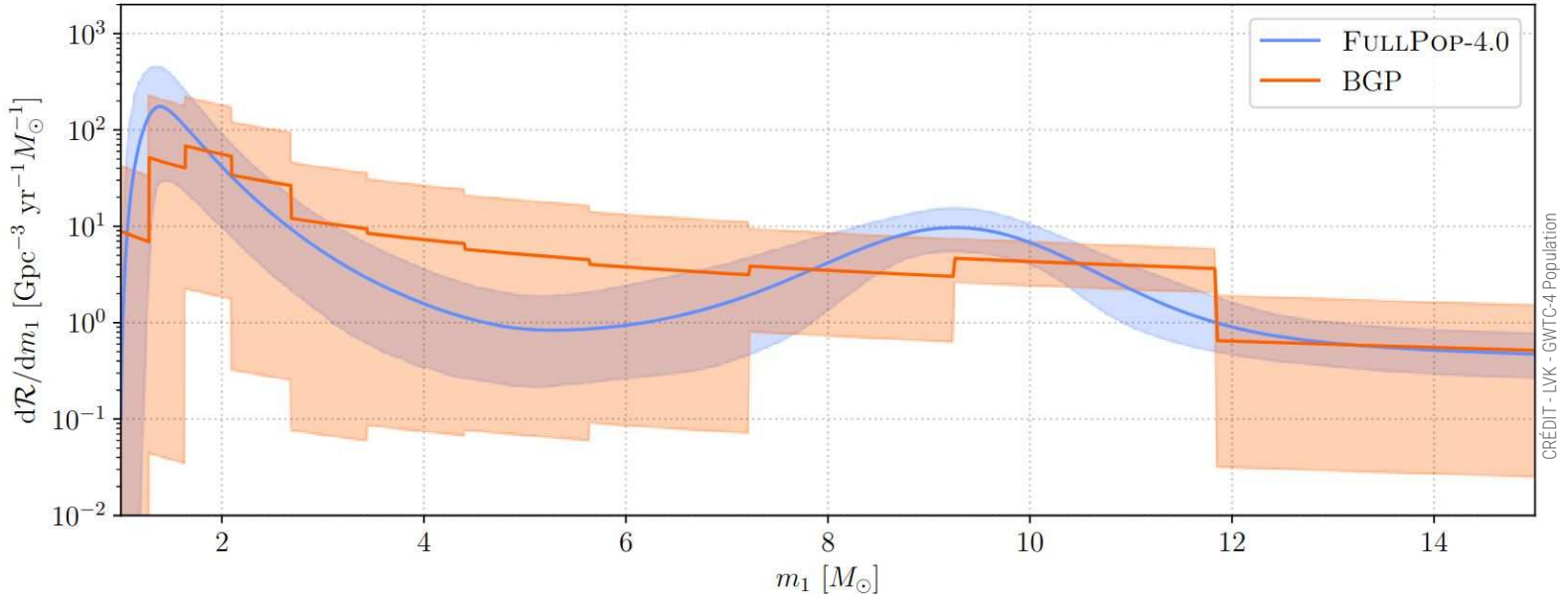

BBH population

Pic à 10 $M_\odot$ → Exigence de transfert de masse stable entre deux étoiles binaires → créer des trous noirs autour de 10 $M_\odot$

Pic à 35 $M_\odot$ → Beaucoup d'hypothèses différentes

Déficit de masse après 45 $M_\odot$ → instabilité de paire des supernova → instabilité du coeur des supernova quand on dépasse une certaine masse → pas de formation de trous noir → mystère pourquoi on voit tout de même des trous noirs dans cette région

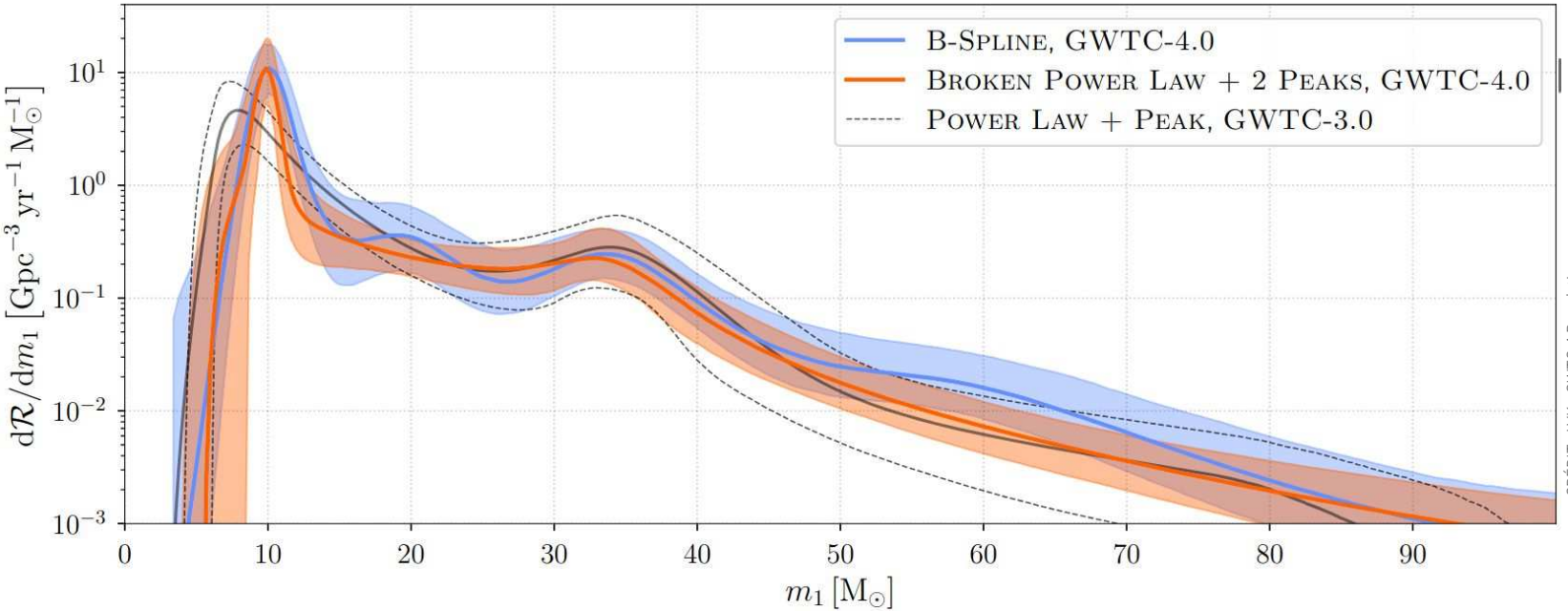

CRÉDIT - LVK - GWTC-4 Population

GW230814 - Test RG

SNR de 42.4

BBH
33.7 et 28.2

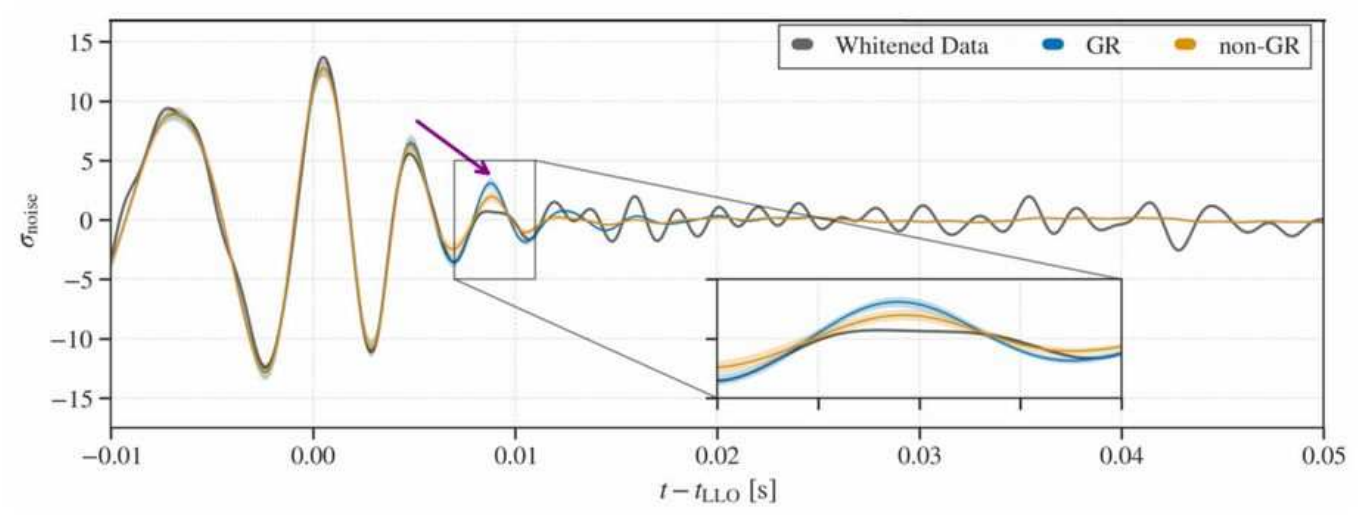

GW250114 - Test RG

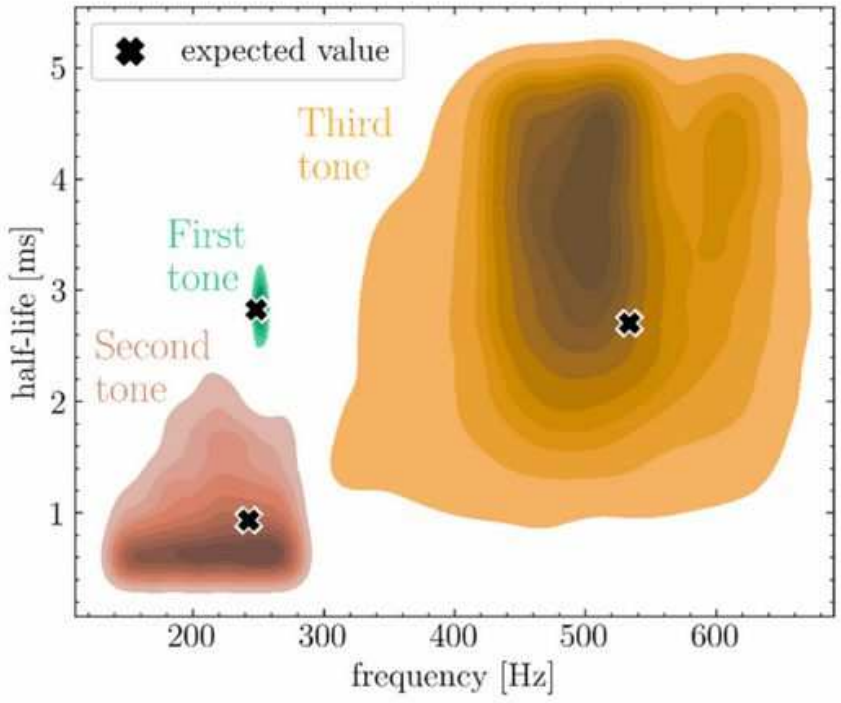

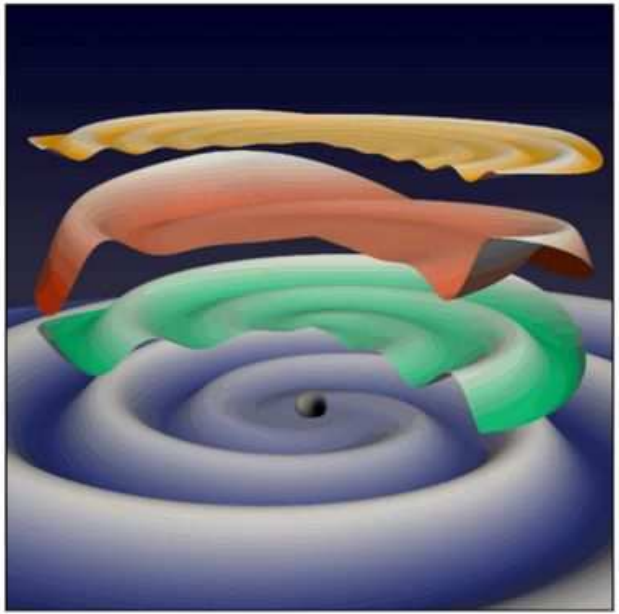

Forme d'onde et approximations GR

- NR: "exact"
- PN: $v^2 \sim (m_1 + m_2)/r \ll 1$
- PM: $(m_1 + m_2)/r \ll 1$
- GSF: $m_2/m_1 \ll 1$
- ringdown: $|g_{\alpha\beta} - g^{\mathrm{Kerr}}_{\alpha\beta}| \ll 1$

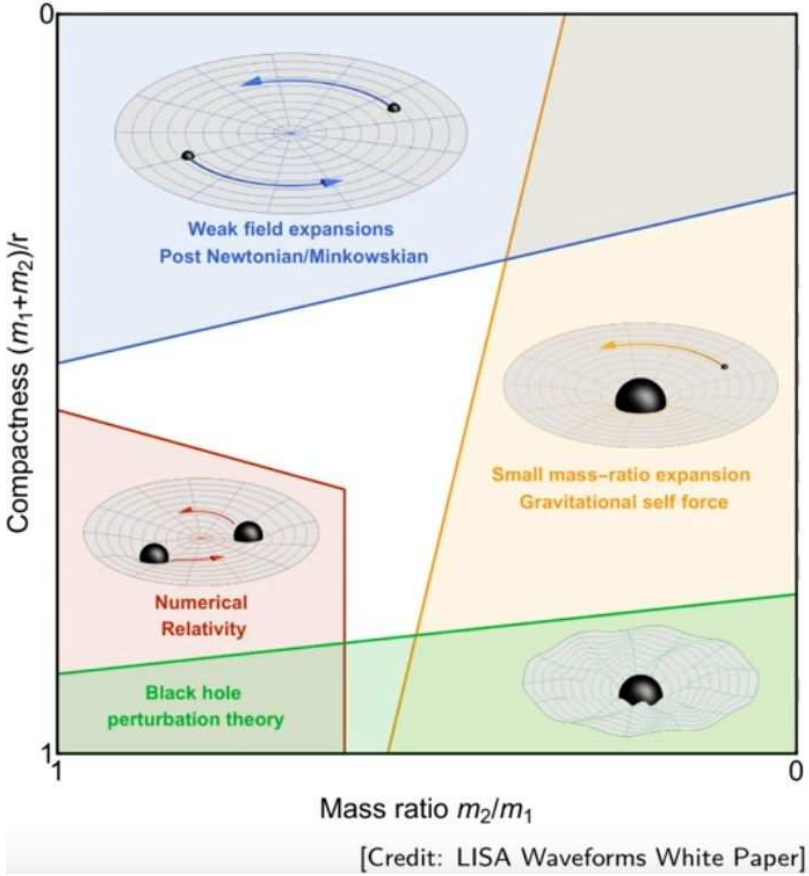

[Credit: LISA Waveforms White Paper]

Forme d'onde et approximations GR

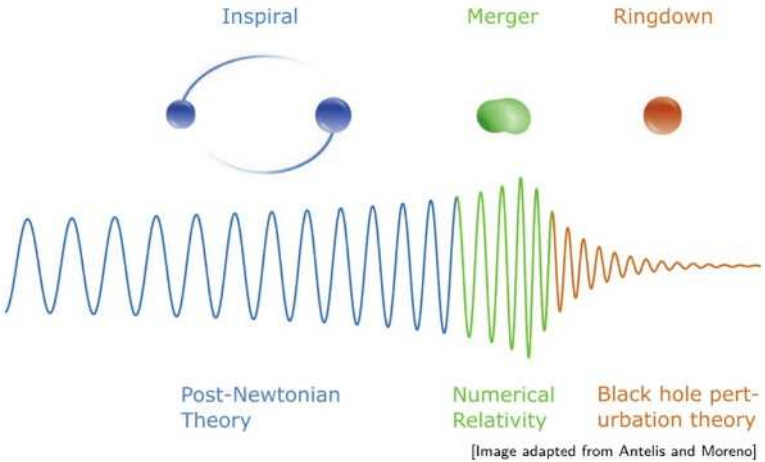

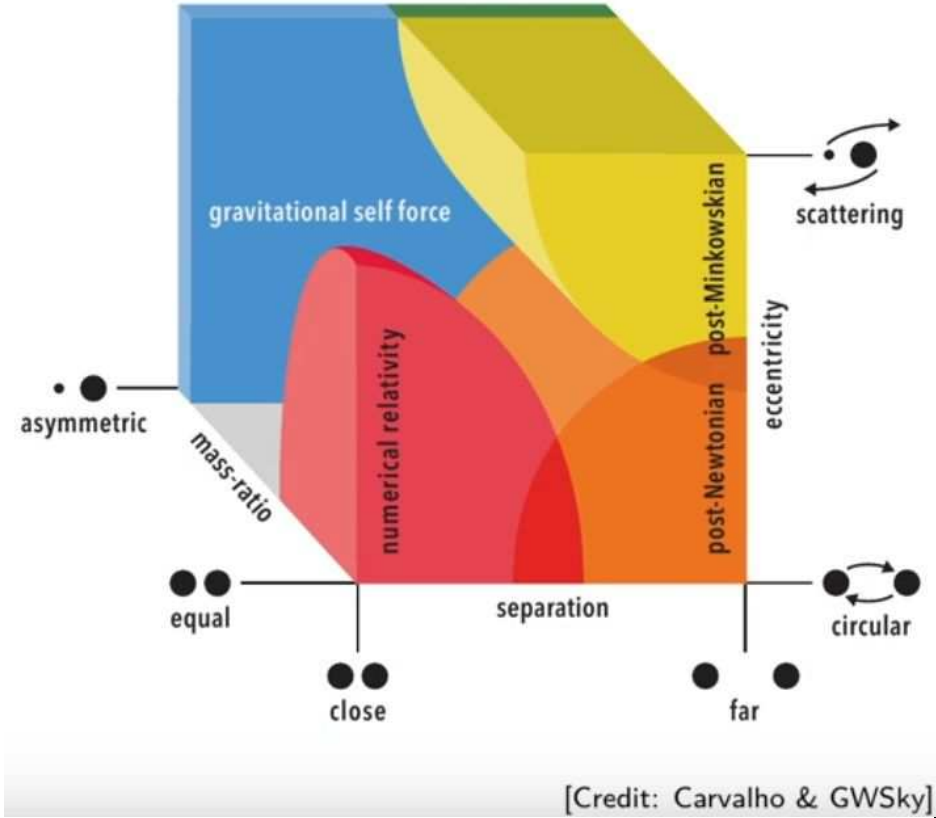

Impact de la calibration

Étude des trous noirs et des étoiles à neutrons

- Première détection en 2015 par les détecteurs LIGO (GW150914) → coalescence de 2 trous noirs (BBH)

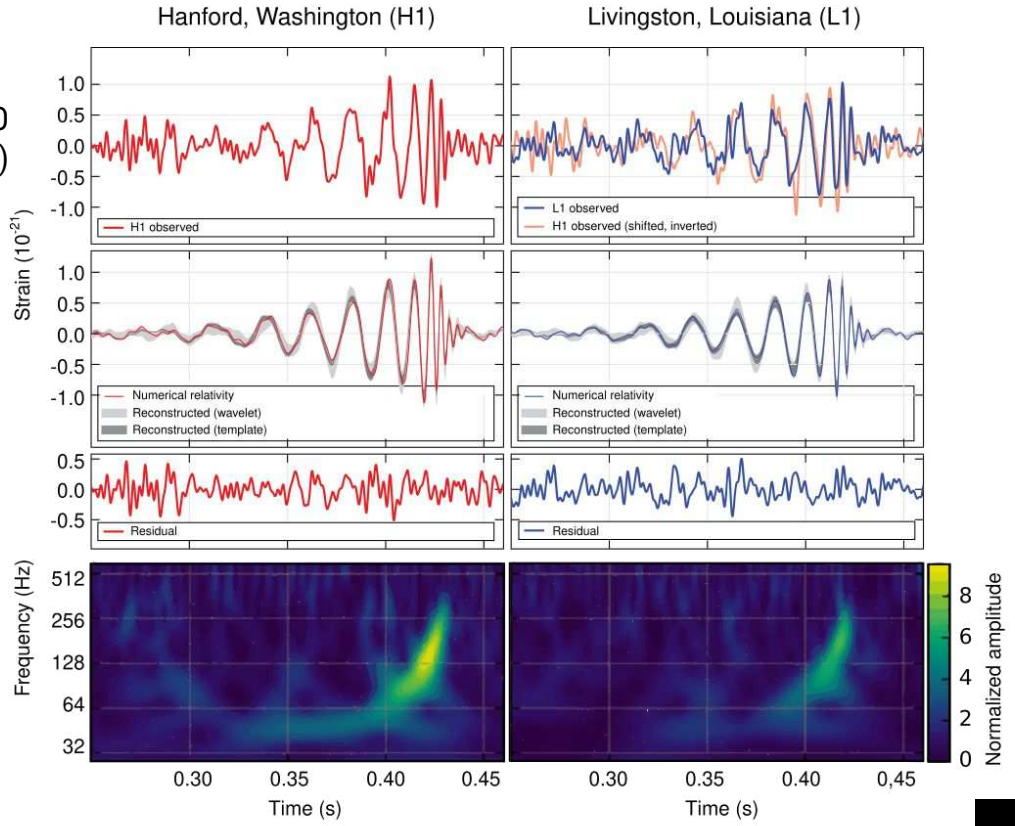

Impact de la calibration

Étude des trous noirs et des étoiles à neutrons

- Première détection en 2015 par les détecteurs LIGO (GW150914) → coalescence de 2 trous noirs (BBH)
- Depuis, plusieurs centaines d'autres coalescences détectées (BBH, BNS, NSBH)
- Permet de faire des études de populations → information sur les processus à l'origine de la création des trous noirs et des étoiles à neutrons

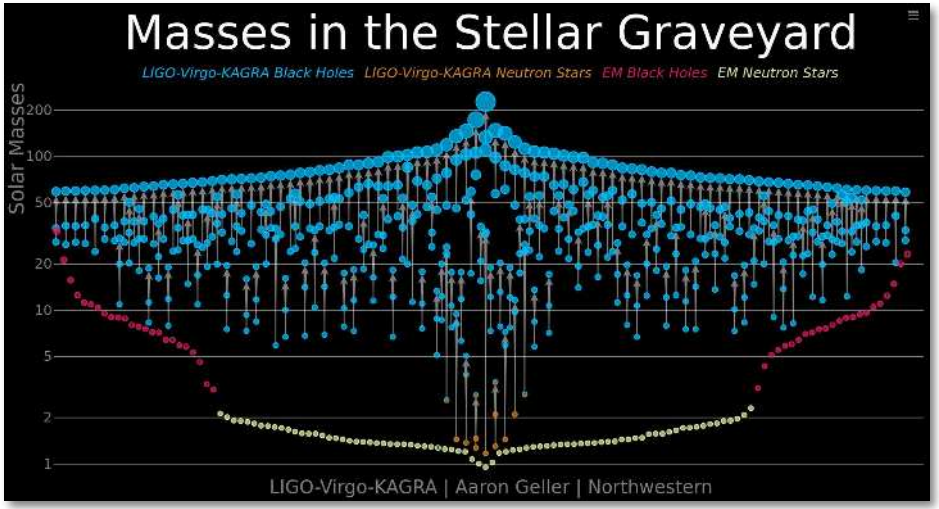

Impact de la calibration

Astrophysique Multi Messagers (MM)

- Première détection multimessager OG/EM en 2017 (GW170817) → BNS avec contrepartie électromagnétique

- OG détectées par LIGO et Virgo, 1.7 s plus tard détection d'un sursaut gamma (GRB) par INTEGRAL et Fermi.

- Importance de la détection en réseaux → localisation précise

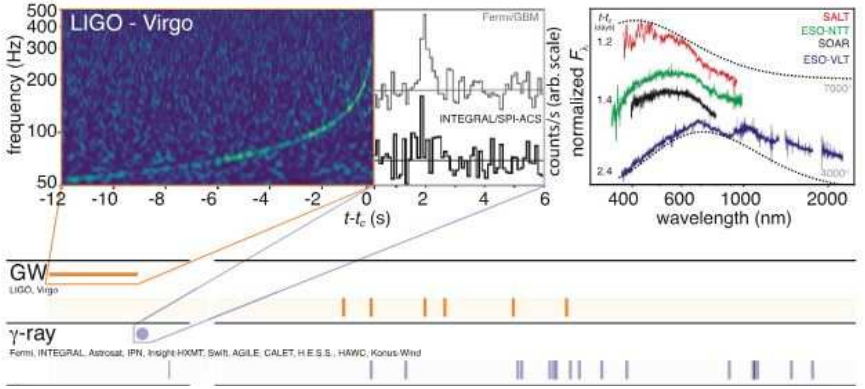

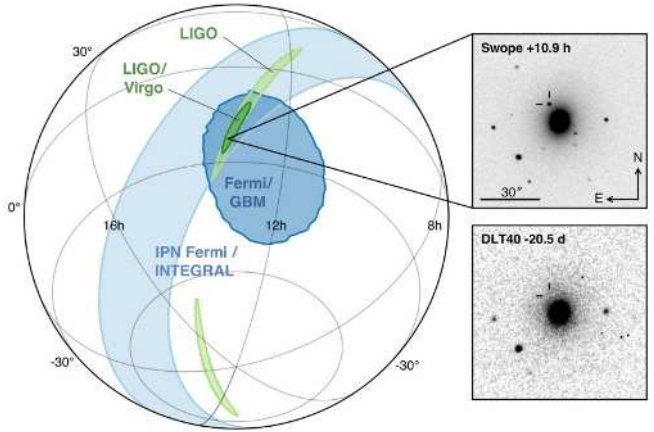

Impact de la calibration

Astrophysique Multi Messagers (MM)

- Première détection multimessager OG/EM en 2017 (GW170817) → BNS avec contrepartie électromagnétique

- OG détectées par LIGO et Virgo, 1.7 s plus tard détection d'un sursaut gamma (GRB) par INTEGRAL et Fermi.

- Importance de la détection en réseaux → localisation précise

- Puis détections à travers tout le spectre E.M. jusqu'à plusieurs jours plus tard.

Détections MM permettent :

- Étude de l'origine des GRB
- Étude des kilonovas
- Mesure de la vitesses des OG
- Mesure de la constante de Hubble

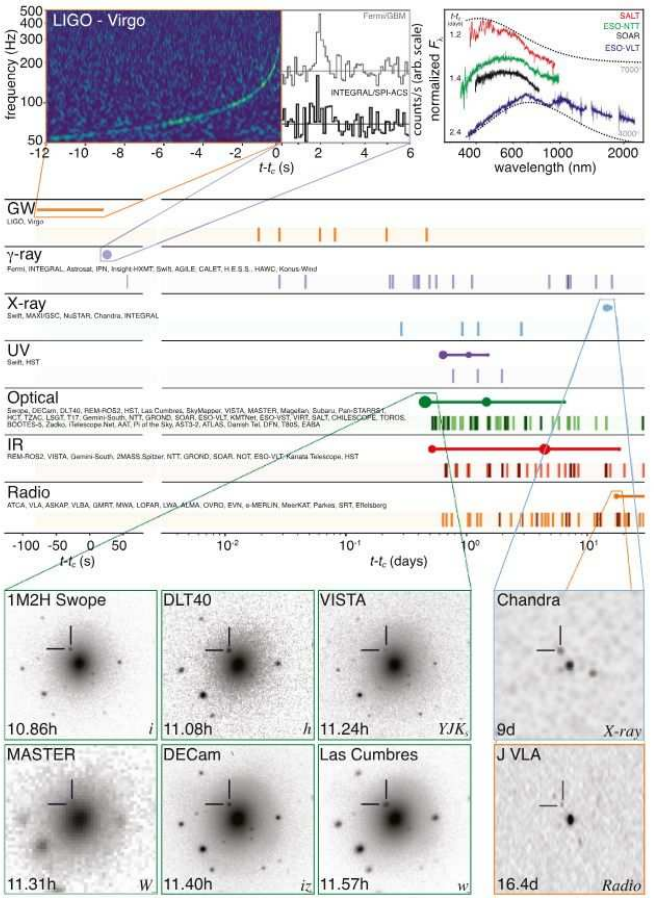

Physique des ondes gravitationnelles

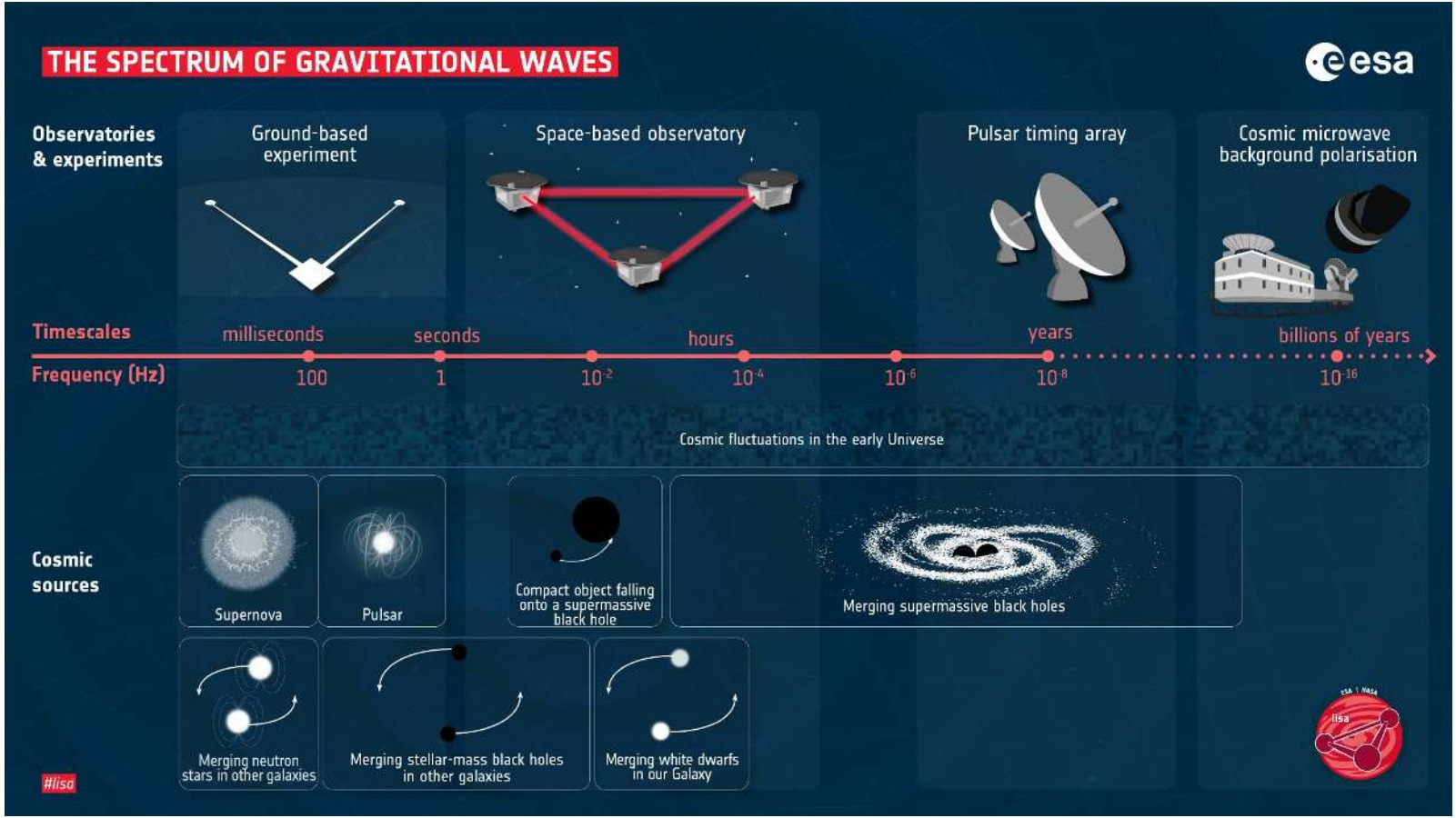

Méthode de détection avec Advanced Virgo

Interféromètre terrestre avec des bras de 3 km :

- Source Laser, proche-IR (1064 nm)
- Lame séparatrice (BS)
- Miroirs de bout de bras (NE, WE)

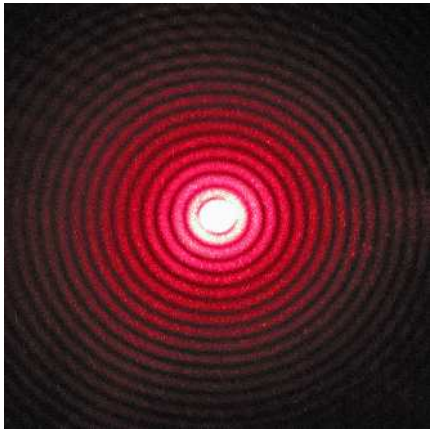

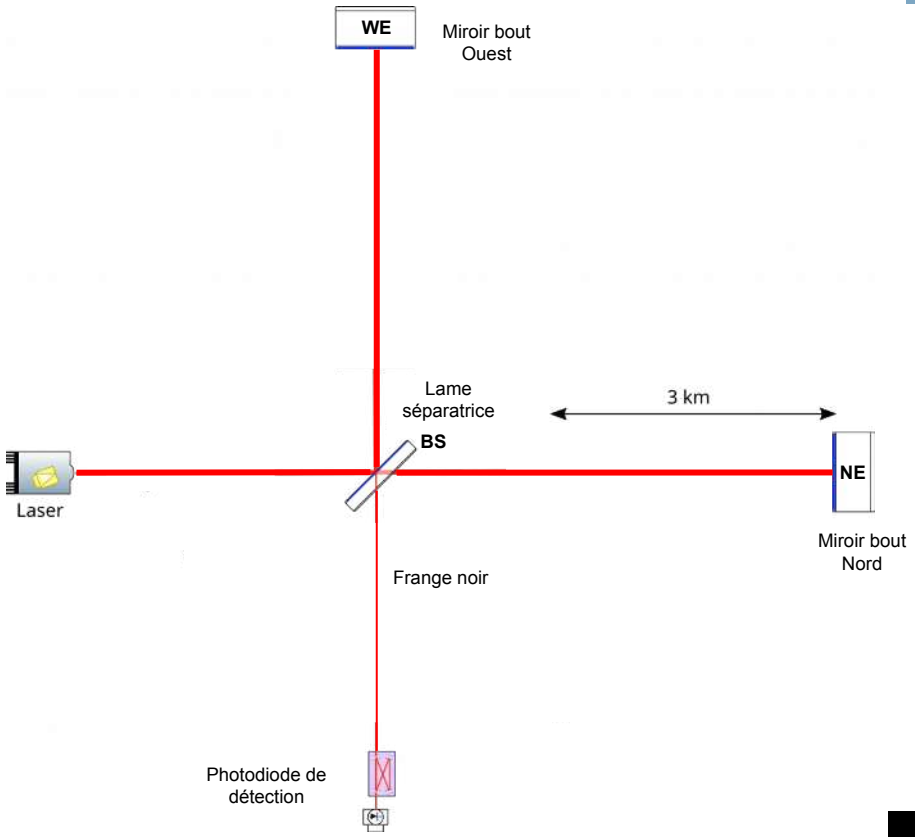

Cavité Fabry-Perot résonante

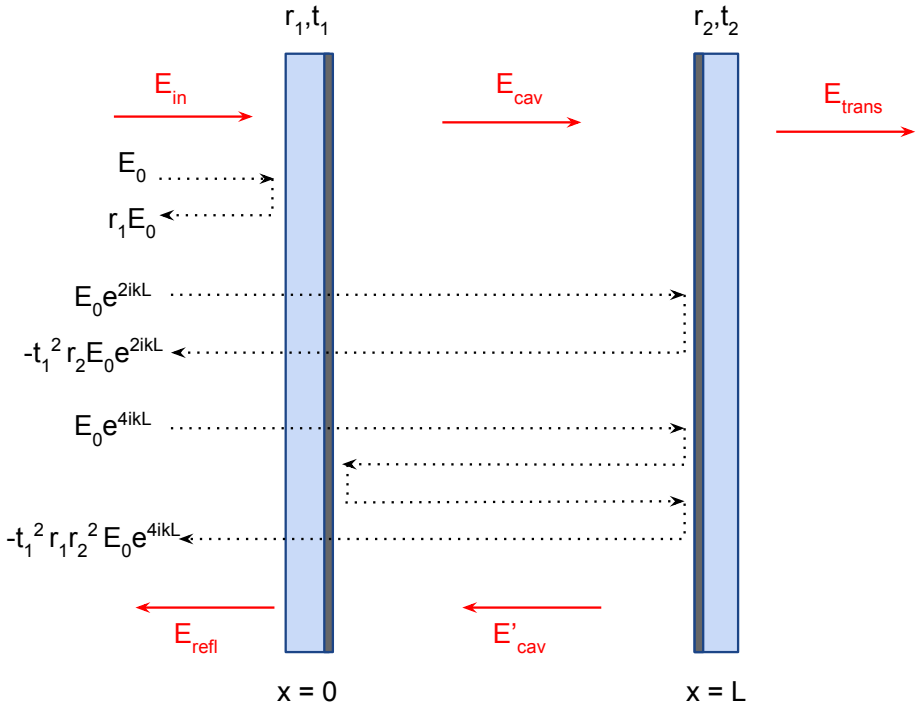

Super attenuator system

- Pendulum : longitudinal displacement
- Blade springs : vertical displacement
- Torsion threads : rotation

Resonant frequency < 1Hz

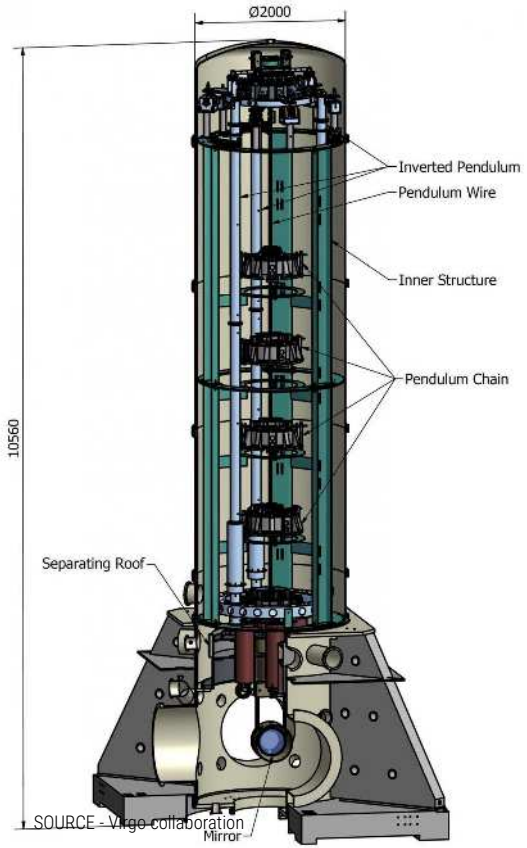

Contrôle de l'interféromètre

Mouvement des miroir dus à différents "bruits" (sismiques, quantiques, etc)

Nécessaire de contrôler très précisément la position des miroirs et la longueurs des cavités résonantes pour détecter les OG

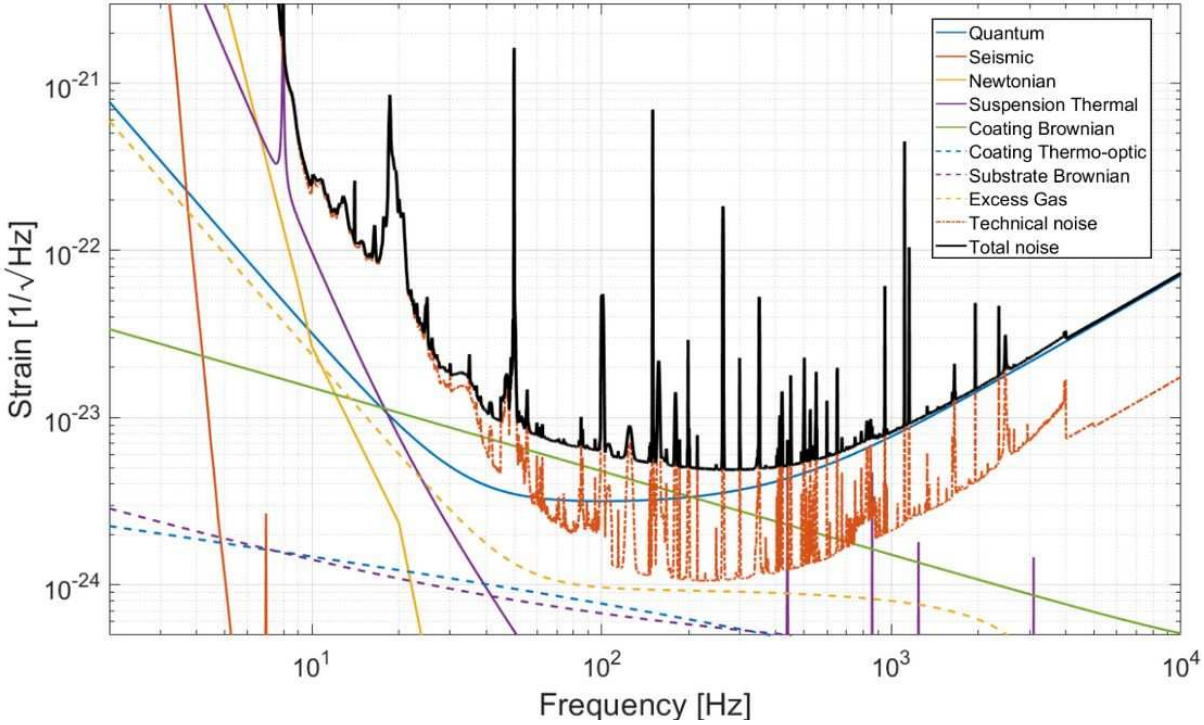

Réponse d'antenne à un signal d'OG

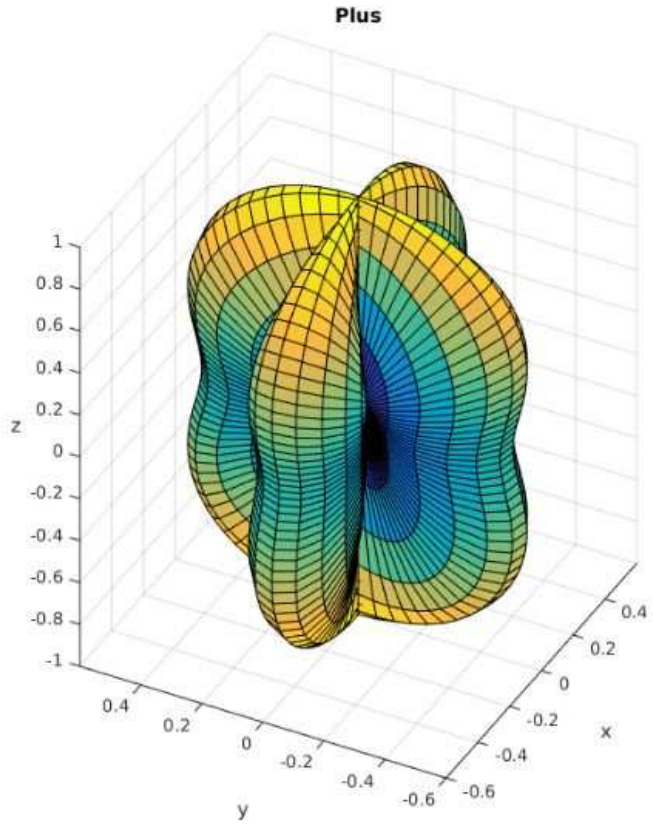

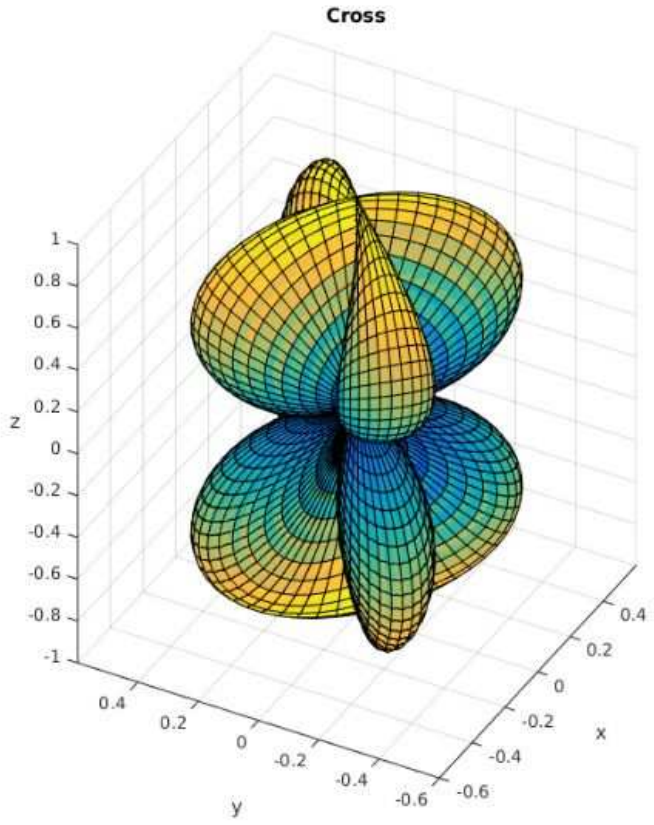

Système de contrôle de Virgo

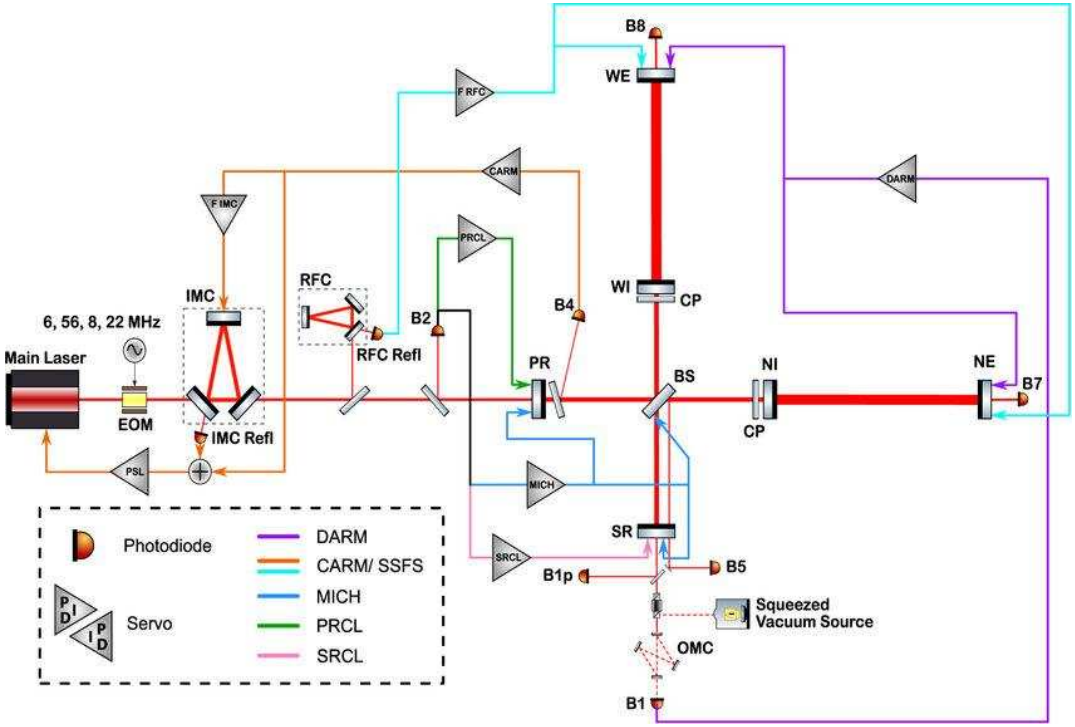

Chaîne d'acquisition des actionneurs E.M.

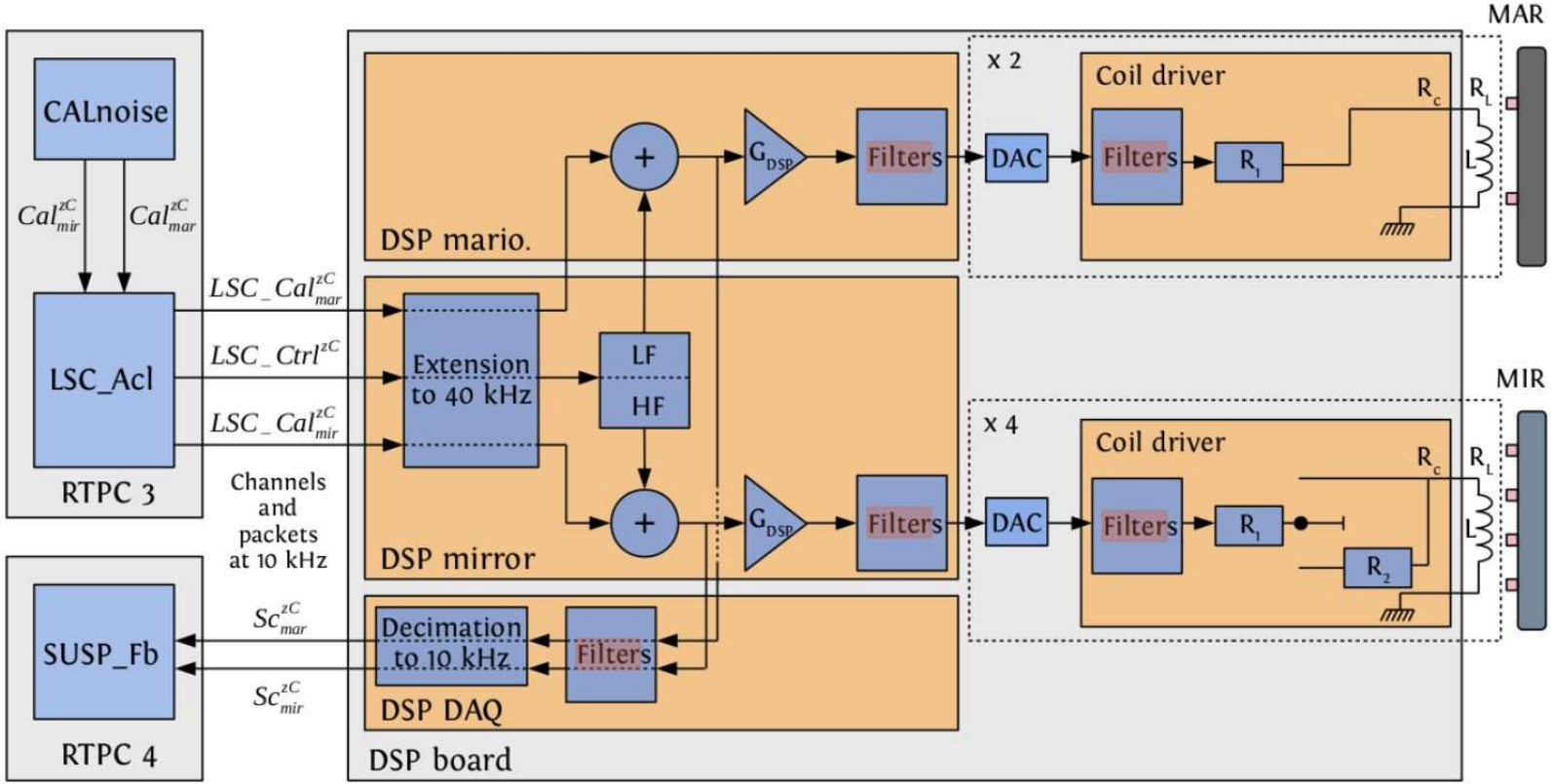

Sensibilité O4 des détecteurs LIGO et Virgo

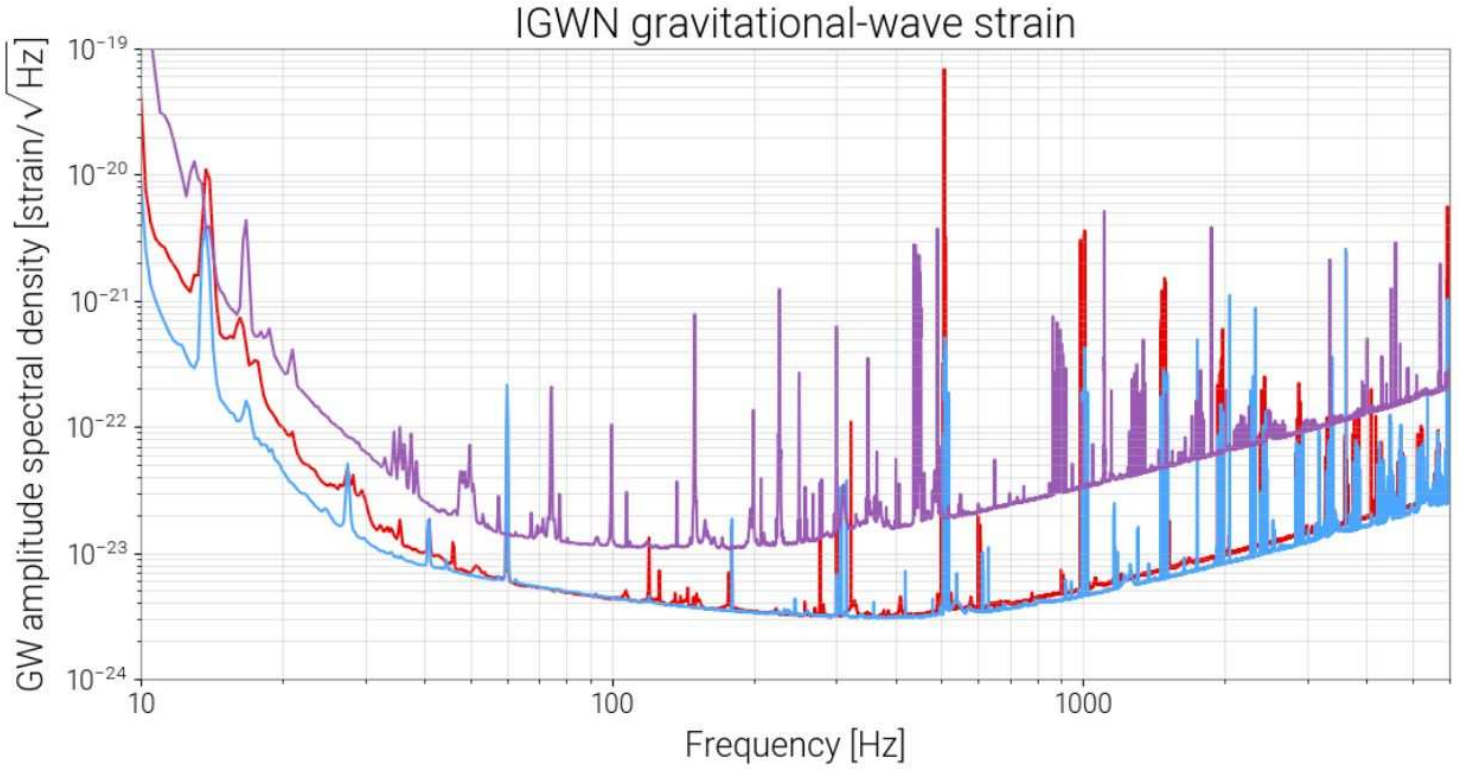

H → ~150 Mpc
L→ ~150 Mpc
V→ ~55 Mpc

Calibration lines injections

Lines injections :

- Sinusoidal signals sent to move the mirrors using the different actuators (Pcal and Electromagnetic)
- Example of the 420Hz lines injected with E.M. actuators on NE, WE and BS mirrors
- Lines injected seen in the Fourier transform of the DARM signal

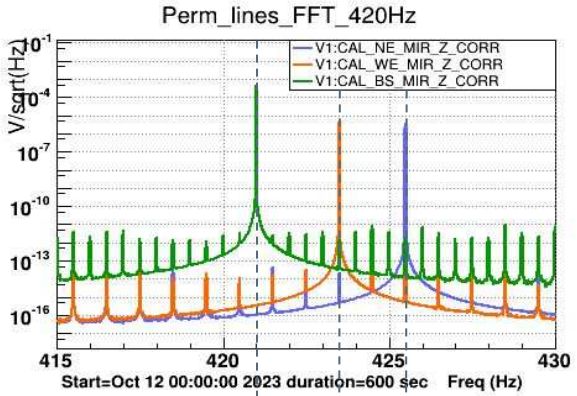

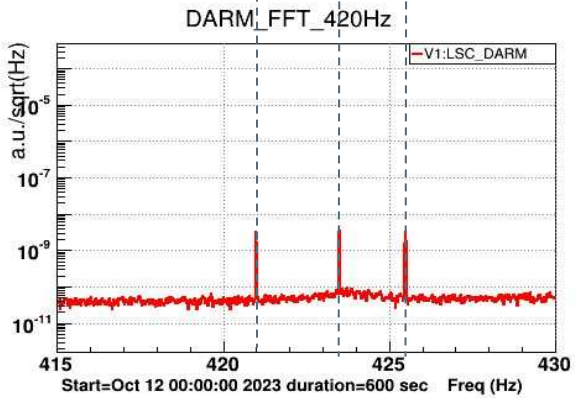

PCal optical layout

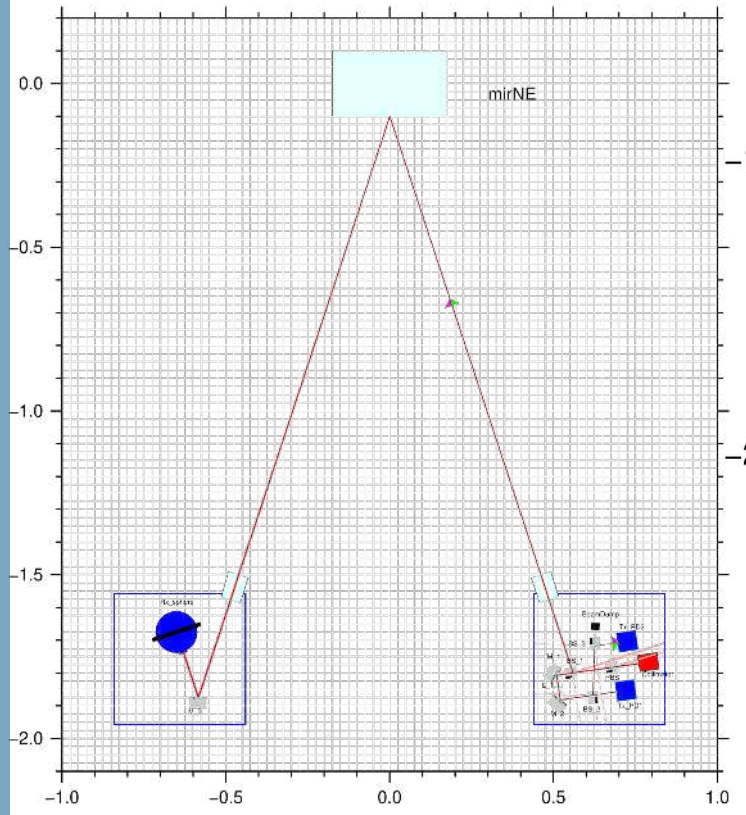

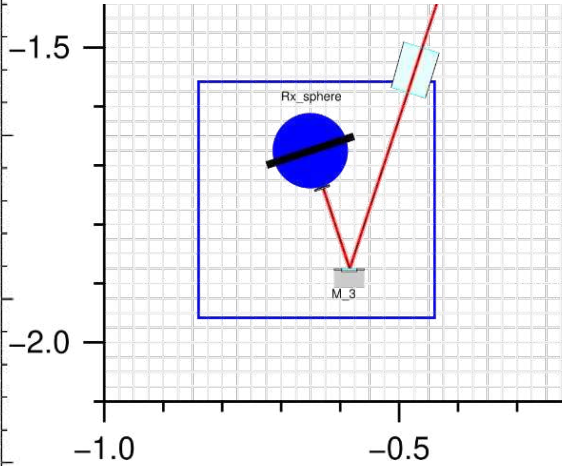

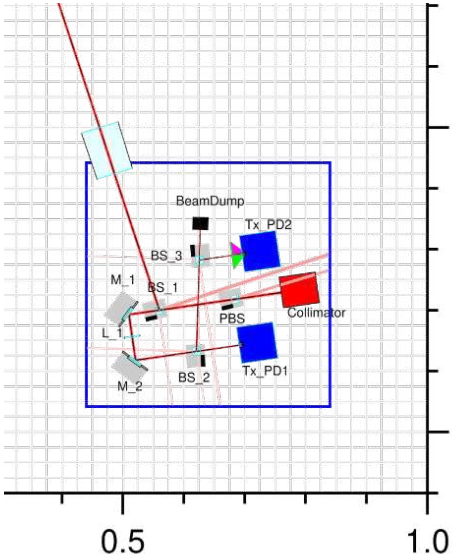

Bruit des capteurs de puissances sans laser

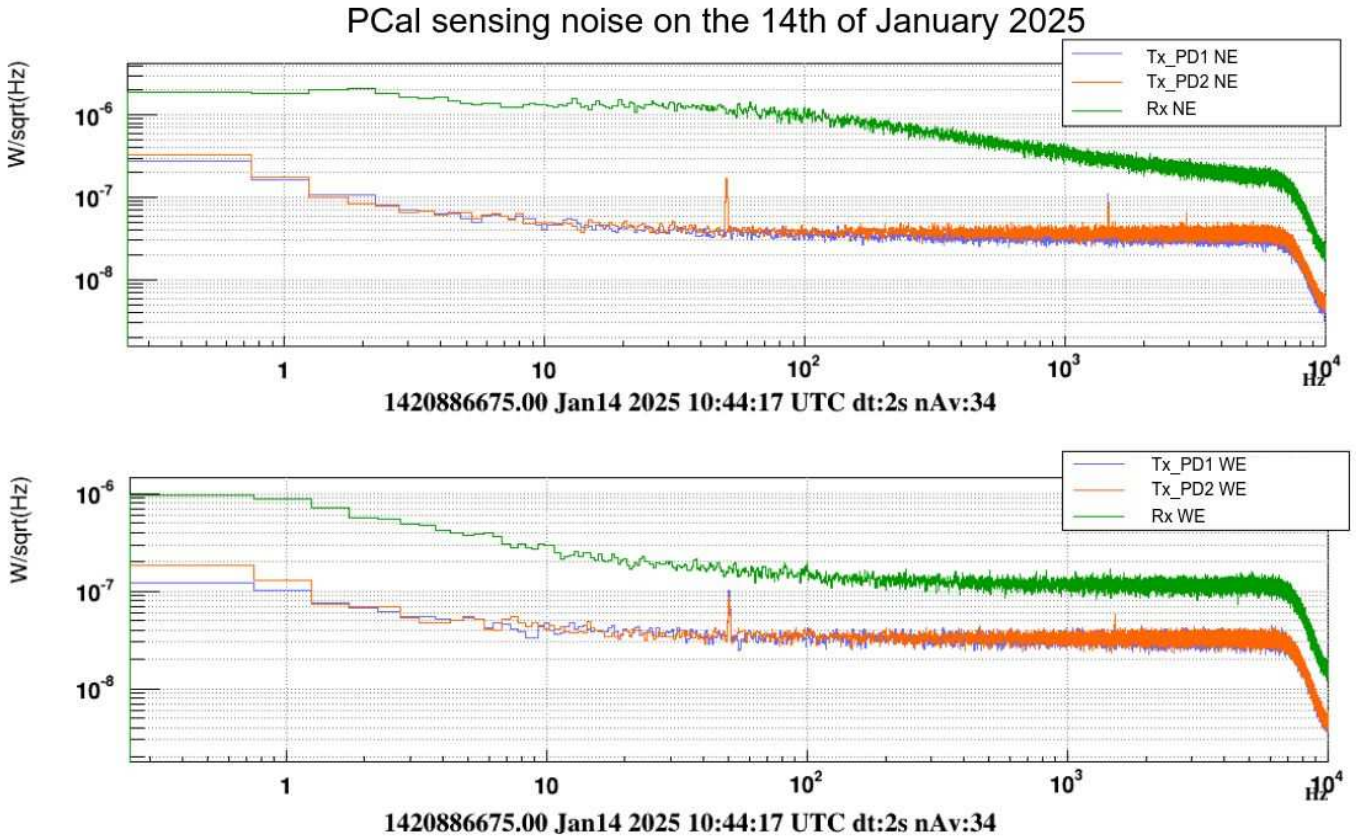

Bruit capteurs de puissances sans boucle

NE

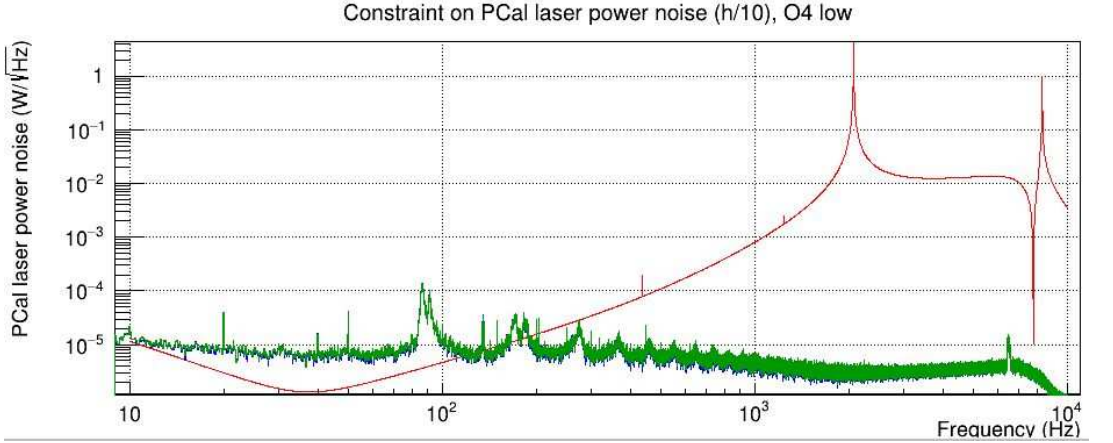

WE

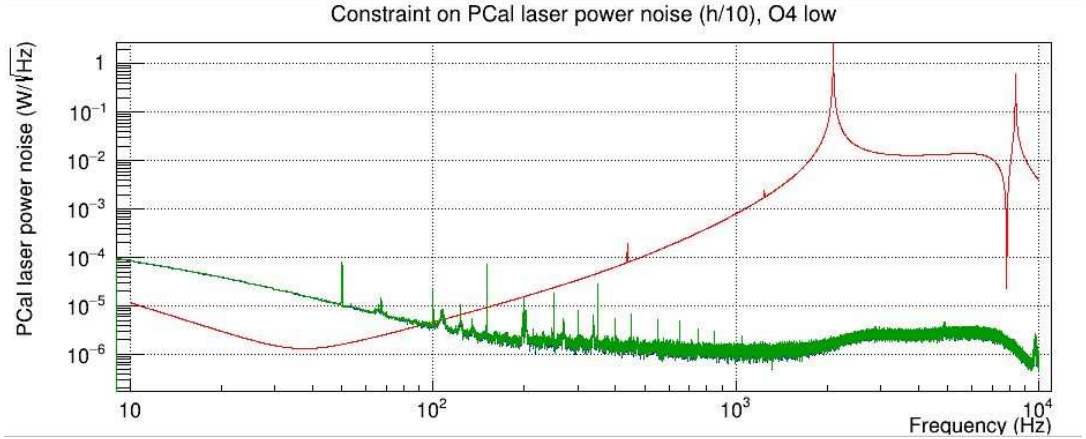

Boucle de contrôle laser PCal

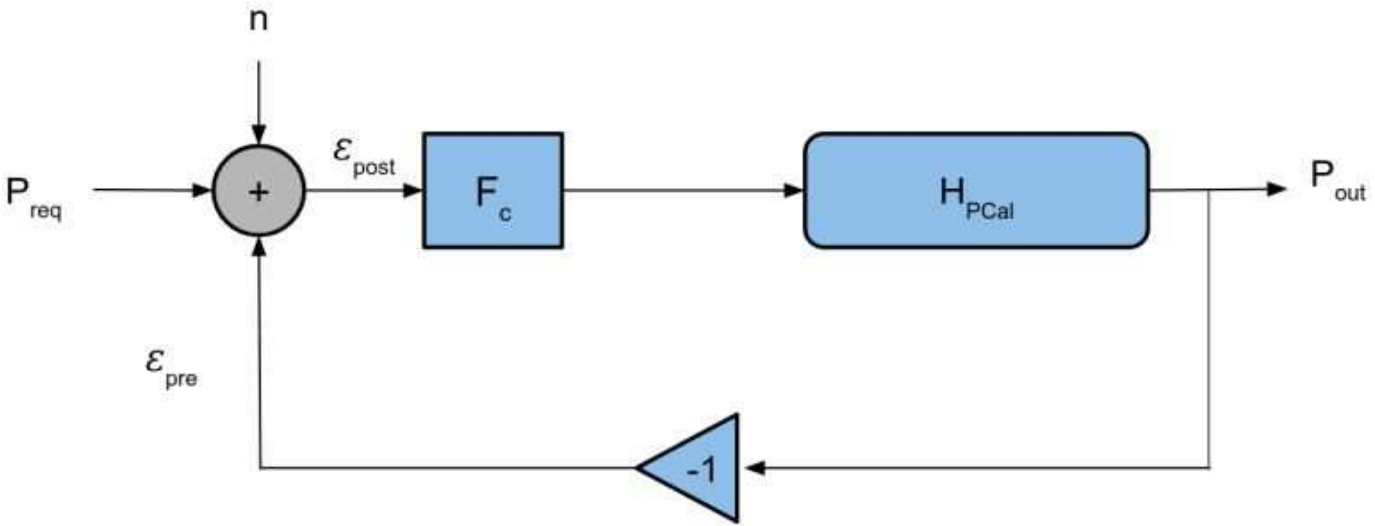

Figure 3.14: Representation of the PCal laser control loop.

PCal laser power noise constraint for O4

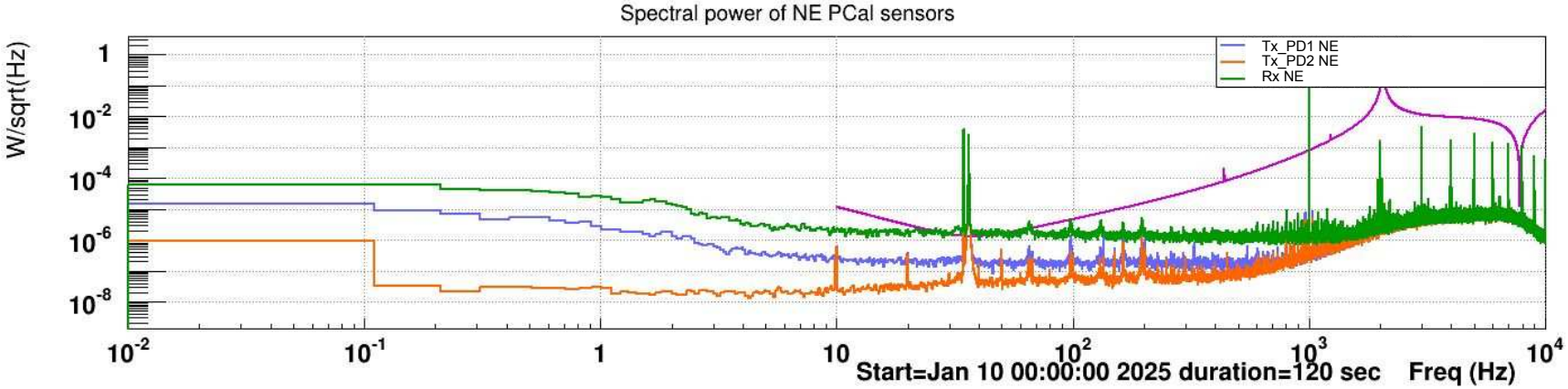

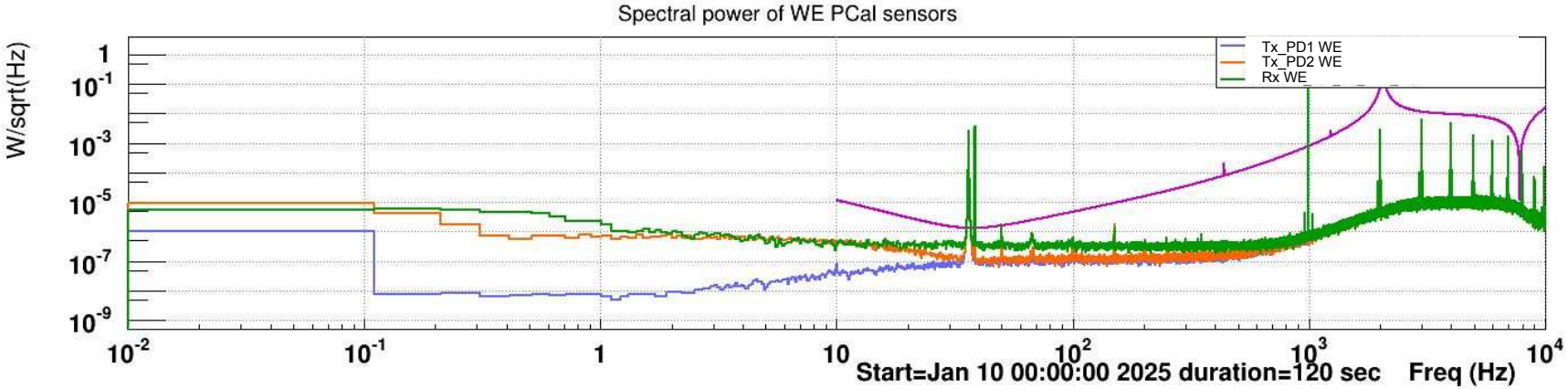

Investigation ghost beam setup intercalibration

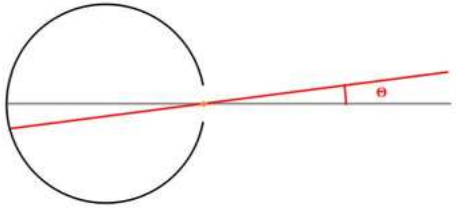

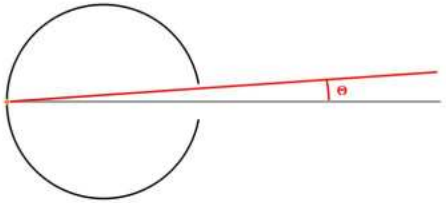

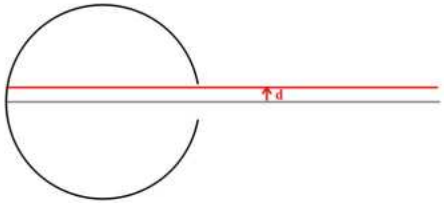

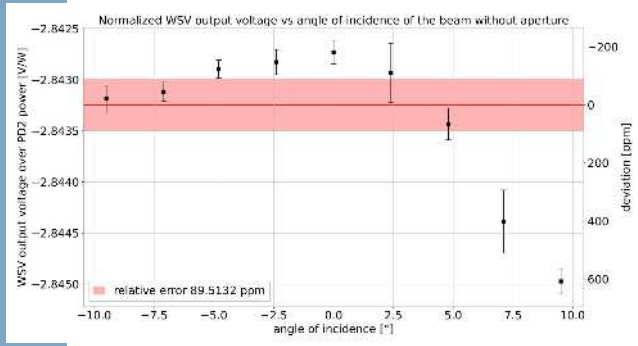

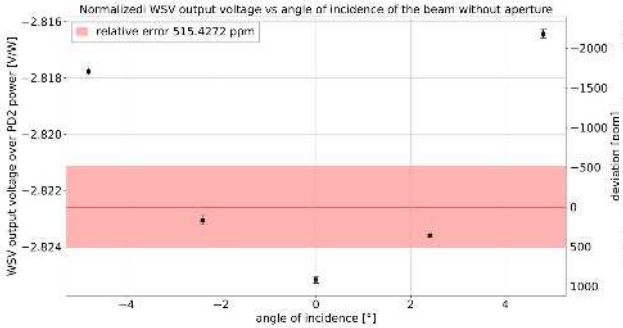

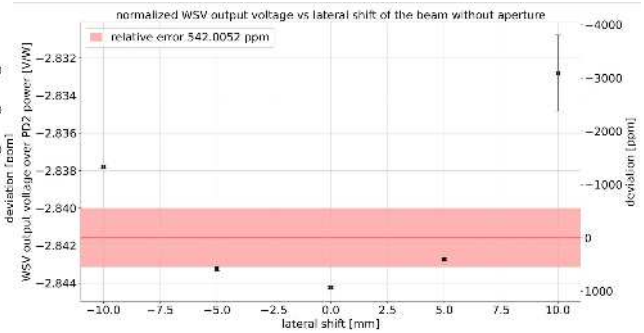

Investigation ghost beam setup intercalibration

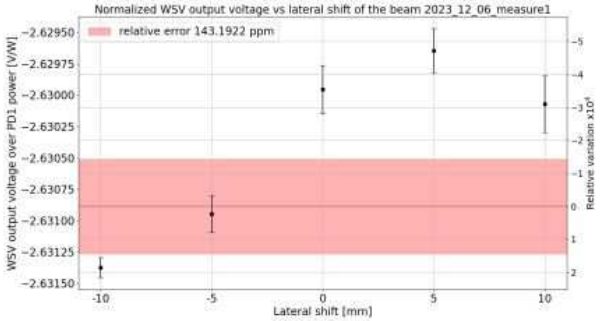

(a) Diaphragm closed

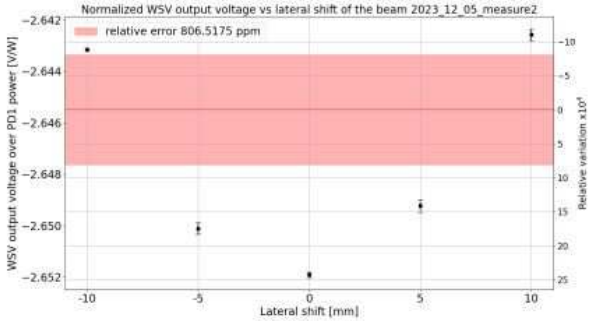

(b) Diaphragm open

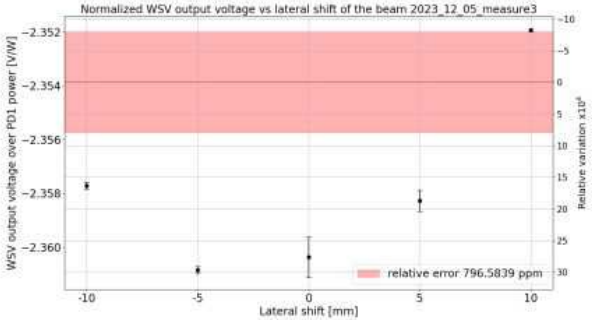

(c) Diaphragm open, dichroic mirror after BS1

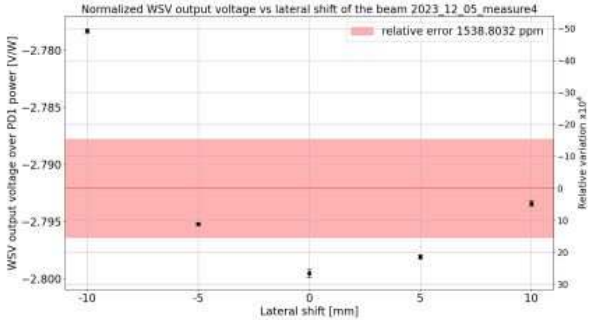

(d) Diaphragm open, dichroic mirror after collimator

Calibration TSA/TSB à NIST

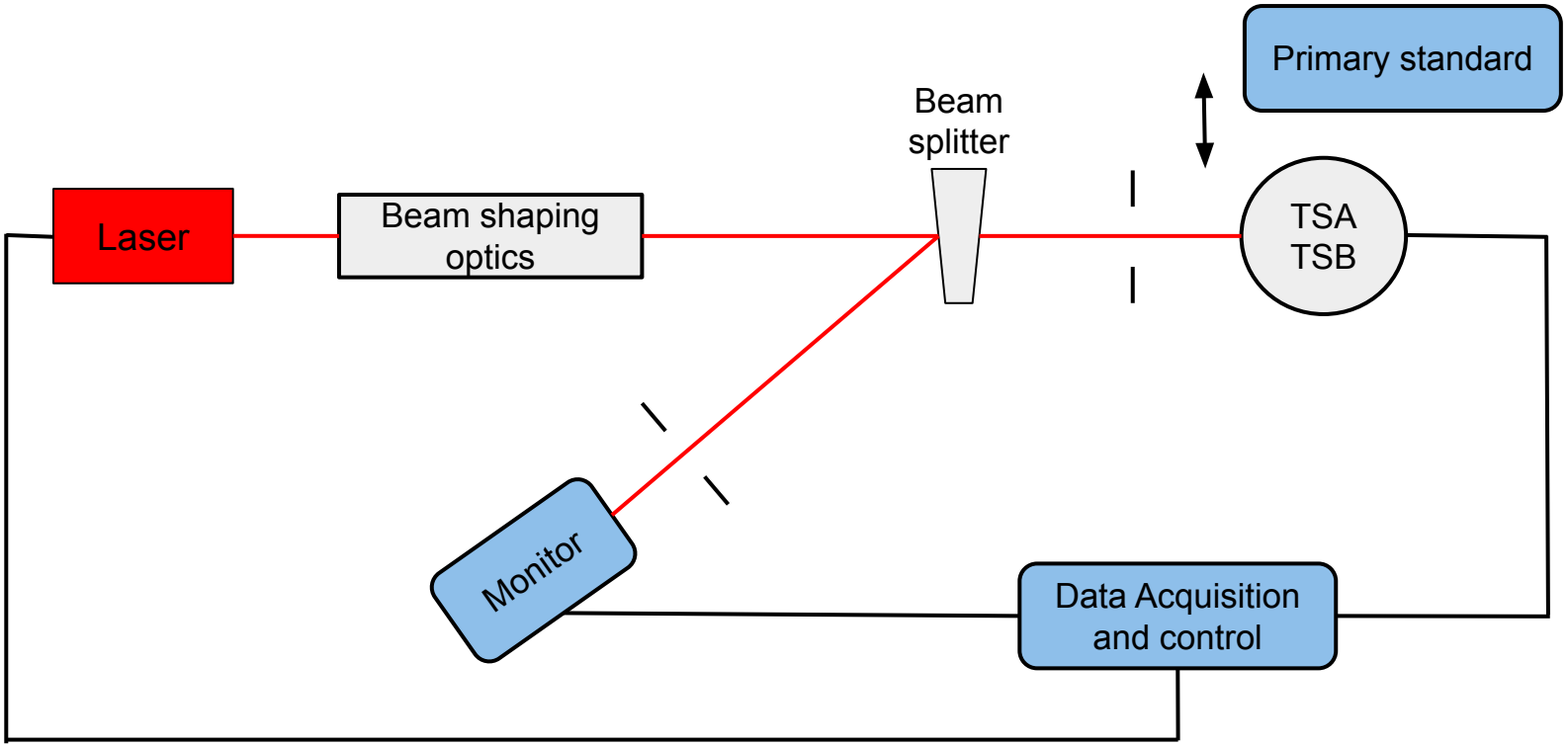

Calcul responsivité consensus à NIST et PTB

	CR	u(CR) [%]	DoE [%]	u(DoE) ($\sigma = 2$) [%]
TSA	-4.35988	0.08	-0.21	0.32
TSB	-4.27856	0.08	-0.23	

$$CR = (1 + \Delta_{RR}) \cdot R_{RR}$$

$$u(CR) = \sqrt{(\Delta_{RR} \cdot u(\Delta_{RR}))^2 + u^2(R_{RR})}$$

$$\Delta_{RR} = \sum_{l=1}^{2} \omega_l \Delta_l$$

$$\text{with} \quad \Delta_l = \frac{R_l}{R_{RR}} - 1$$

$$\text{and} \quad \omega_l = \frac{u^{-2}(\Delta_l)}{\sum_{k=1}^{2} u^{-2}(\Delta_k)}$$

$$\text{where} \quad u(\Delta_l) = \sqrt{u^2(R_l) + u^2(R_{RR}) + u_{ts}^2}$$

$$\text{with} \quad u(\Delta_{RR}) = \frac{1}{\sqrt{\sum_{l=1}^{2} u^{-2}(\Delta_l)}}$$

$$u(R_{PTB}) = 0.1\%$$

$$u(R_{RR}) = u(R_{NIST}) = 0.075\%$$

$$u_{ts} = 0.001\%$$

Calcul responsivité consensus à NIST et PTB

	CR	u(CR) [%]	DoE [%]	u(DoE) ($\sigma = 2$) [%]
TSA	-4.35988	0.08	-0.21	0.32
TSB	-4.27856	0.08	-0.23	

$$u(R_{PTB}) = 0.1\%$$

$$u(R_{RR}) = u(R_{NIST}) = 0.075\%$$

$$u_{ts} = 0.001\%$$

$$DoE = \Delta_{PTB} - \Delta_{NIST} = -(\frac{R_{NIST}}{R_{RR}} - 1)$$

$$u(DoE) = \sqrt{u^2(\Delta_{NIST}) + u^2(\Delta_{PTB})} = \sqrt{(u^2(R_{NIST}) + u^2(R_{RR}) + u_{ts}^2) + (u^2(R_{PTB}) + u^2(R_{RR}) + u_{ts}^2)}$$

Système pneumatique intercalibration

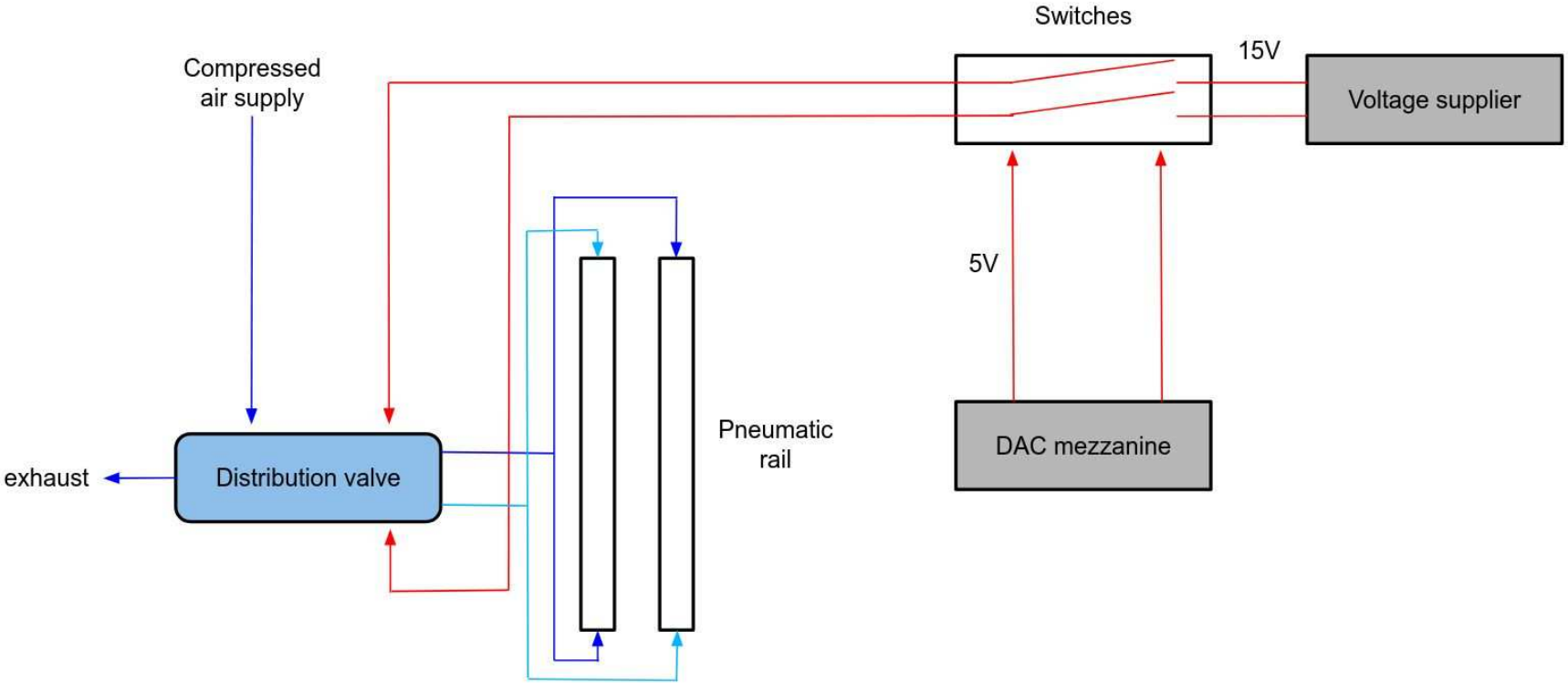

Calibration canaux ADC

$$V_{out} = a \cdot V_{in} + b + \epsilon$$

$$\sigma_{sys} = \sqrt{\frac{\sum_{i=1}^{N} \epsilon_i^2}{\chi^2_{max}}}$$

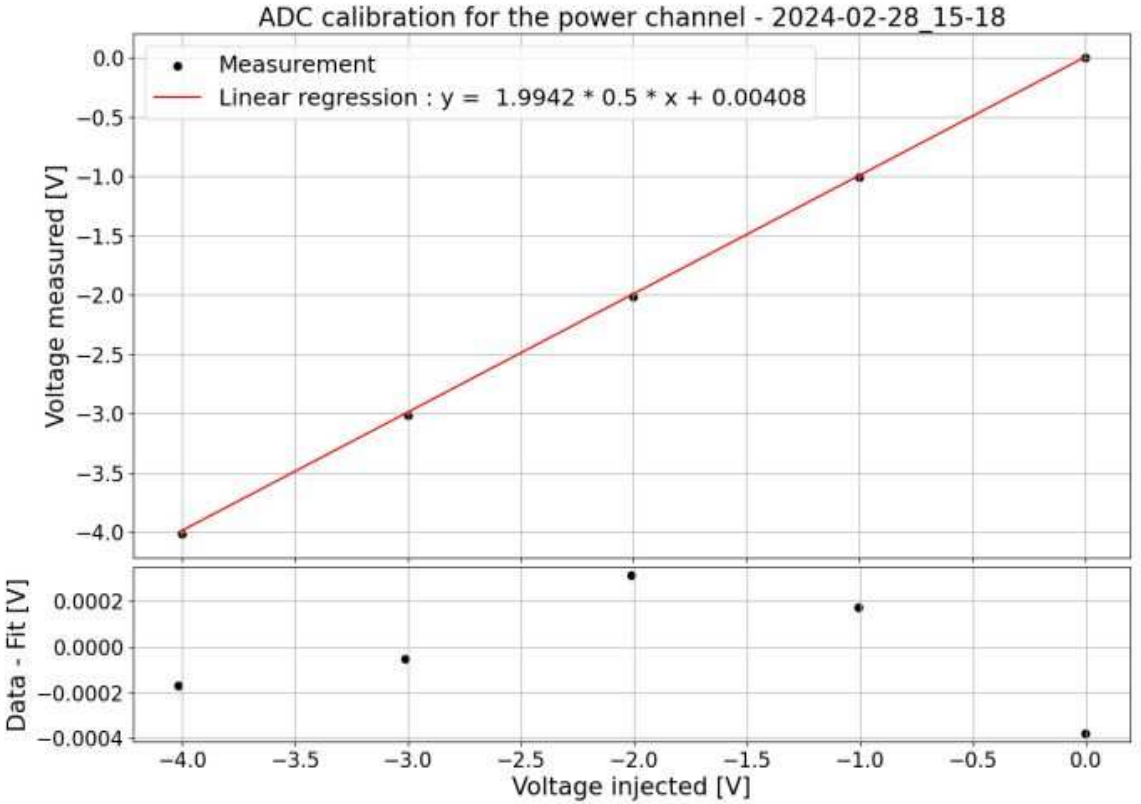

Mesure background intercalibration

$$\sigma_{bg} = \sqrt{(\sigma_{ADC})^2 + (\sigma_{V_{bg}})^2}$$
$$= \sqrt{0.197^2 + 0.01^2}$$
$$= 0.197 \text{ mV}$$

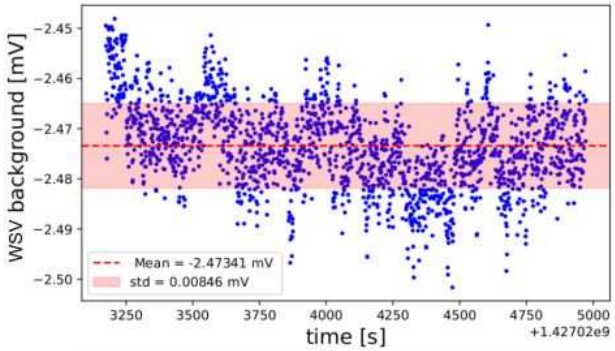

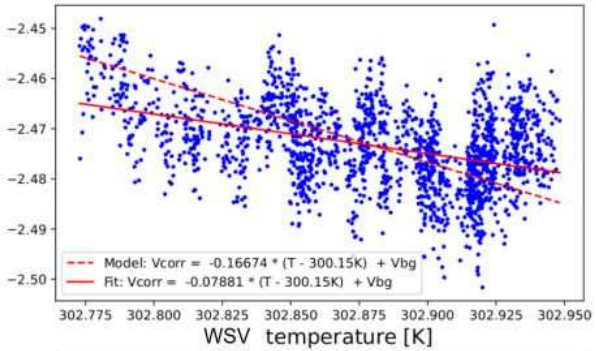

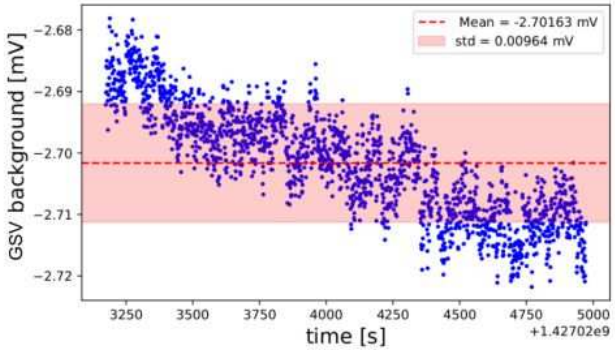

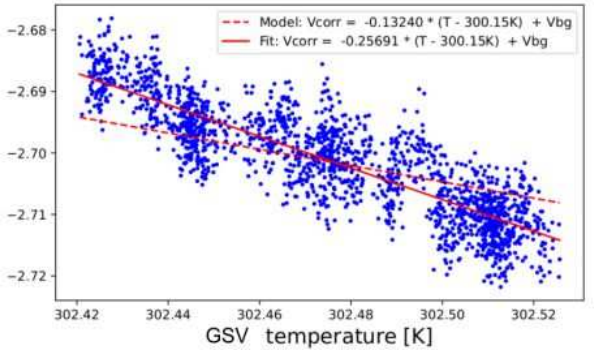

PCal intercalibration: Temperature dependence of background

Protocol for background voltage temperature dependence :

- Insulates the test sphere with bubble wrap
- Put it in an oven at 40°C (313.K) for 30 min
- Record the background voltage and temperature of the sphere while it's cooling down to room temp

Compute temperature dependence coefficient *m* :

- Fit the measurements data following this model

$$V^{bg}(\mathcal{T}) = m \cdot (\mathcal{T} - 300.15\ \mathrm{K}) + V'^{\,bg}$$

Where $V'^{\,bg}$ is the value of the background voltage at 300.15K

Temperature background voltage correction :

$$V_{bg}(\mathcal{T}) = m \cdot (\mathcal{T} - \mathcal{T}^{meas}) + V_{bg}^{meas}$$

Current *m* values :

$$m_{WSV} = -0.1667 \pm 0.0013\ \mathrm{mV/K}$$
$$m_{GSV} = -0.1324 \pm 0.0017\ \mathrm{mV/K}$$

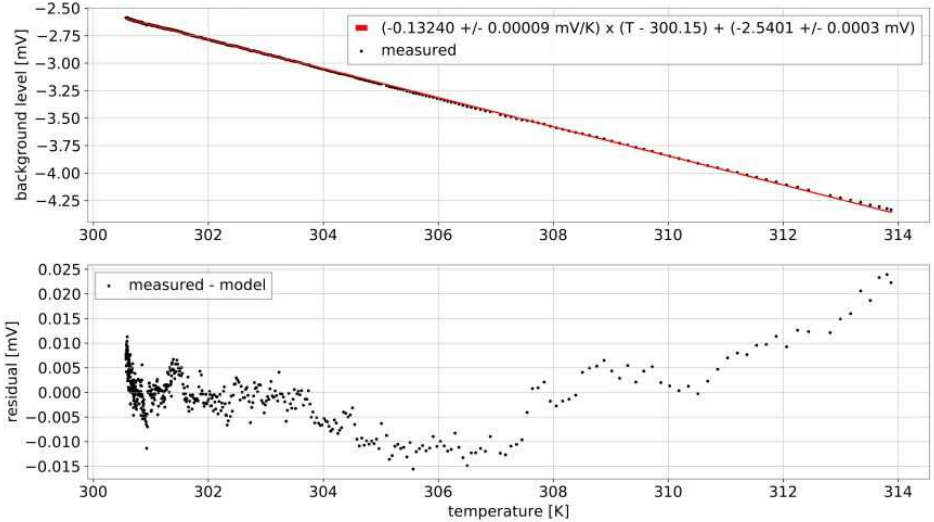

PCal intercalibration: Temperature dependence of responsivity

Protocol for responsivity temperature dependence :

- Insulates the test sphere with bubble wrap
- Put it in an oven at 40°C (313.K) for 30 min
- Do a responsivity ratio (α) measurement of the test sphere while it is cooling down to room temp

Compute temperature dependence coefficient κ :

-The temperature dependency of test sphere model as

$$\rho_{test}(\mathcal{T}) = \rho'_{test} \cdot (1 + \kappa \cdot (\mathcal{T} - 300.15\ \mathrm{K}))$$

Where ρ' is the value of the responsivity at 300.15K

- The temperature dependant background voltage is subtracted using the previous measurement result and we can model α as

$$\alpha(\mathcal{T}) = \frac{\rho'_{test}}{\rho'_{ref}} \cdot (1 + \kappa \cdot (\mathcal{T} - 300.15\ \mathrm{K})) = \alpha' \cdot (1 + \kappa \cdot (\mathcal{T} - 300.15\ \mathrm{K}))$$

- We down-sampled to 1 point every 0.5 K and fit the α model to the data
- Error bars are increased until the p-value of the fit reach 0.05 → 0.04% uncertainty

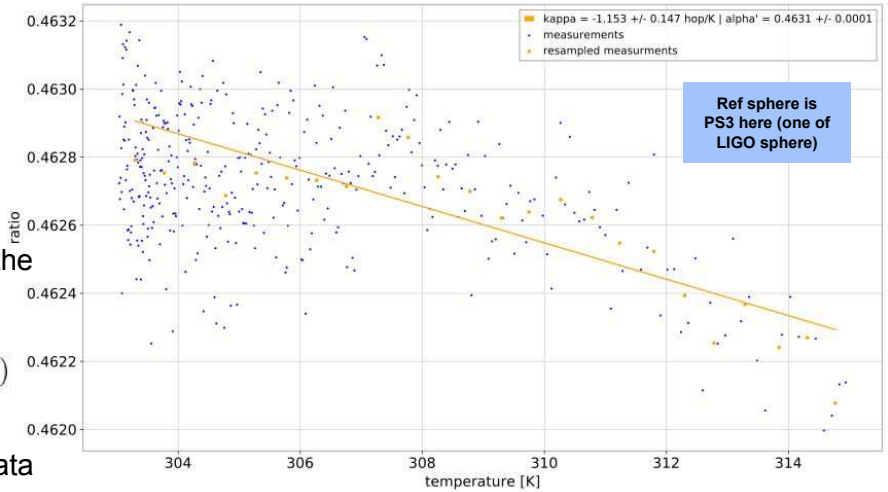

Current κ values :

$$\kappa_{GSV} = -115 \pm 31\ \mathrm{ppm/K}$$
$$\kappa_{WSV} = -187 \pm 29\ \mathrm{ppm/K}$$

Temperature variation are ~0.01 - 0.02 %/K, very small but still corrected

Impact des différentes corrections sur la tension

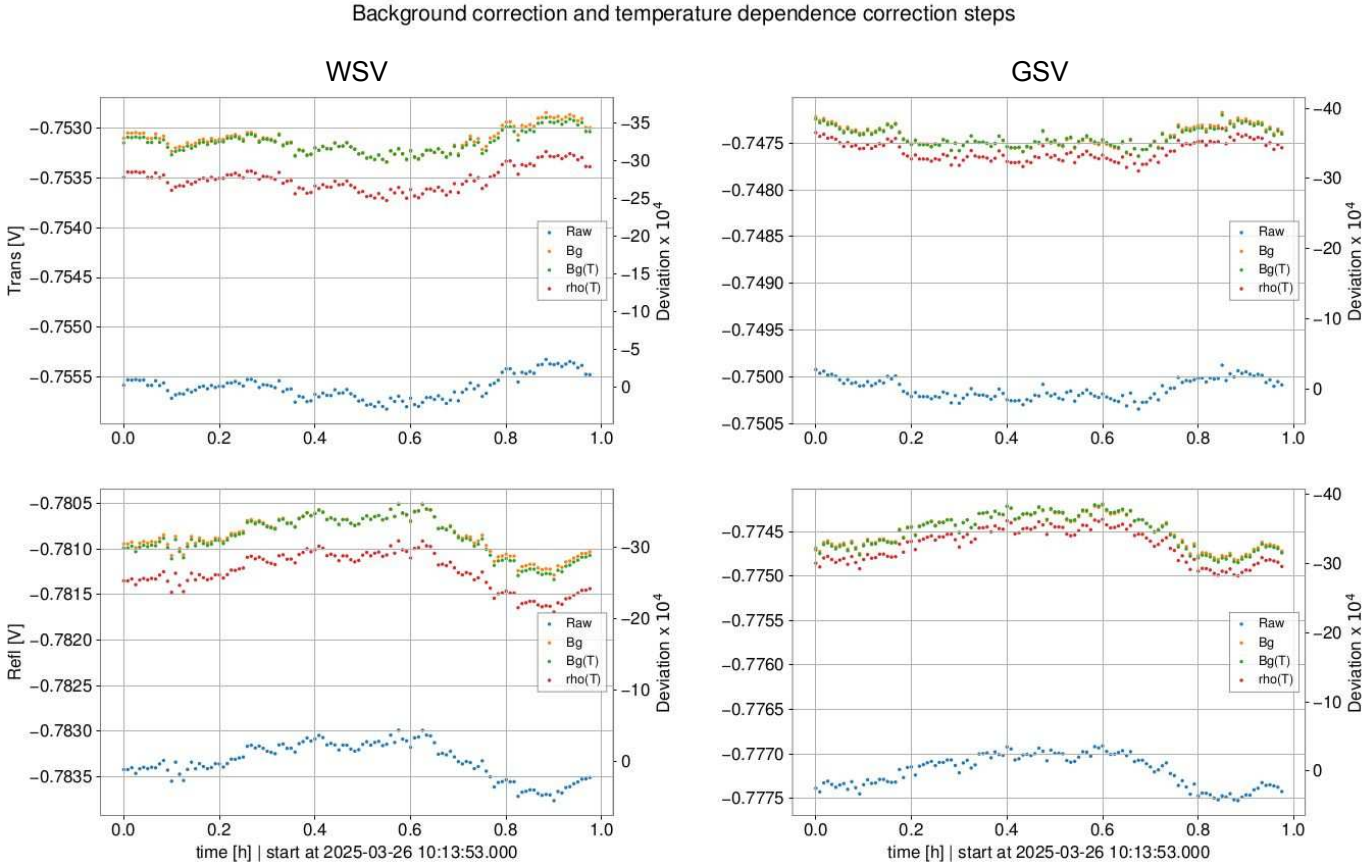

Mesure du ratio α

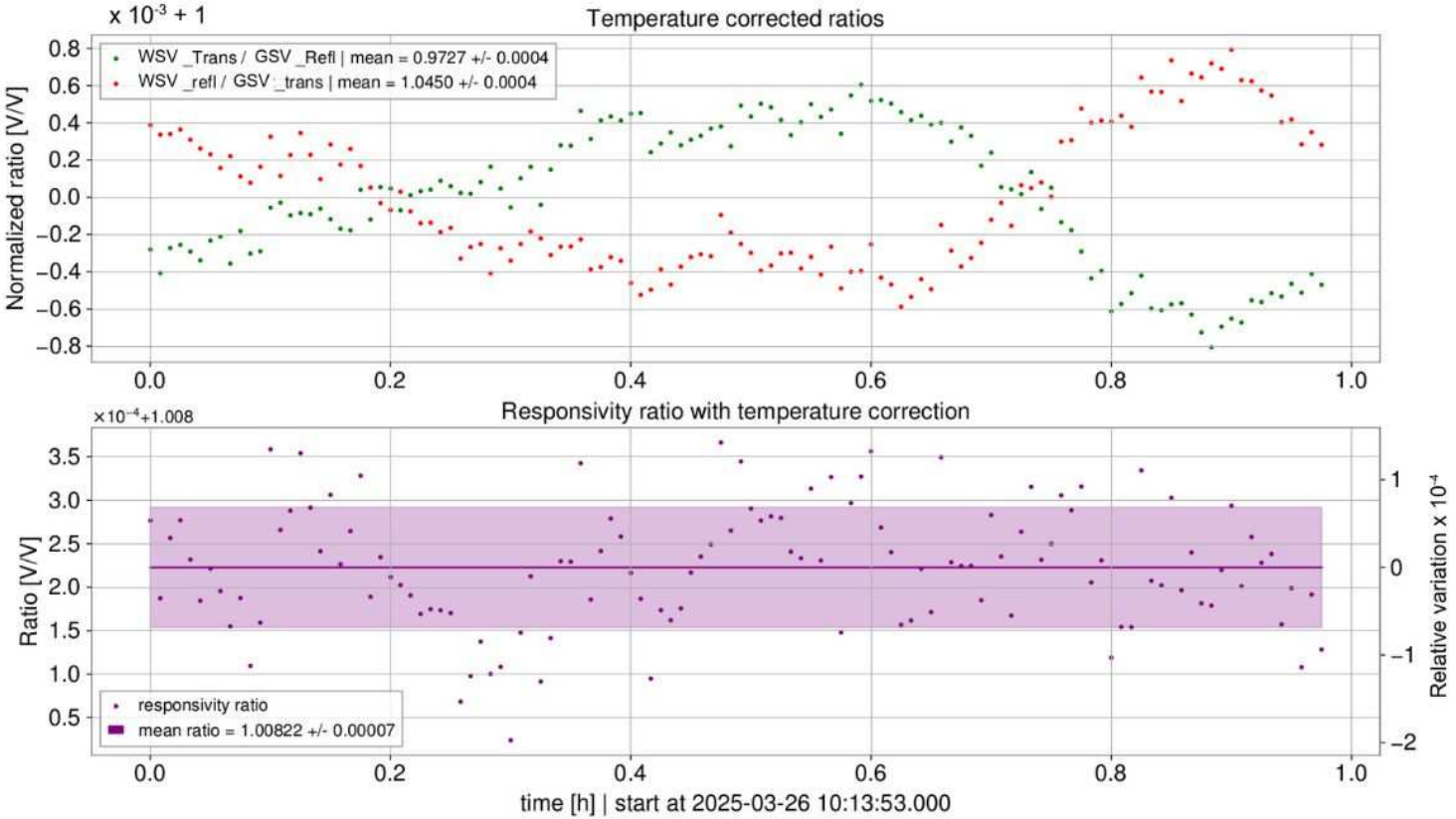

Intercalibration des sphères intégrantes

Première estimation de la responsivité de WSV en avril 2024 en utilisant la méthode “dernière valeur”

$$\rho'_{WSV} = -2.61787 \pm 0.00288 \text{ V/W}$$

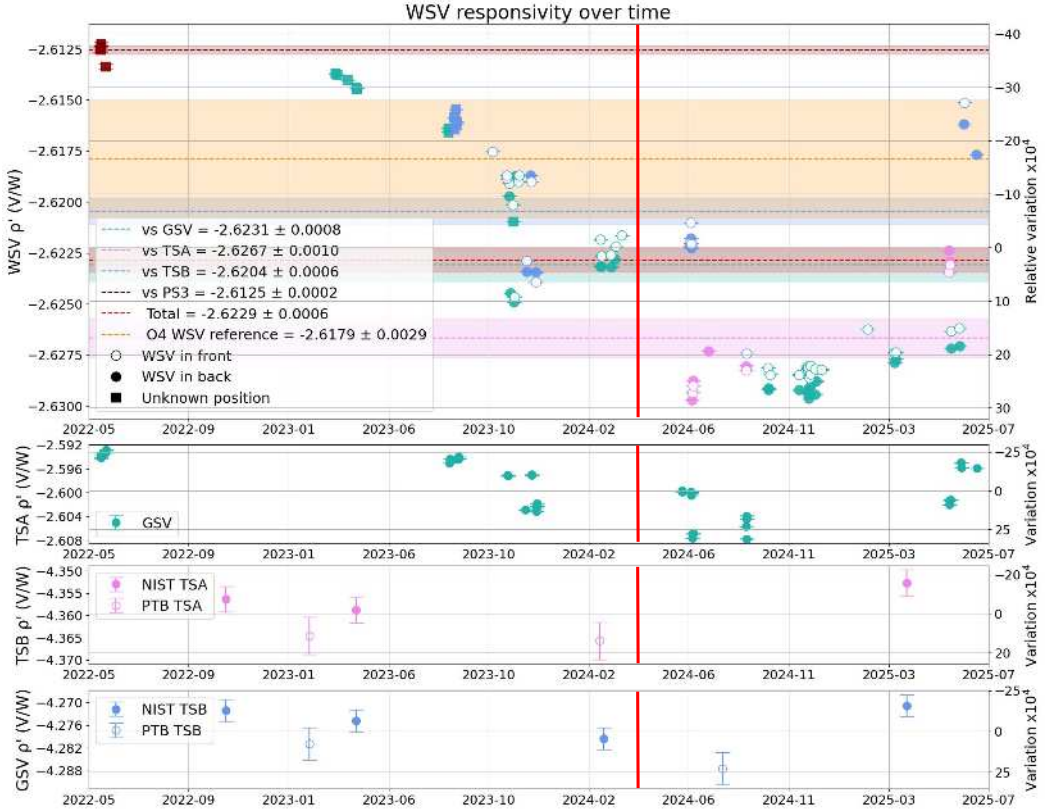

Intercalibration : Responsivity evolution

Highlighting of a **~0.2%** discrepancy between the responsivity computed with TSA and TSB

This difference is seen with both WSV and GSV

Similar difference seen at LIGO starting in July 2024 →Need to confirm with further measurements

→ Addition of a 0.16% uncertainty

$$\sigma = \frac{\bar{\rho}_{WSV_A} - \bar{\rho}_{WSV_B}}{\sqrt{2}}$$

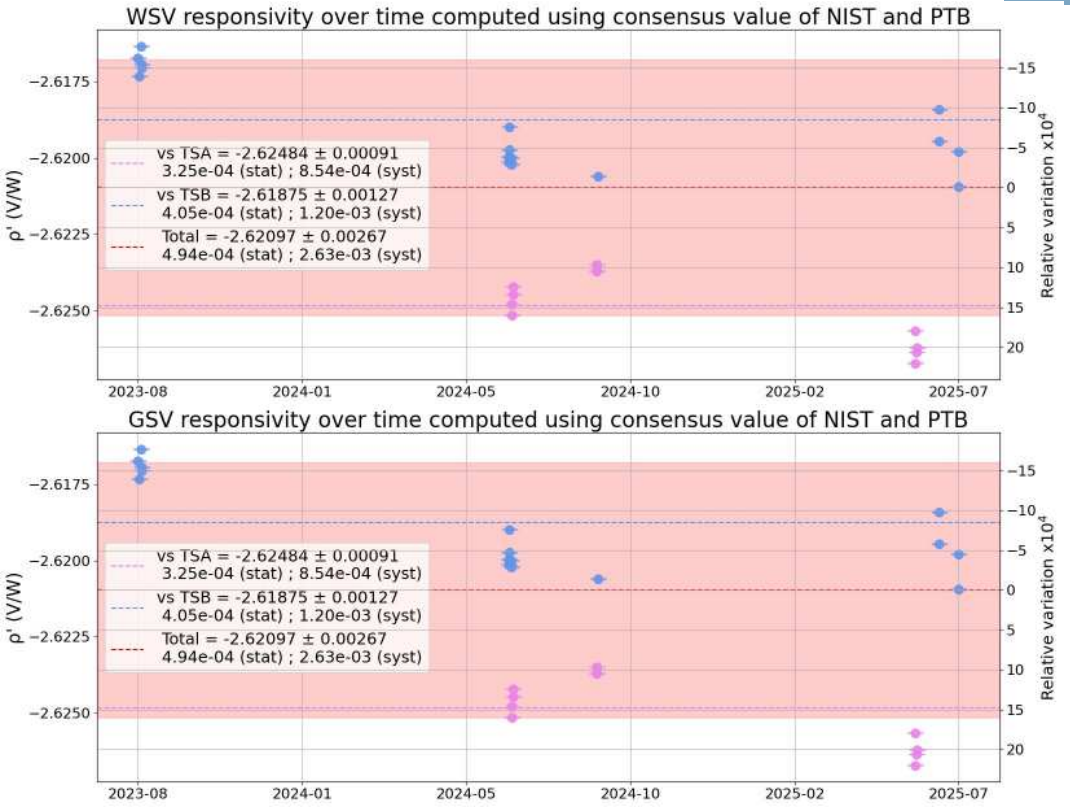

Incertitudes PCal estimées au début de 04

Source	Relative uncertainty [%]	
TS responsivity	0.08	
α' ratio GSV/TS	0.03	
α' ratio WSV/GSV	0.03	
ρ_{WSV} temperature dependence	0.04	
Output voltage	ADC conversion	0.02
	Background voltage	0.02
	Temperature dependence	0.04
	Total	0.05
Total	**0.11**	

Source	Relative uncertainty [%]	
Rx responsivity	0.15	
Deformation model	0.30	
Optical efficiency	0.40	
Pendulum model	Incident angle, $\cos(\theta)$	0.16
	ETM mass, M	0.05
	ETM rotation	0.09
	Total	0.19
Total	**0.56**	

Différence entre LIGO et Virgo intercalibration

LIGO

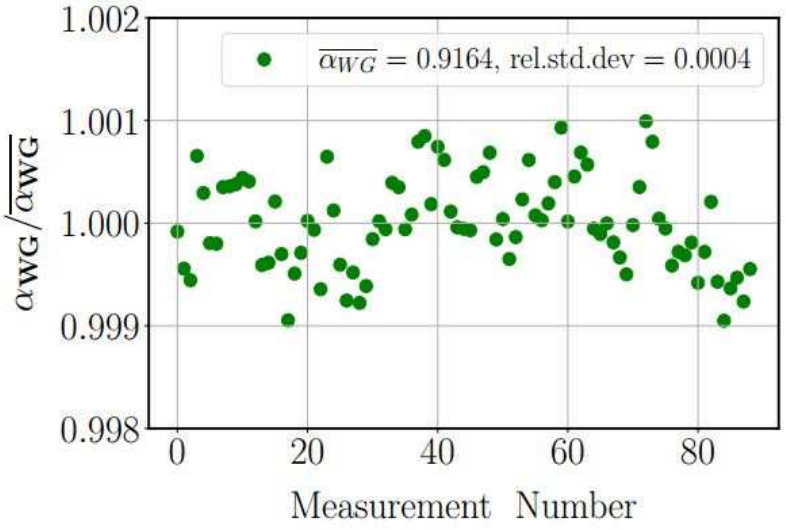

Virgo

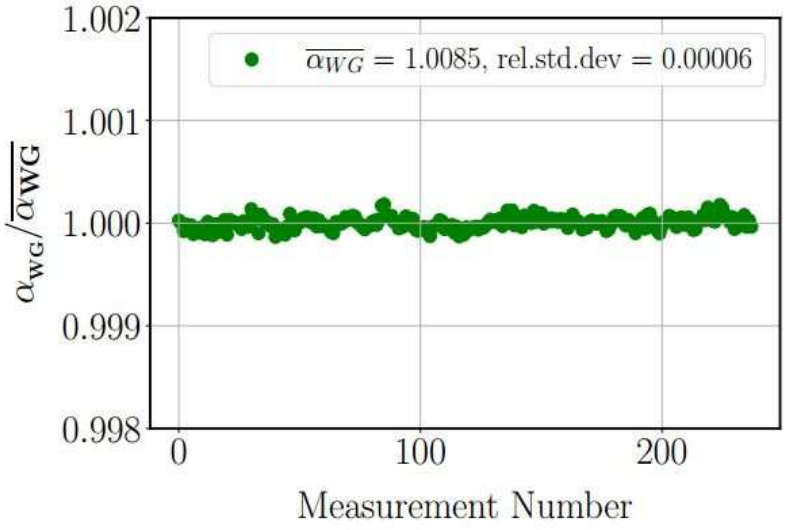

Evolution des Gold Standard de LIGO et Virgo

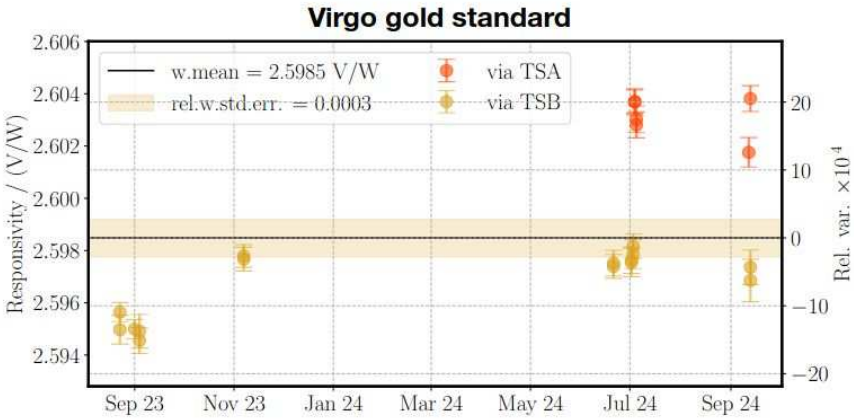

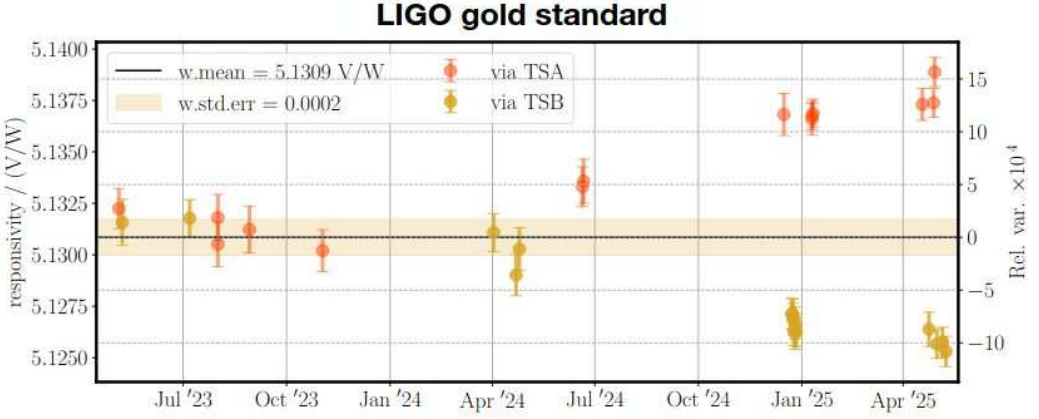

CRÉDIT - Dripta Bhattacharjee

Calibration des sphères Rx à LIGO

Measurement uncertainty	O2 (%)	O3 (%)	O4 (%)
LHO	0.75%	0.42%	0.29%
LLO	0.75%	0.54%	0.15%

Regular Rx/WS and optical efficiency measurements made at LHO and LLO end stations.

Slow variations of ~ +/- 0.2 % over 2.5 years

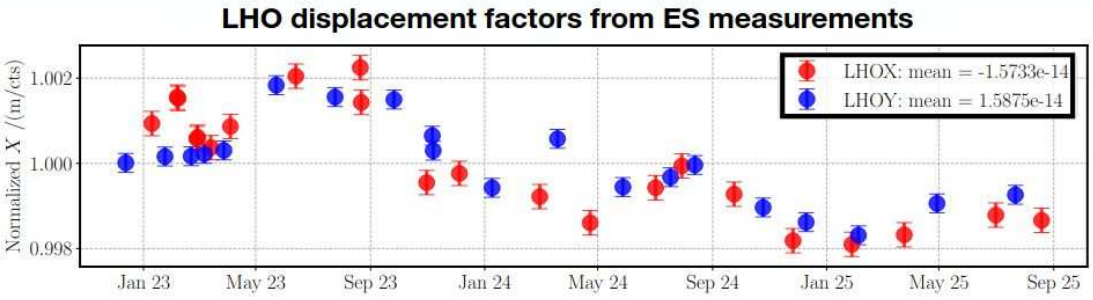

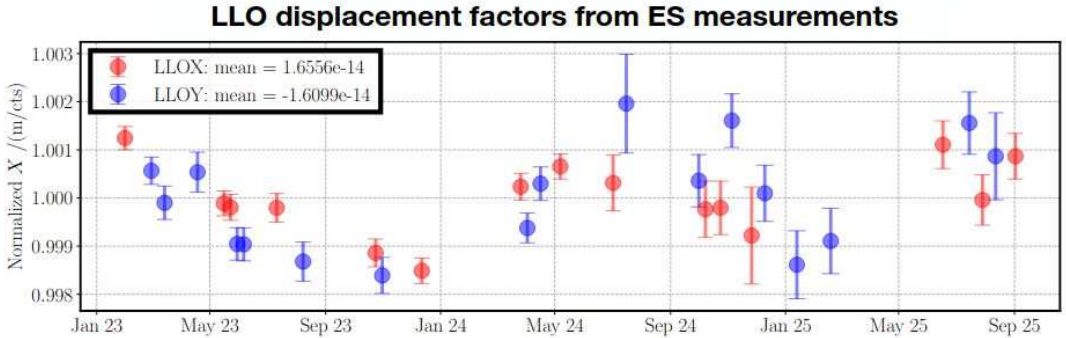

Measurement at LLO used two different sensors as WS

CRÉDIT - Dripta Bhattacharjee

Calibration photodiodes PCal pour O4

NE	G^{new} (W/V)	O^{new} (W)
Tx_PD1	-0.775253	-0.000758
Tx_PD2	-0.858946	-0.000843

WE	G^{new} (W/V)	O^{new} (W)
Tx_PD1	-0.740169	0.000648
Tx_PD2	-0.783431	0.001054

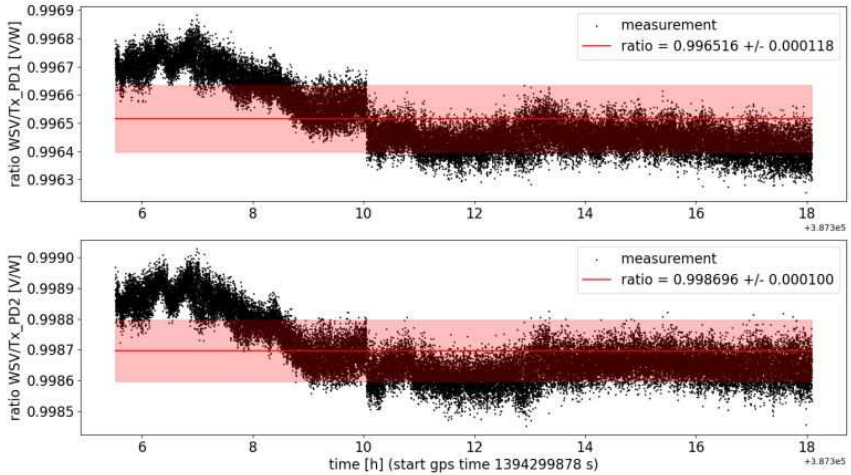

(a) NE

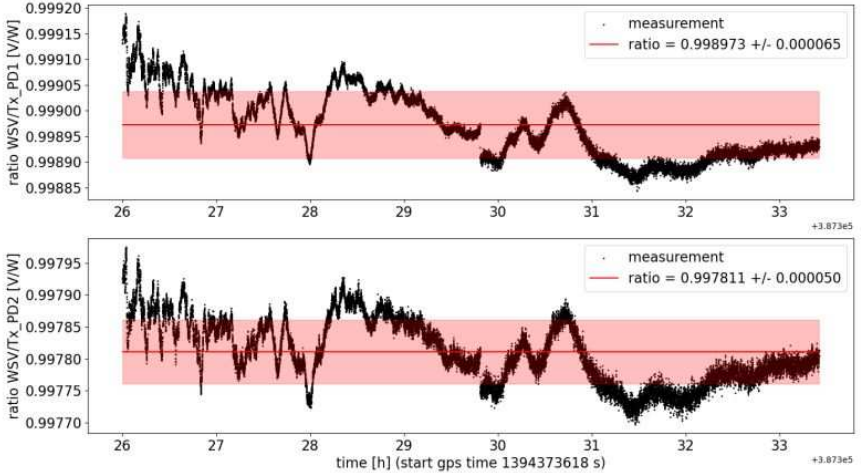

(b) WE

Calibration sphères Rx PCal 04

Rx	G^{new} [W/V]	O^{new} [W]
NE	0.730861	-0.002632
WE	0.690639	-0.001155

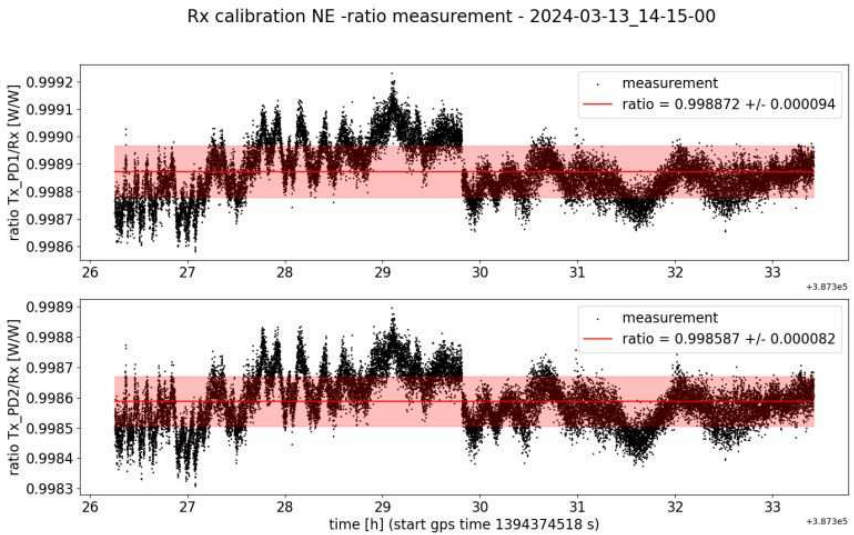

(a) NE

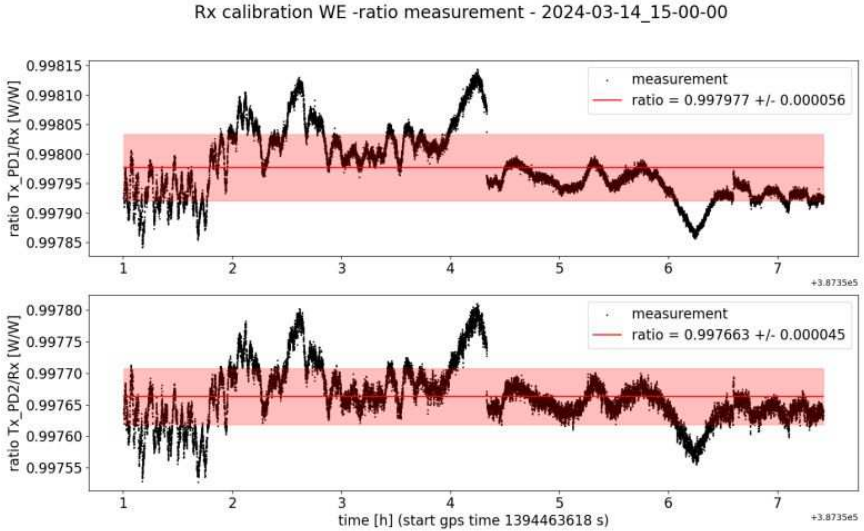

(b) WE

Evolution calibration canaux ADC PCal 04

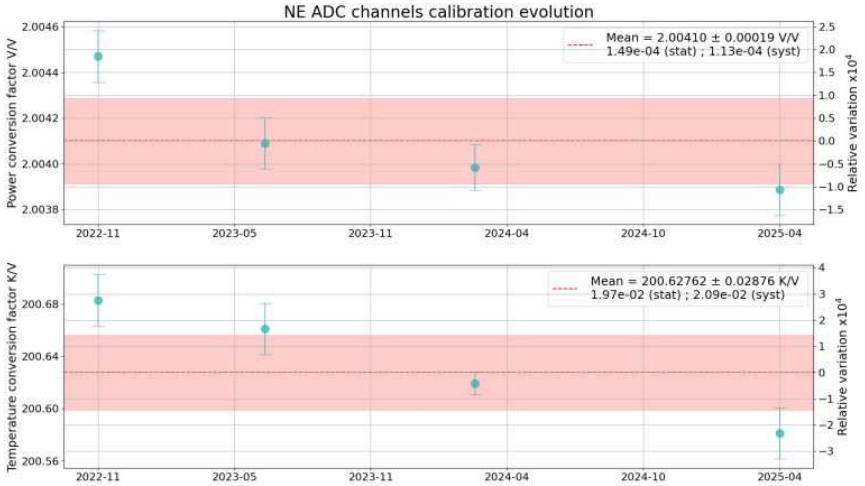

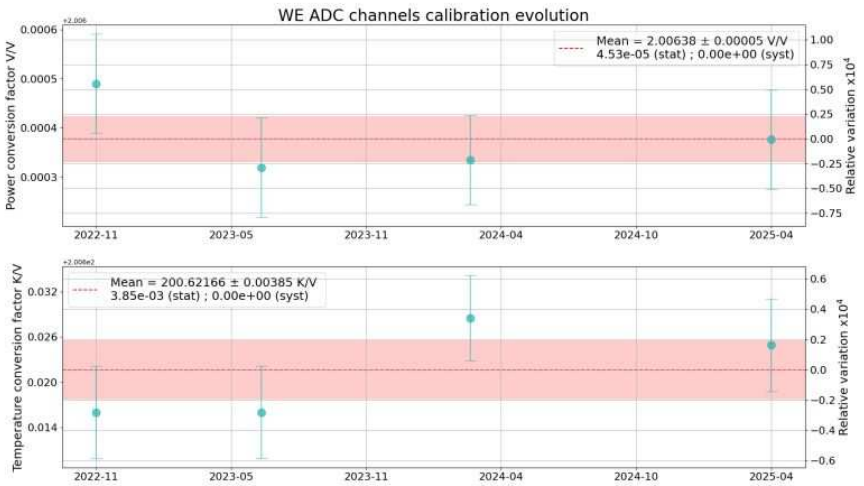

Evolution calibration photodiodes PCal 04

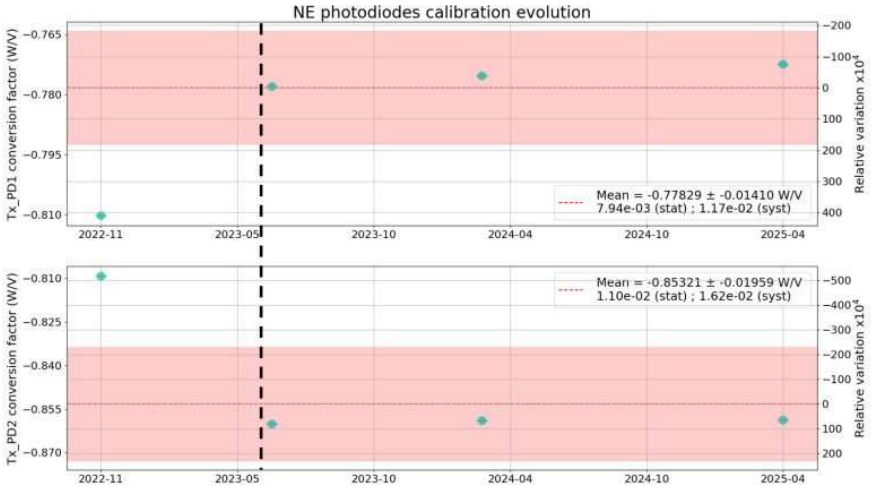

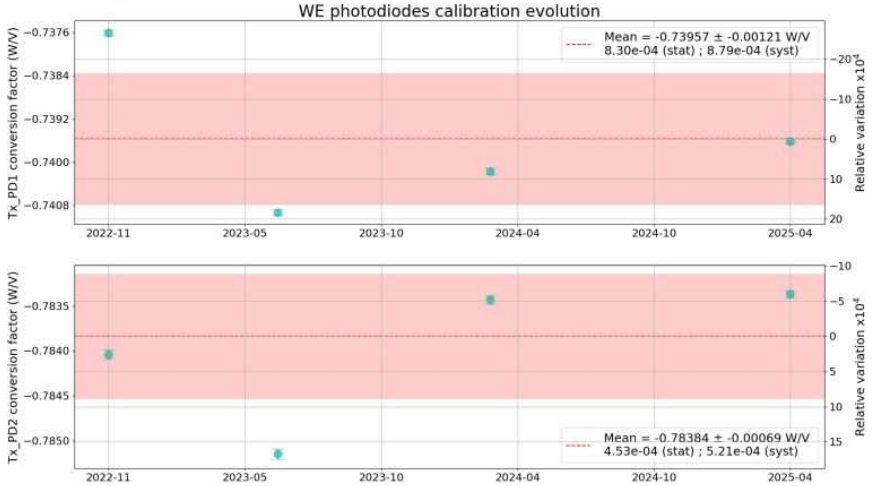

Calibration des capteurs de puissances

Monitoring de la puissance mesurée par les capteurs du PCal

Augmentation des variations pour NE au début du run
→ causées par la dépendance au variation d'humidité de Tx_PD1 (photodiode de la boucle de contrôle)

Changement de la photodiode de boucle pour NE → diminution des variations → ± 0.15 % comme pour WE

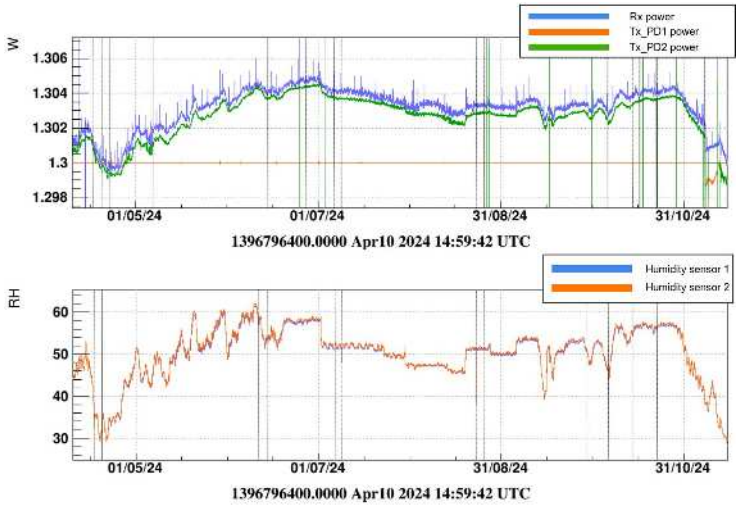

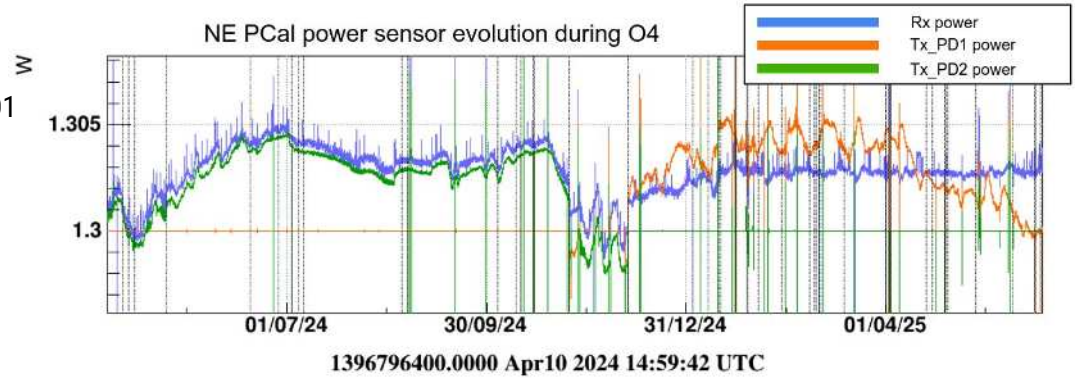

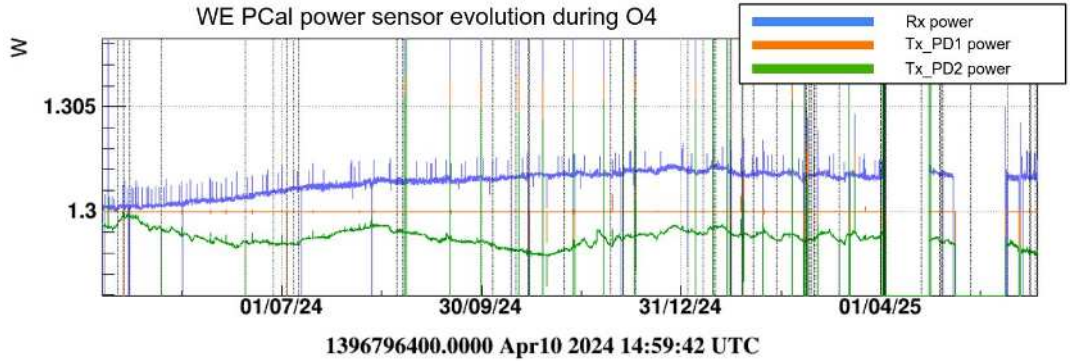

Calibration de l'électronique de détection

Chaîne d'acquisition du PCal :
- Photodiode
- Process analogique → filtre anti-repliement + Analog to Digital Converter (ADC)
- Process digital → filtre anti-repliement + sous échantillonage (delai 49 µs)

Timing :
- Receveur GPS principal placé dans le bâtiment central et distribue le timing à tous les autres bâtiments grâce à un signal IRIG-B envoyé à des TDBox
- Les TDBox distribuent aux DAQBox, RTPCs…

Mesure de la réponse fréquentielle :

- une LED placée devant Tx_PD1

- Connectée à la TDBox → permet de générer un signal synchronisé avec l'horloge interne de la DAQBox

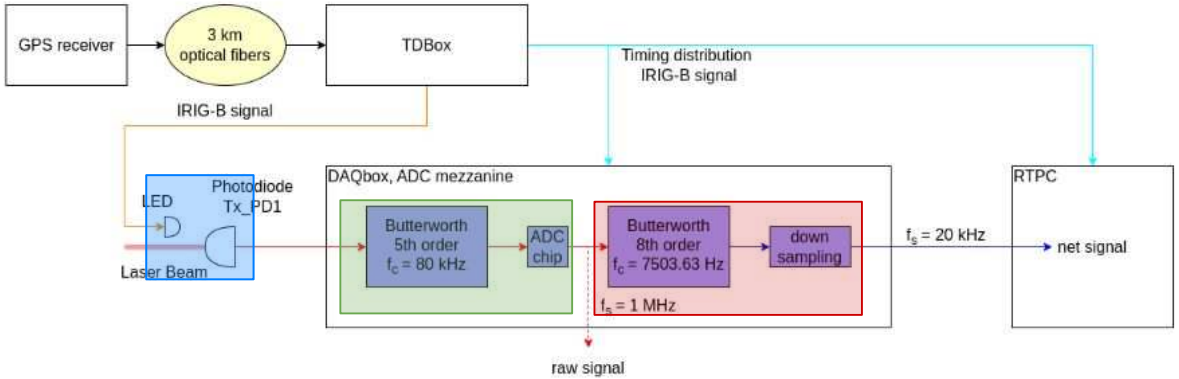

Calibration de l'électronique de détection

1- Mesure de la réponse pour Tx_PD1

- Laser PCal éteint
- Utilise la LED pour flasher un signal IRIG-B à Tx_PD1
- Calcul de la fonction de transfert entre le signal IRIG-B et l'output de la photodiode
- Fit de la fonction de transfert (modèle nominal + retard)

2- Mesure de la réponse pour Tx_PD2 ou Rx

- Injection d'un bruit blanc avec le laser PCal
- Calcul de la fonction de transfert entre Tx_PD1 et Tx_PD2
- Fit avec un délai résiduel

- Reproduire la même chose pour Rx

	PCal	NE			WE		
Nominal model	Sensor	Tx_PD1	Tx_PD2	Rx	Tx_PD1	Tx_PD2	Rx
	Analog filter	5^{th} order Butterworth filter f_c= 80 kHz					
	Digital filter	8^{th} order Butterworth filter f_c= 7503.65 kHz					
	Down sampling delay	-49 μs					
Residual delay		0.62 μs	0.54 μs	1.45 μs	0.72 μs	0.66 μs	1.38 μs

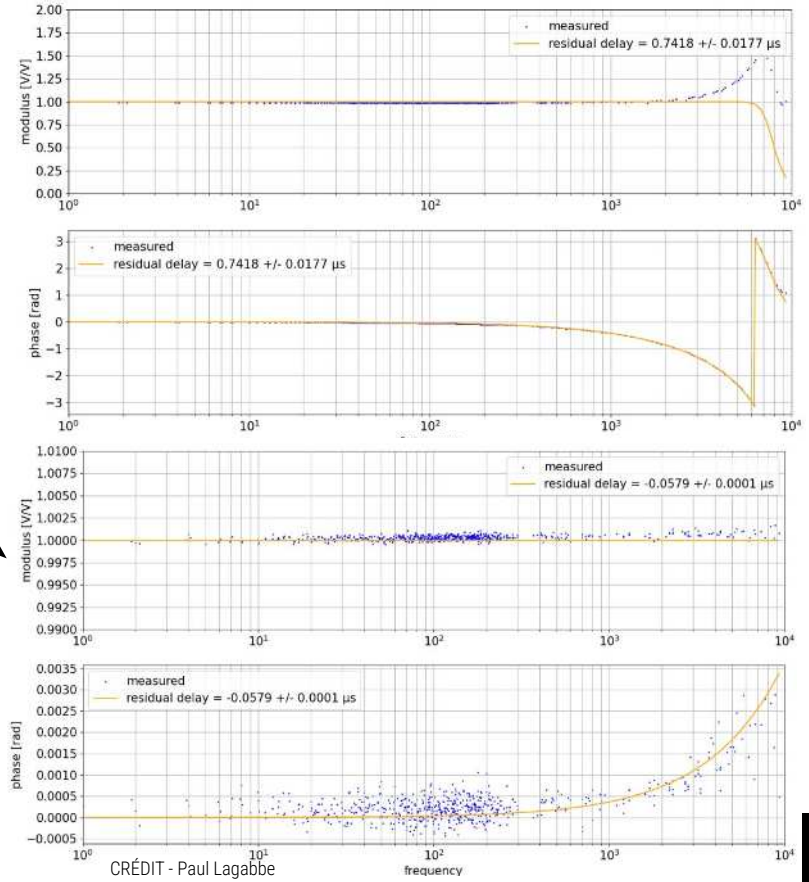

CRÉDIT - Paul Lagabbe

Pertes optiques

Pertes optiques :

- Miroir directeur M3
- Viewport entre le banc et la tour du miroir de bout de bras

$$P_{ref}(f) = \frac{P_{Rx}}{(1 - l_{vp})(1 - l_M)} \cdot S^{-1}_{PCal}(f)$$

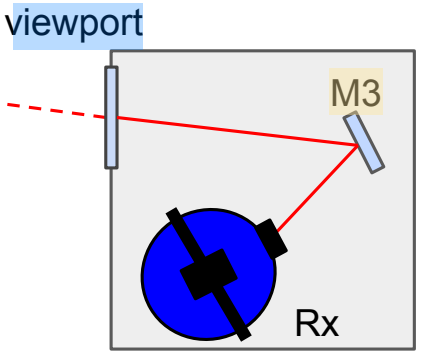

$$l_M = 0.107 \pm 0.012\%$$

$$l_{vp} = 0.57 \pm 0.096\%$$

Incertitude sur les pertes optiques → 0.1%

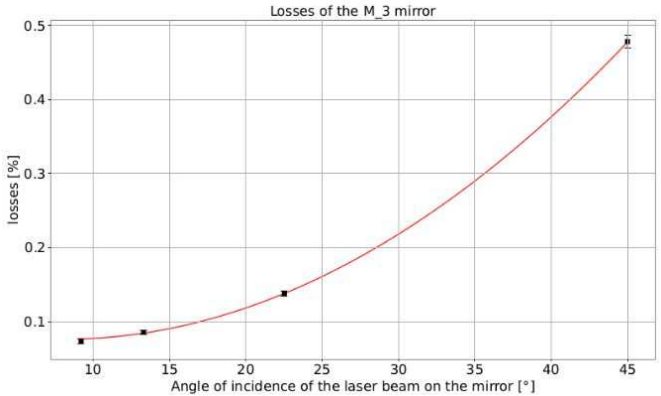

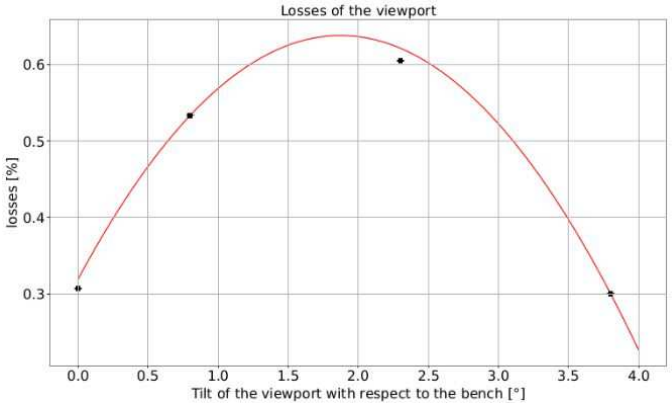

CRÉDIT - Paul Lagabbe

PCal mechanical stability during O4

Additional mechanical response measurements were performed at the beginning of the break in April 2024 and before the restart of the run in June 2025
Residual between the two models computed in March 2024 and April 2024 shows a stability within 0.7% for NE and 0.5 % for WE

NE residual

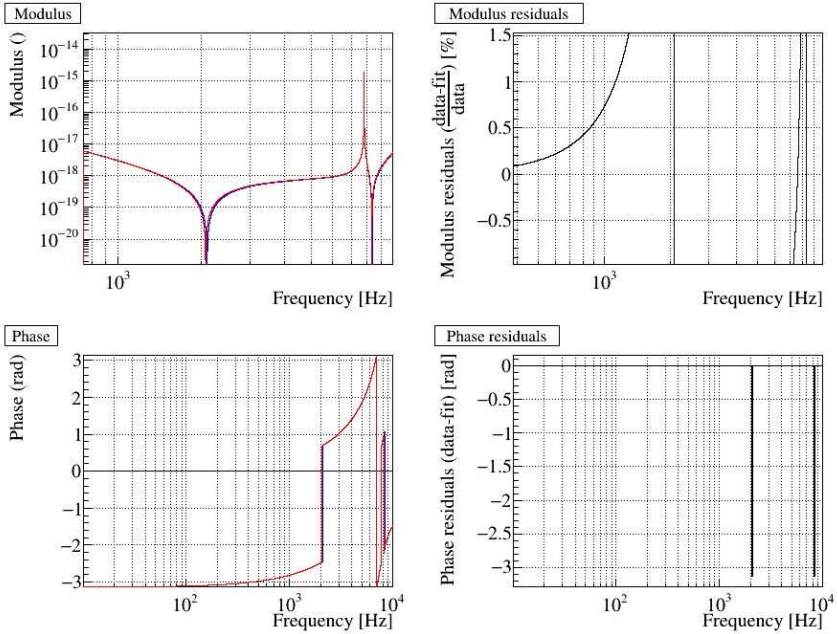

WE residual

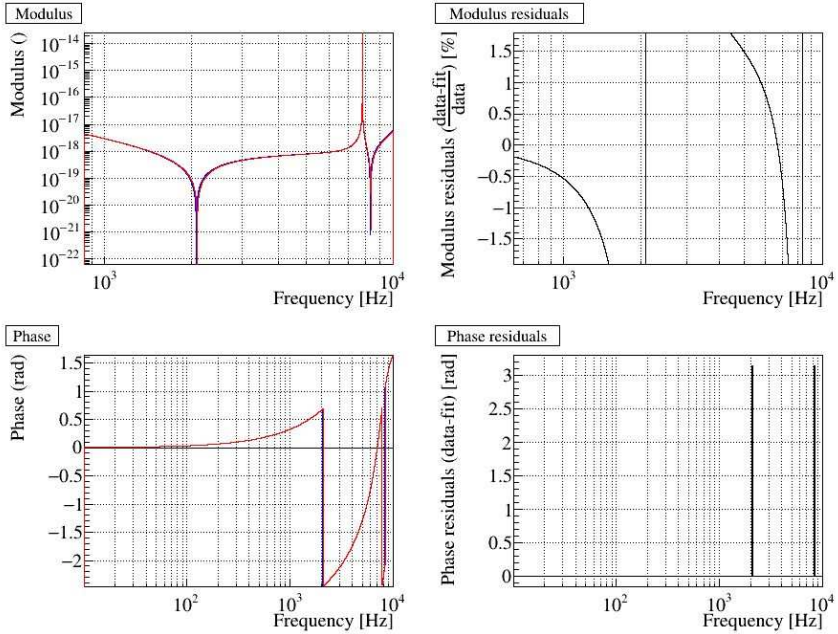

Mechanical response measurement

The uncertainty on the mechanical response is composed of:

- Uncertainty on the pendulum response

$$\sigma_{pend} = \sqrt{\sigma_\theta^2 + \sigma_{Mass}^2 + \sigma_{Rotation}^2}$$
$$= \sqrt{0.16^2 + 0.05^2 + 0.09^2} = 0.2\%$$

- Uncertainty on the mirror vibration modes

$$\sigma_{drum} = 0.7\%$$

NE

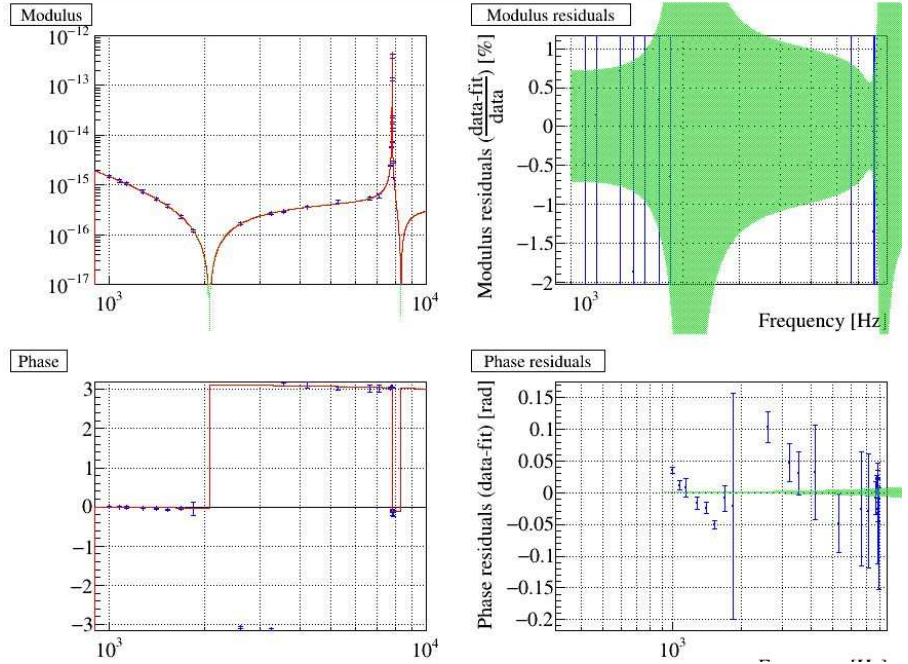

Mechanical response measurement

The uncertainty on the mechanical response is composed of:

- Uncertainty on the pendulum response

$$\sigma_{pend} = \sqrt{\sigma_{\theta}^2 + \sigma_{Mass}^2 + \sigma_{Rotation}^2}$$
$$= \sqrt{0.16^2 + 0.05^2 + 0.09^2} = 0.2\%$$

- Uncertainty on the mirror vibration modes

$$\sigma_{drum} = 0.7\%$$

BUT the uncertainty on the vibration modes must be weighted with regard to its contribution over the pendulum response one at 1Khz

$$\sigma_{Pcal\_model} = \sqrt{\sigma_{pend}^2 + \sigma_{drum}^2 \cdot \frac{A_{drum}(1\ kHz)}{A_{pend}(1\ kHz)}}$$
$$= \sqrt{0.2^2 + 0.7^2 \cdot 0.22} = 0.38\%$$

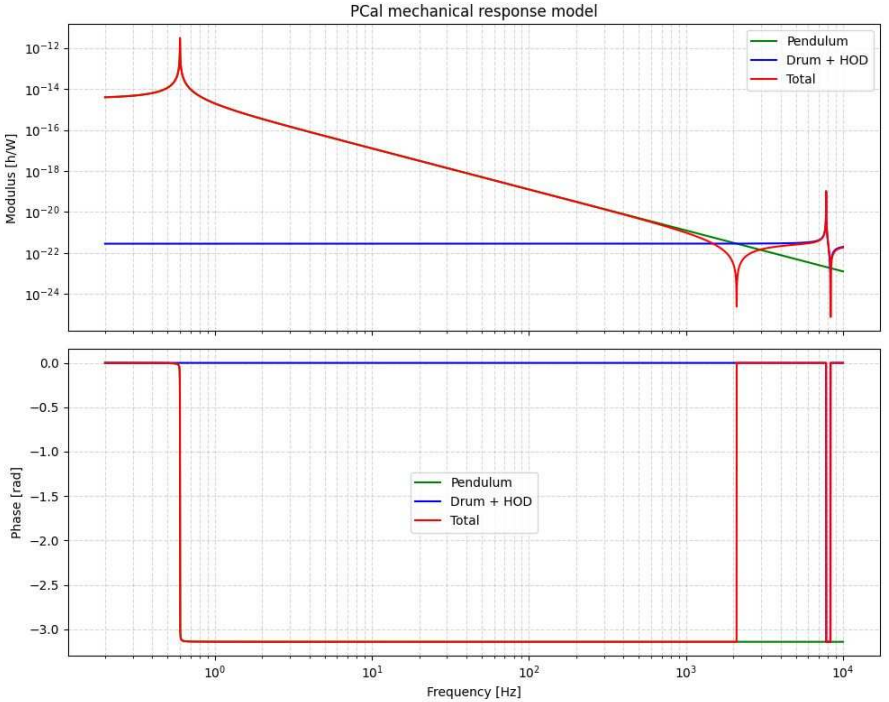

Variation réponse mécanique

		fixed	fitted				Usage
		G_p (h/W)	G_d (h/W)	f_d (Hz)	Q_d	G_{hod} (h/W)	
March 2024	NE	3.51e-15	3.32e-23	7798.1	5.69e5	2.58e-22	O4 model
		-	±3.26e-25	±0.1	±1.52e6	±1.82e-24	
	WE	-3.51e-15	-3.42e-23	7814.7	1.12e7	-2.52e-22	O4 model until April 2025
		-	±5.54e-25	±0.1	±1.94e6	±1.87e-24	
April 2025	NE	3.51e-15	3.36e-23	7798.1	2.31e8	2.50e-22	Monitoring
	WE	-	±1.46e-23	±0.1	±9.52e11	±1.64e-24	
		-3.51e-15	-3.23e-23	7814.3	2.13e8	-2.59e-22	Monitoring
		-	±1.36e-25	±0.1	±1.39e11	±9.56e-25	
June 2025	NE	3.51e-15	3.41e-23	7798.2	1.46e6	2.55e-22	Monitoring
		-	±4.14e-25	±0.1	±6.35e6	±2.11e-24	
	WE	-3.51e-15	-3.37e-23	7814.8	3.31e3	-2.60e-22	O4 model after June 2025
		-	±4.28e-25	± 0.3	±8.6e2	±1.47e-24	

Table 6.9: PCal mechanical response model fitted parameters for NE and WE.

Final PCal displacement model

PCal NCal comparison:

After all the calibration steps
→ WE PCal and NCal: in agreement
→ NE PCal and NCal: **0.9% discrepancy**

Reason of this discrepancy is unknown (higher optical losses ?)

Since NCal uncertainty is ± 0.12% < PCal uncertainty
→ Addition of a correction factor of 0.9% in the PCal displacement model
→After which PCal and NCal for NE are in agreement
→ Stable throughout the rest of the run

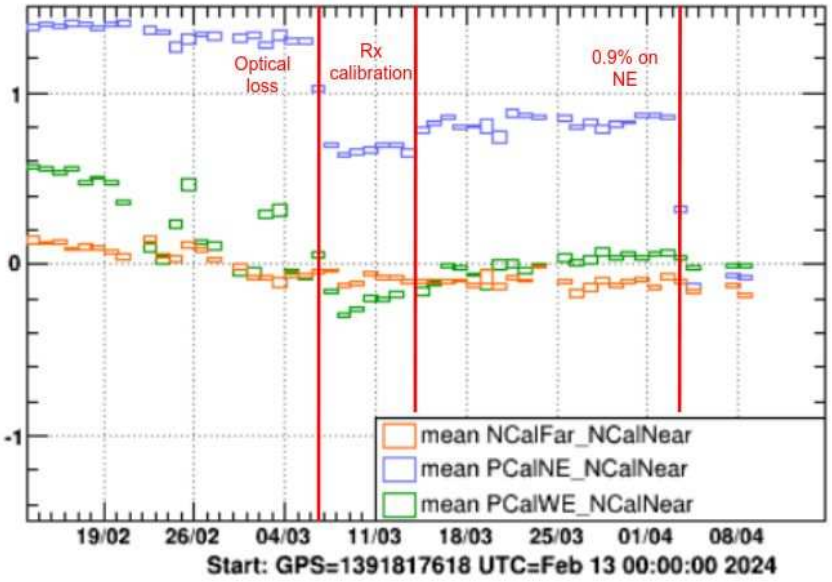

NCal → Absolute reference of mirror displacement for O4

Amélioration PCal O3 → O4

Avant tous les capteurs de puissance étaient des photodiode Silicon → corrélation avec variations de température

Banc injection → remplacé par photodiode InGaAs → plus stable avec la température

Banc réflexion → sphère intégrante

→ car réponse indépendante de l'angle d'incidence du faisceau laser dans la sphère

→ et sphère peuvent mesurer jusqu'à 3 W de puissance → permet mesure directe du faisceau sans jeter la majorité de la puissance

→ Diminue impact des pertes optiques → moins d'optiques sur banc de réflection

Améliorer la configuration optique : utilisation de cubes séparateurs à la place de miroirs beam splitters qui variaient beaucoup avec l'humidité pendant O4

PCal / NCal comparison during O4

The NE PCal was recalibrated with regard to the NCal with a correction factor of 0.9%

PCal over NCal comparison very stable throughout the run

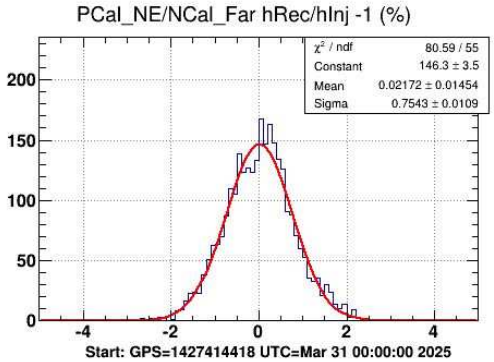

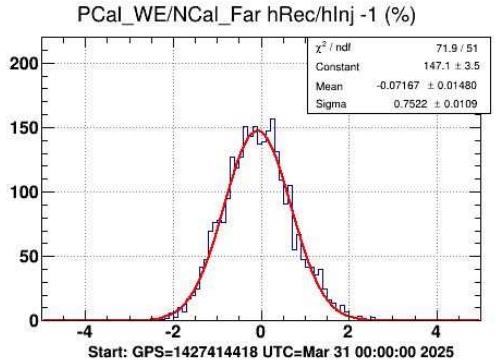

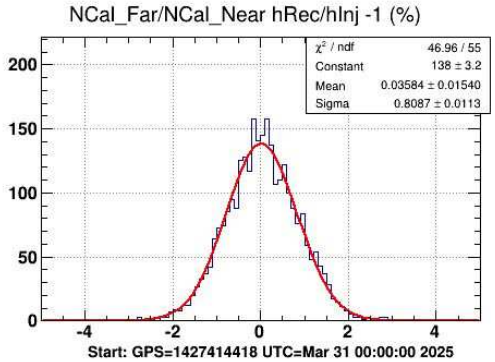

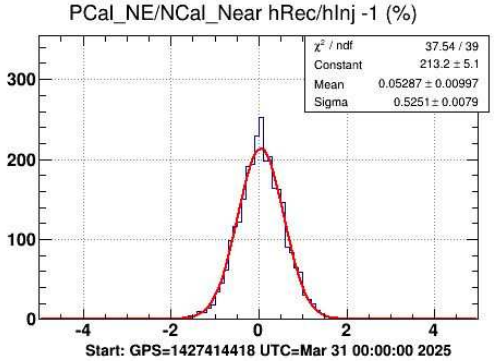

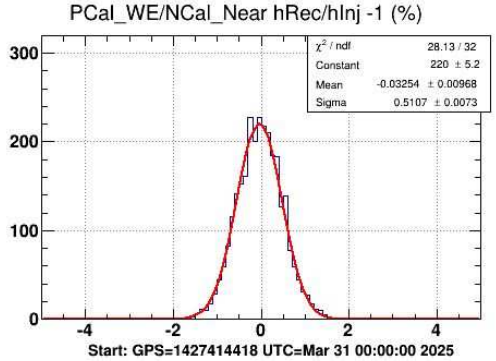

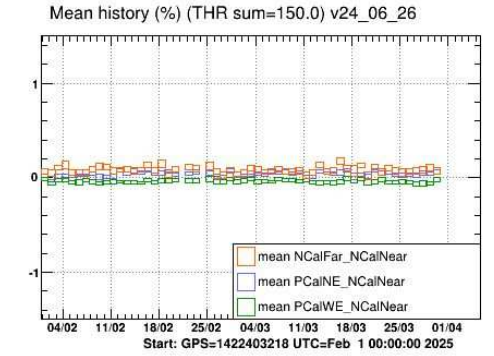

Schémas des mesures de calibrations

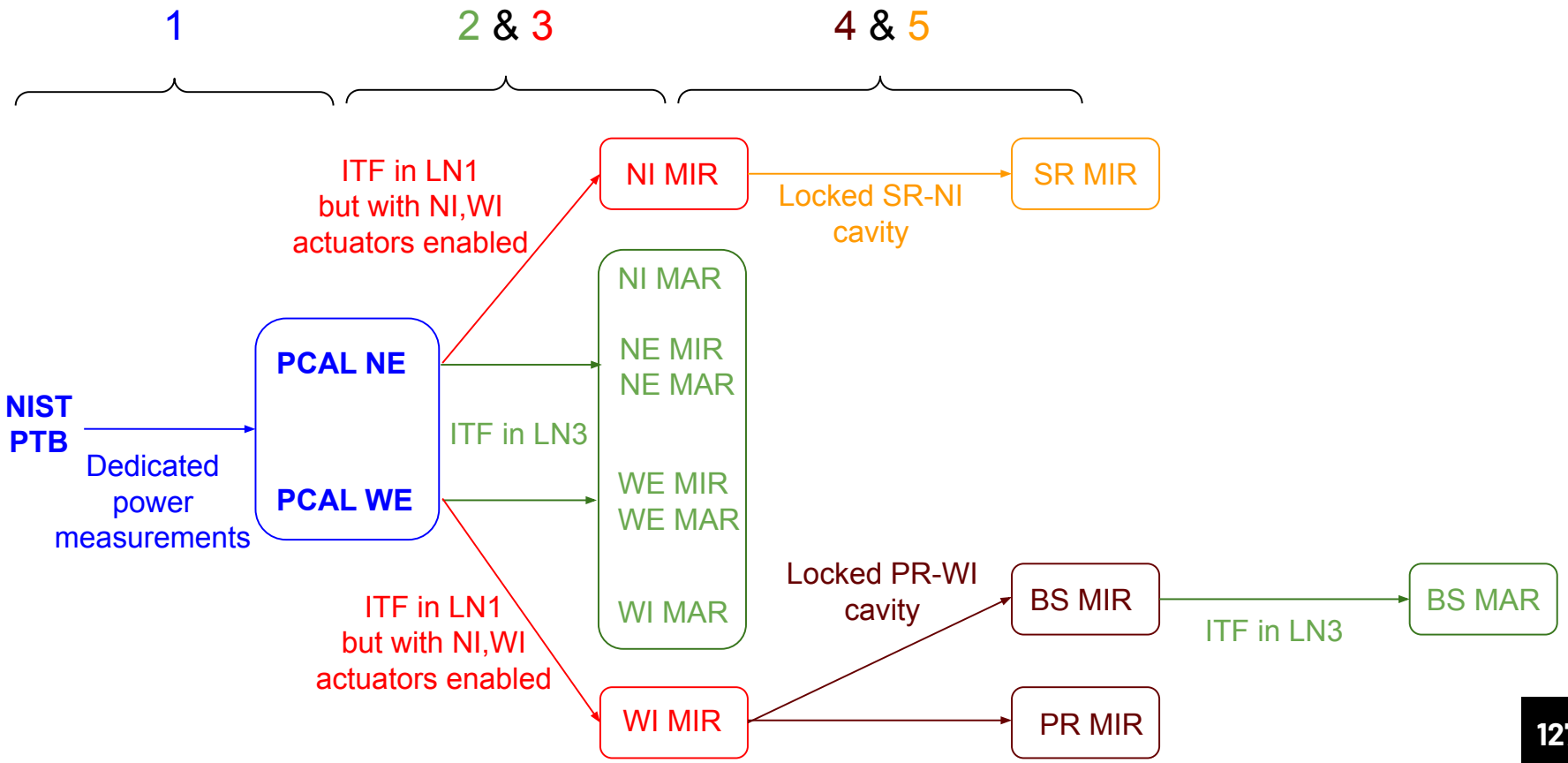

Variation actionneurs EM entre preO4 et O4

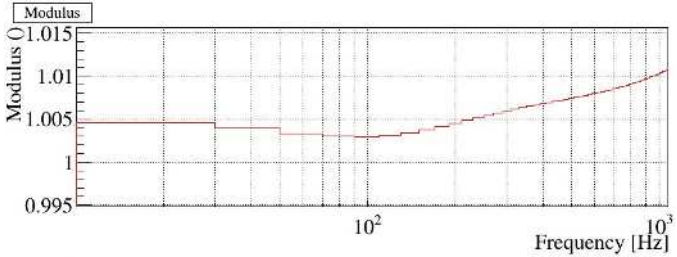

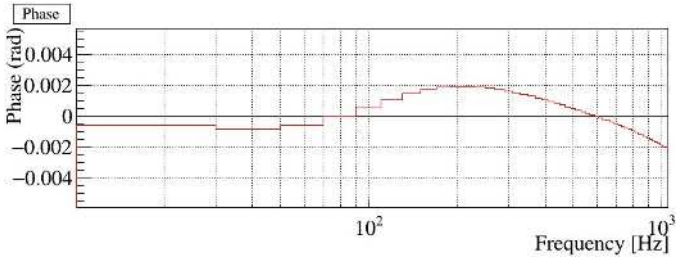

NE

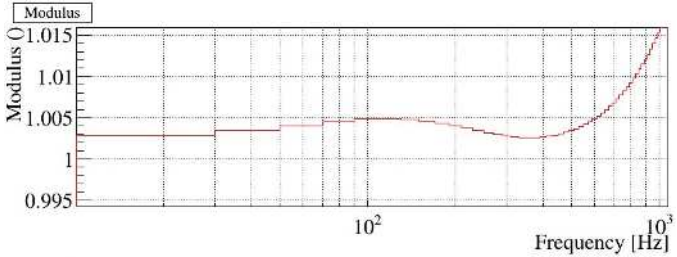

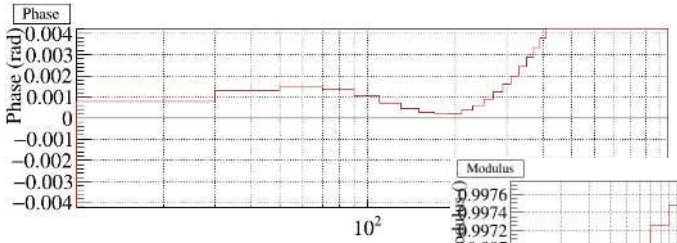

WE

WE

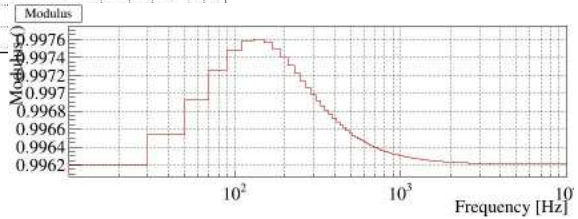

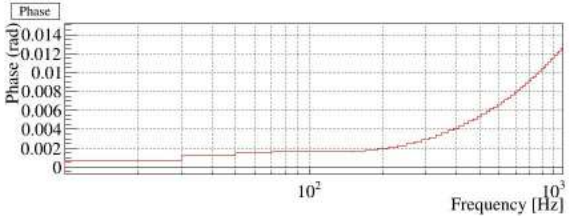

Calcul réponses optiques

$$O_{mir}(f) = \left(\frac{DARM}{CAL_{mir}}\right)(f) \cdot \left(\frac{DARM}{DARM\_NOISE}\right)^{-1}(f) \cdot A_{mir}^{-1}(f) \cdot S^{-1}(f)$$

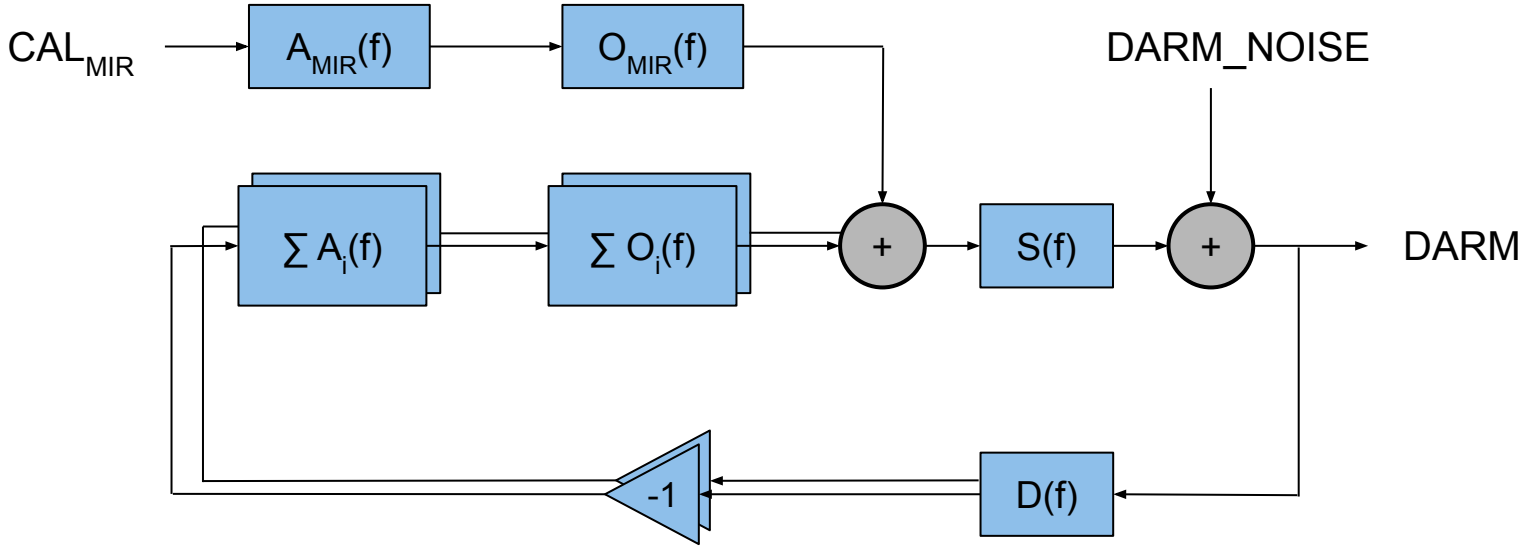

Calcul réponses optiques

Mirror	f_{os} [Hz]	Q_{os}	G_{mir} [W/m]	f_p [Hz]	τ [μs]
NE	7.4 ± 0.7	$7.8 \pm 11 \times 10^7$	$1.916 \pm 0.006 \times 10^9$	169 ± 8	-12 ± 1
WE	7.4 ± 0.7	$9.4 \pm 19 \times 10^7$	$1.919 \pm 0.006 \times 10^9$	167 ± 8	-17 ± 1
BS	17.9 ± 0.1	1.4 ± 0.1	$6.921 \pm 0.009 \times 10^6$	140 ± 1	-43 ± 2

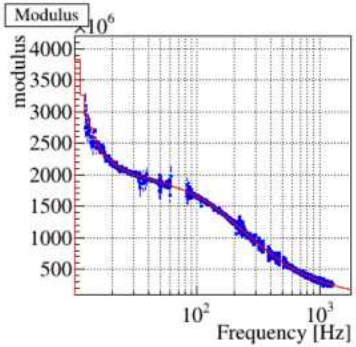

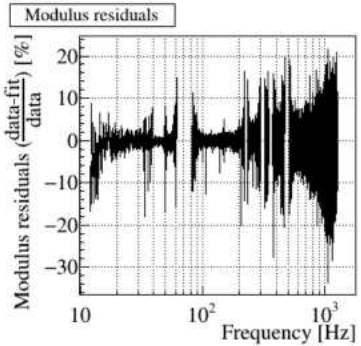

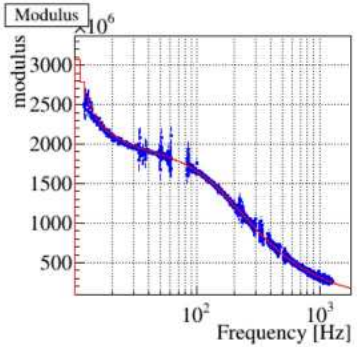

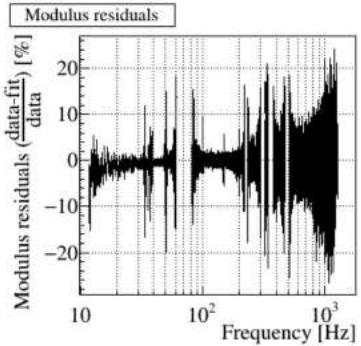

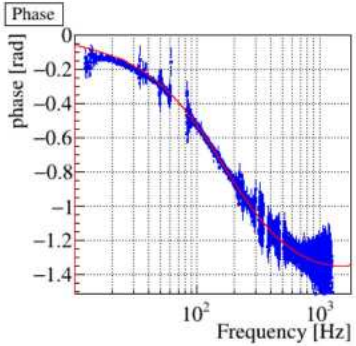

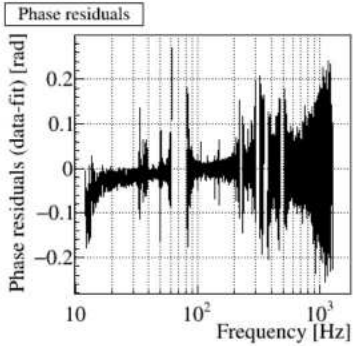

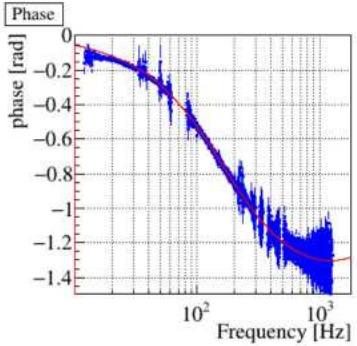

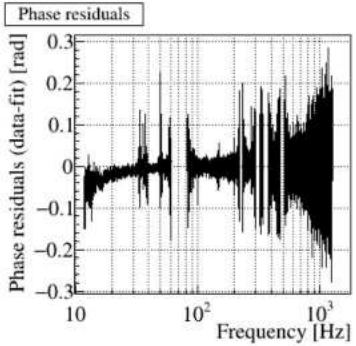

Calcul réponses optiques

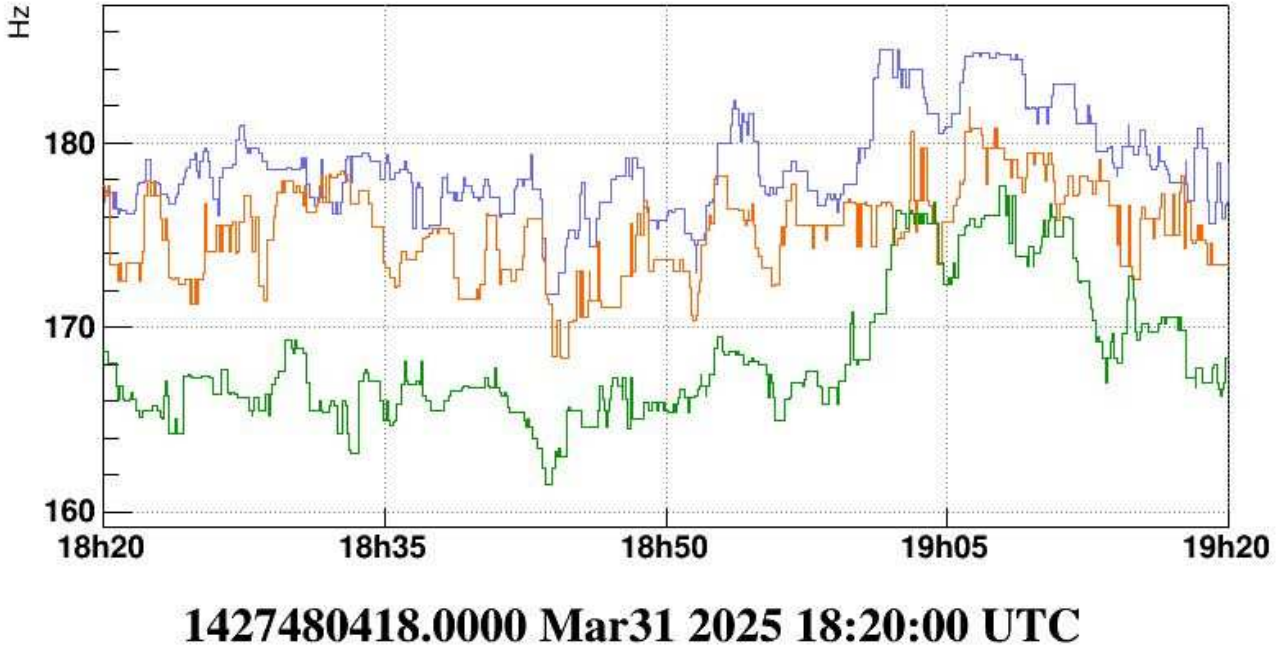

Hrec contribution breakdown

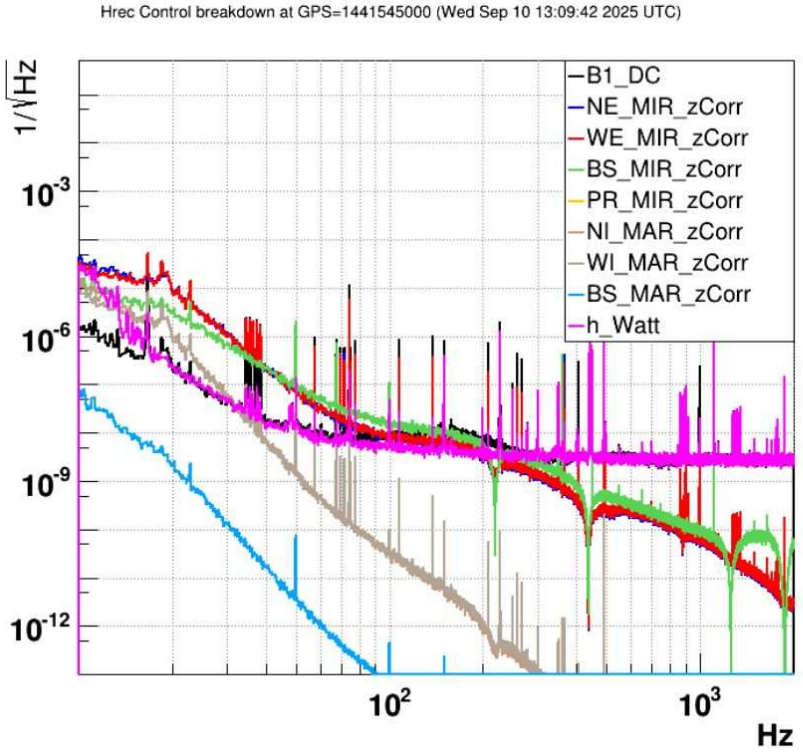

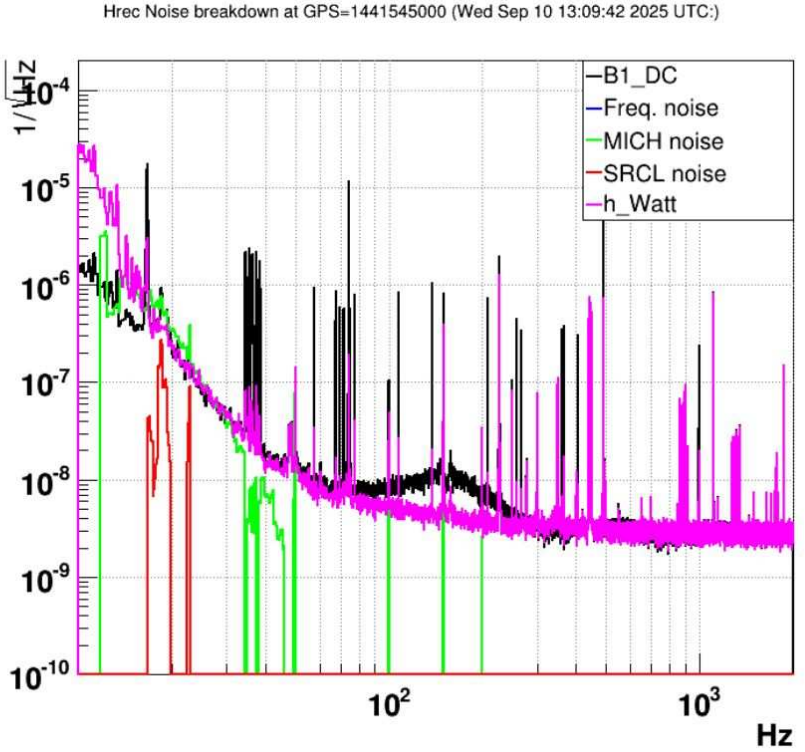

Injection broadband

Pic à 50 Hz et 150 Hz → fréquence de modulation électricité en europe et harmonique

50 Hz
→ 20 % module
→ 50 mrad phase

150 Hz
→ 4% module
→ 20 mrad phase

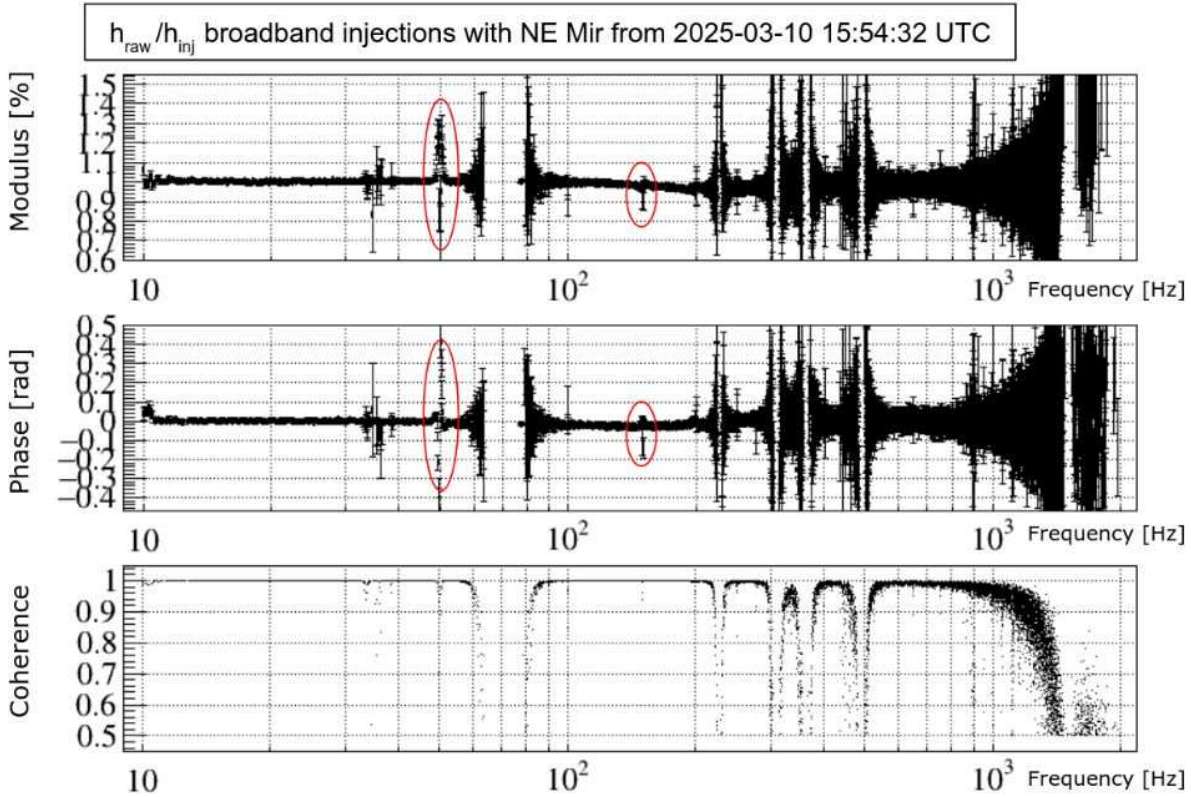

Interpolation avec lignes permanentes

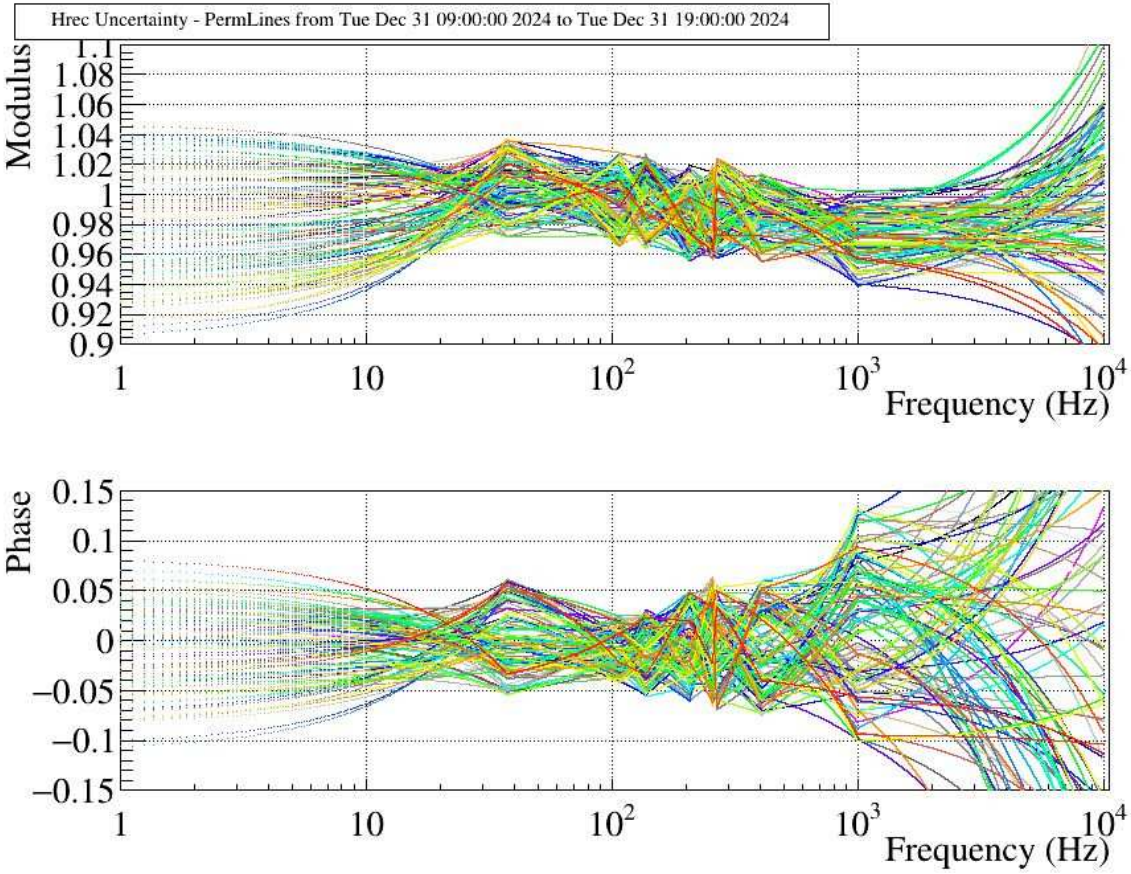

Biais et incertitude pendant O3

3.9 % sur le module

30 mrad sur la phase

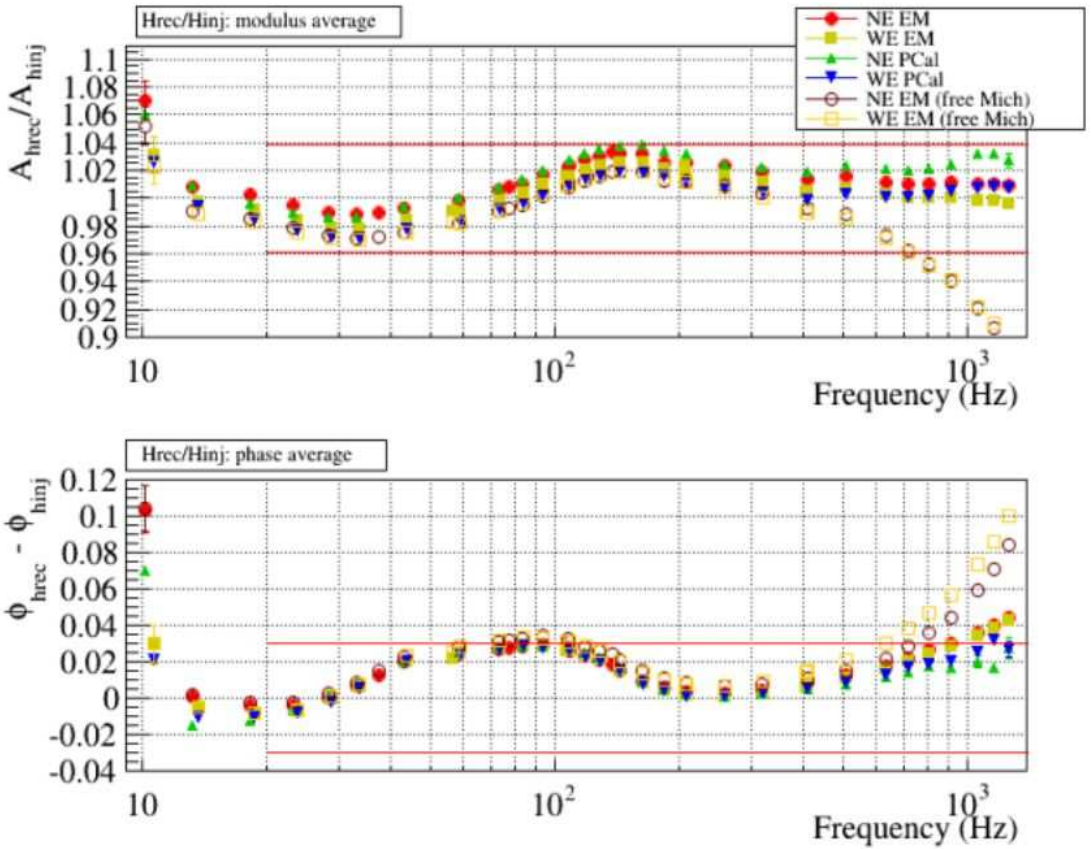

Biais de Hrec après changement WE

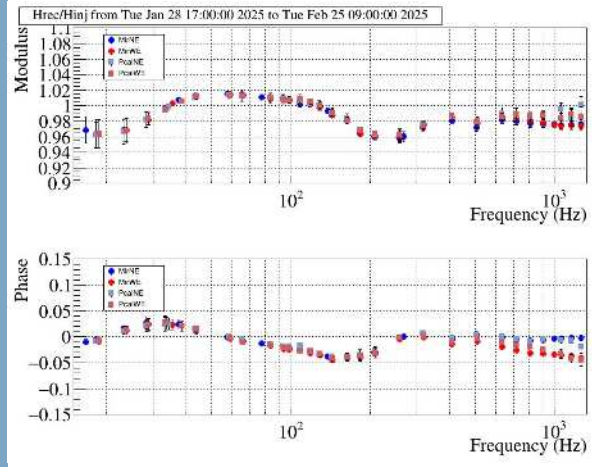

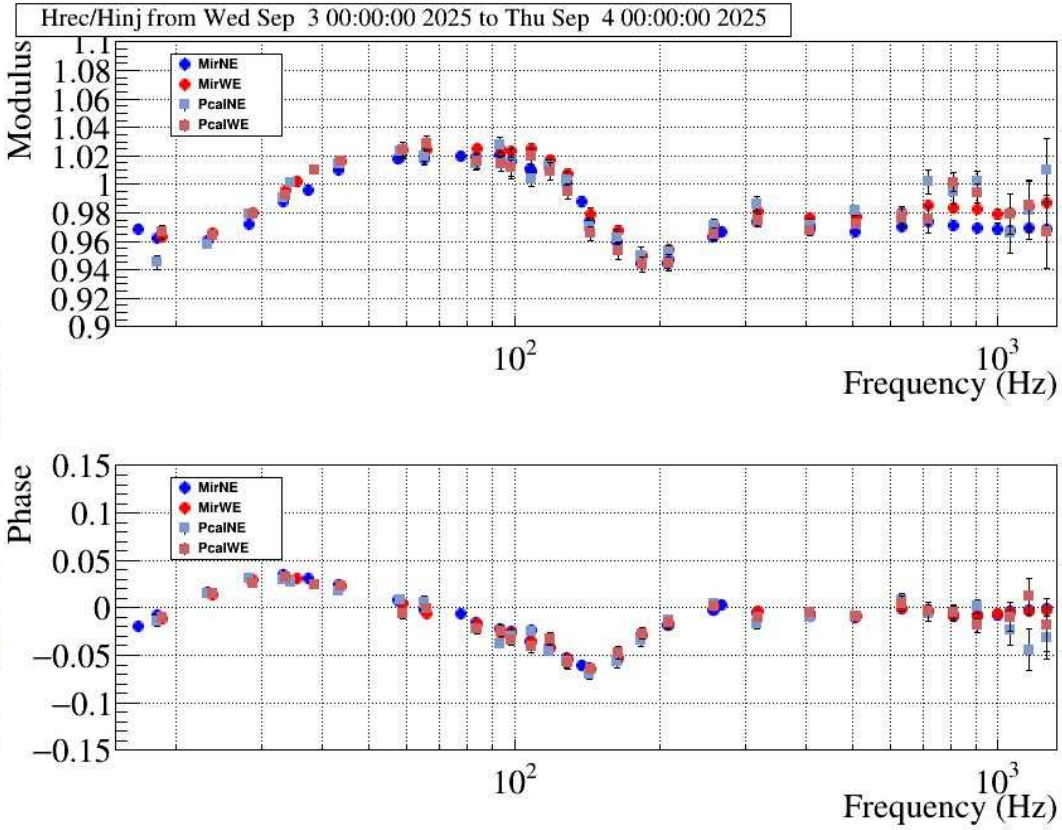

Results and stability during the run

The bias and the uncertainty on the reconstructed signal h(t) were computed monthly during the run
The bias is corrected online and was updated only 4 times during O4

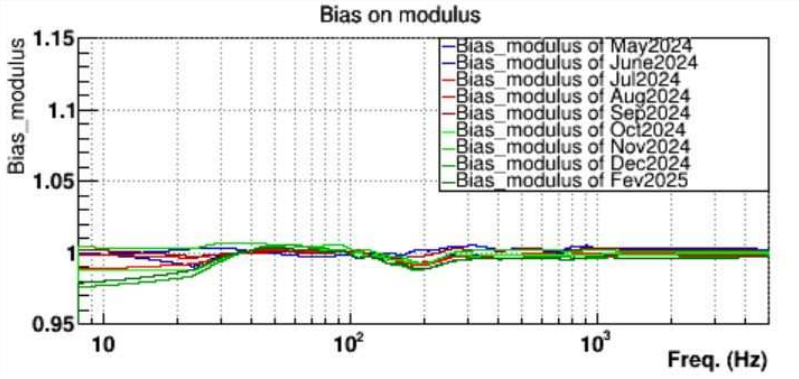

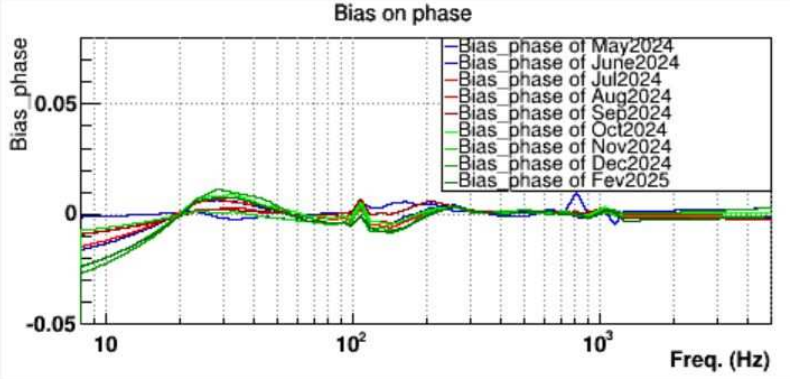

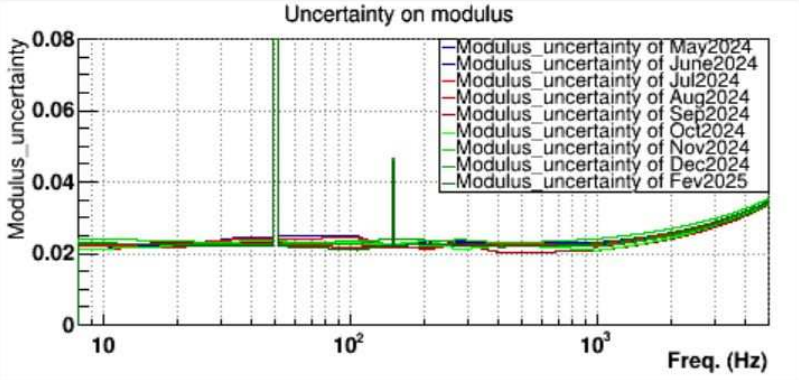

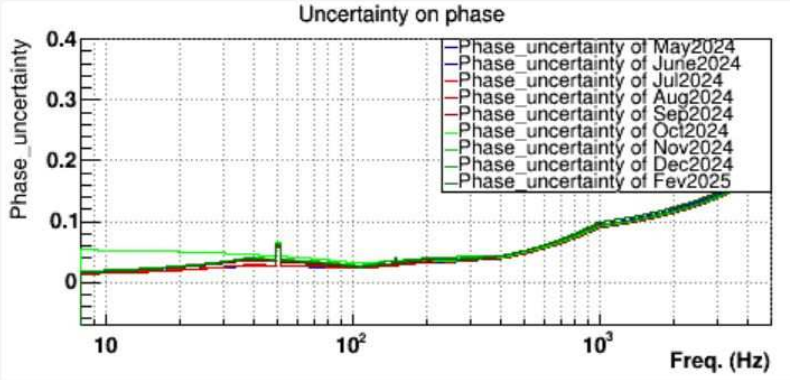

Incertitude h(t) LIGO

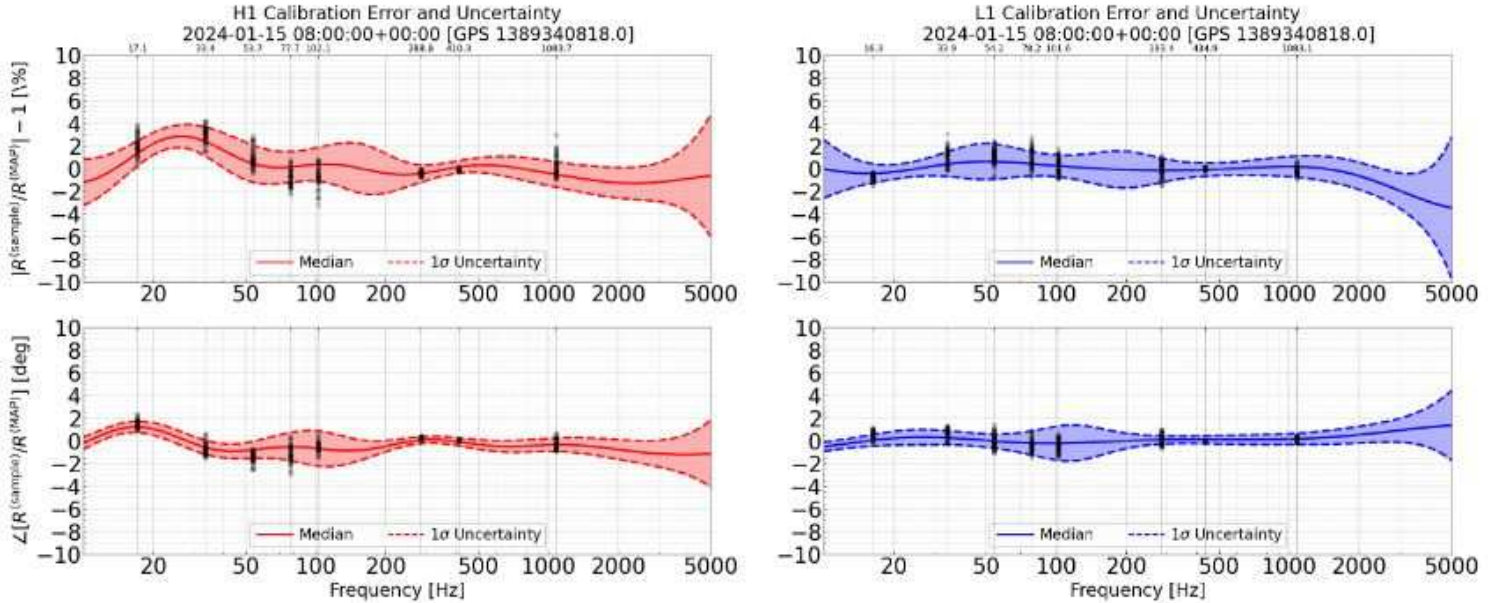

Figure 2. LIGO Hanford (left) and Livingston (right) frequency-dependent calibration error for a one-hour time period in O4a starting at January 15, 2024 08:00:00 UTC. The magnitude of the calibration error is shown in the top plots and the phase of the calibration error (in units of degrees) is shown in the bottom plots. The median systematic error of the calibration is given by the solid line. The 1σ uncertainty on this systematic error is given by the dotted lines. The black dots overlaid on the figure at specific frequencies are direct measurements of the calibration error at a specific frequency during this one-hour time period. These measurements are made using sinusoidal injections with the photon-calibrator system. These uncertainties are representative of typical LIGO calibration uncertainties throughout O4a.

Méthode de calcul du biais et de l'incertitude

Objectif : estimation du biais et de l'incertitude sur la reconstruction du signal h(t) pour toute la bande de fréquence

Lignes hebdomadaires → **BIAS**

Lignes permanentes → **INCERTITUDE**

Lignes Hebdomadaires et Permanentes

Utilise la

Moyenne et l'écart type

Distribution pour chaque ligne

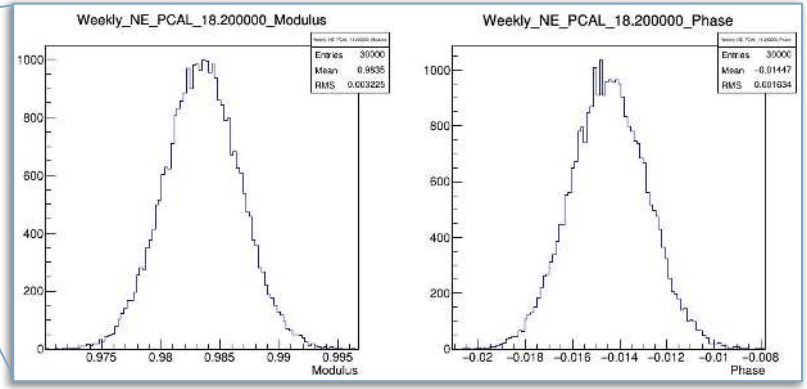

Méthode de calcul du biais et de l'incertitude

Objectif : estimation du biais et de l'incertitude sur la reconstruction du signal h(t) pour toute la bande de fréquence

Lignes hebdomadaires → **BIAS**

Lignes permanentes → **INCERTITUDE**

Lignes Hebdomadaires et Permanentes

Utilise la Moyenne et l'écart type

Distribution pour chaque ligne

Tirage aléatoire suivant les distributions

N jeux de données

	18Hz	...	1258Hz
set 1	##	..	##
...	..	..	..
set N	##	..	##

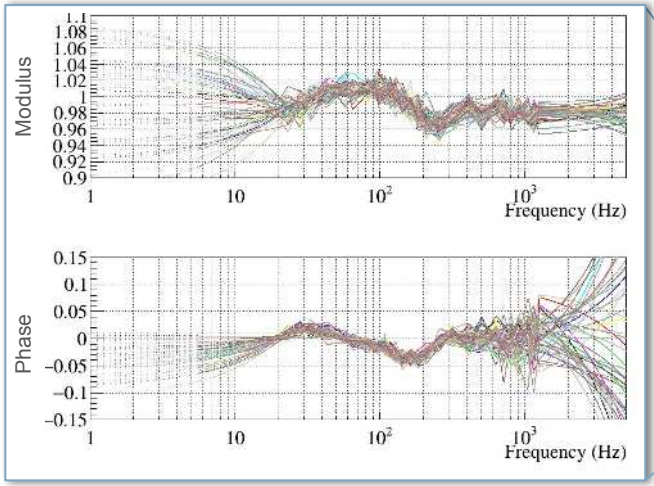

Interpolation entre 0-10 kHz
Un point tout les 0.125 Hz

N jeux de données interpolées

Méthode de calcul du biais et de l'incertitude

Objectif : estimation du biais et de l'incertitude sur la reconstruction du signal h(t) pour toute la bande de fréquence

Lignes hebdomadaires → **BIAS**

Lignes Hebdomadaires et Permanentes → Utilise la Moyenne et l'écart type → Distribution pour chaque ligne

Lignes permanentes → **INCERTITUDE**

Tirage aléatoire suivant les distributions → N jeux de données

	18Hz	...	1258Hz
set 1	##	..	##
...	..	..	..
set N	##	..	##

Interpolation entre 0-10 kHz
Un point tout les 0.125 Hz

N jeux de données interpolées → Distribution de N points pour chaque 0.125 Hz bin en fréquence entre 0-10 kHz → Utilise ces distributions → Moyenne et écart type sur toute la bande en fréquence → Biais et incertitude sur Hrec pour le module et la phase

Diminution de la latence de reconstruction

Latence de reconstruction de h(t) → ~ 10s

Objectif : atteindre ~ 1s de latence pour O5

Méthodes investiguées :

- Reconstruction temporelle
- Reconstruction fréquentielle avec zero padding

Travail bien avancé par stagiaire de M2 (B. Huchon)

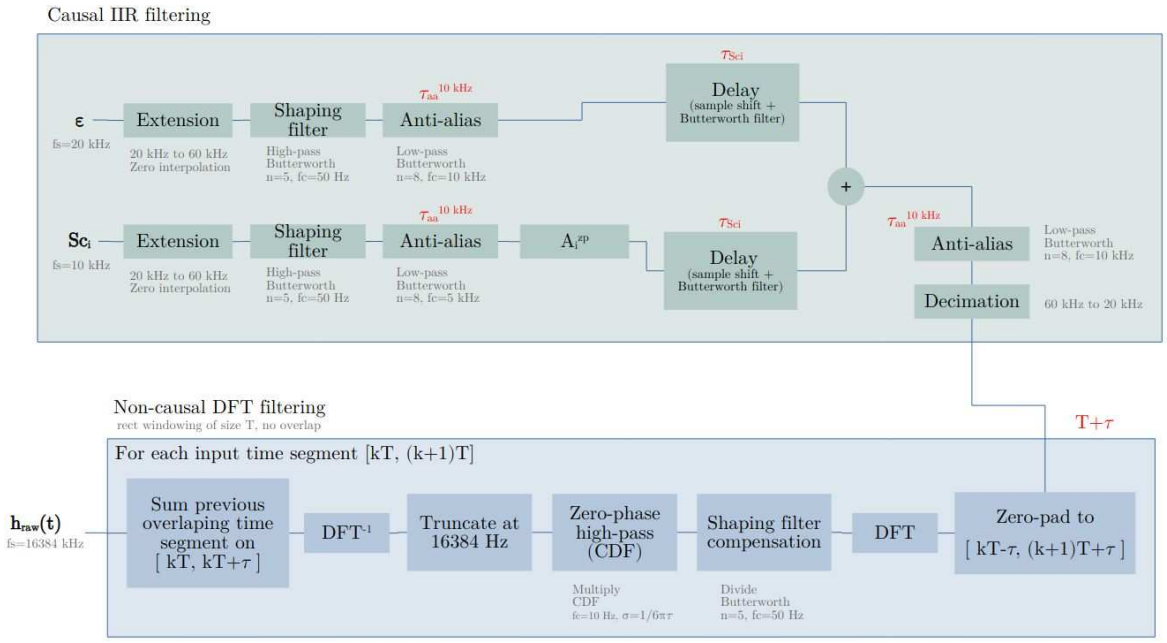

CRÉDIT - Brian Huchon

Latence emission circulaire initiale rrt

- Distribution of O4b+c alerts by hour

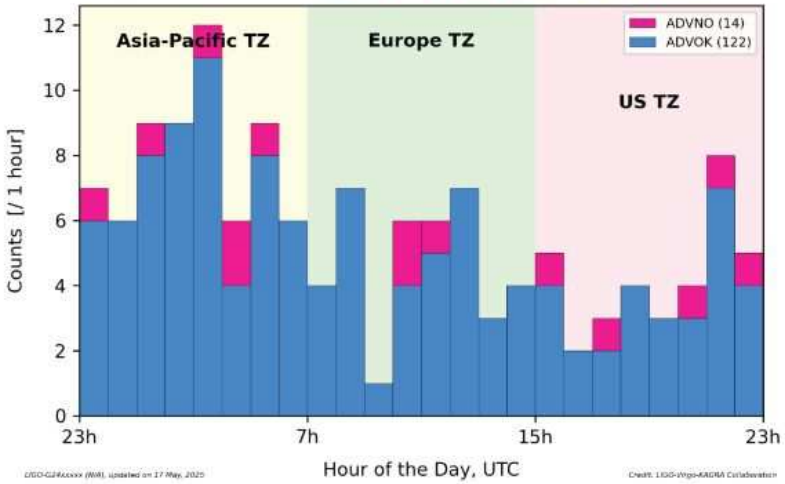

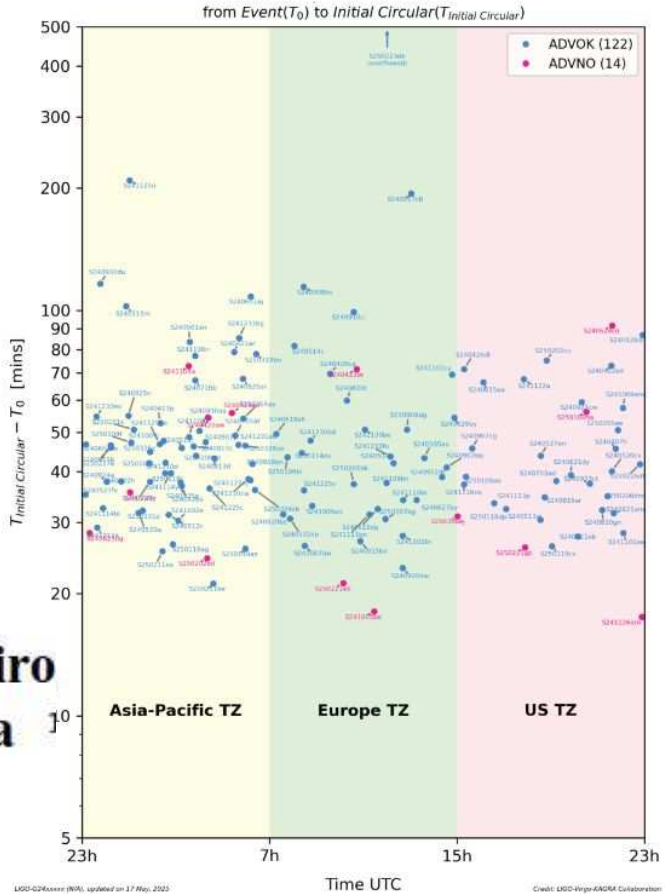

© Takahiro Sawada

Latence emission circulaire initiale rrt

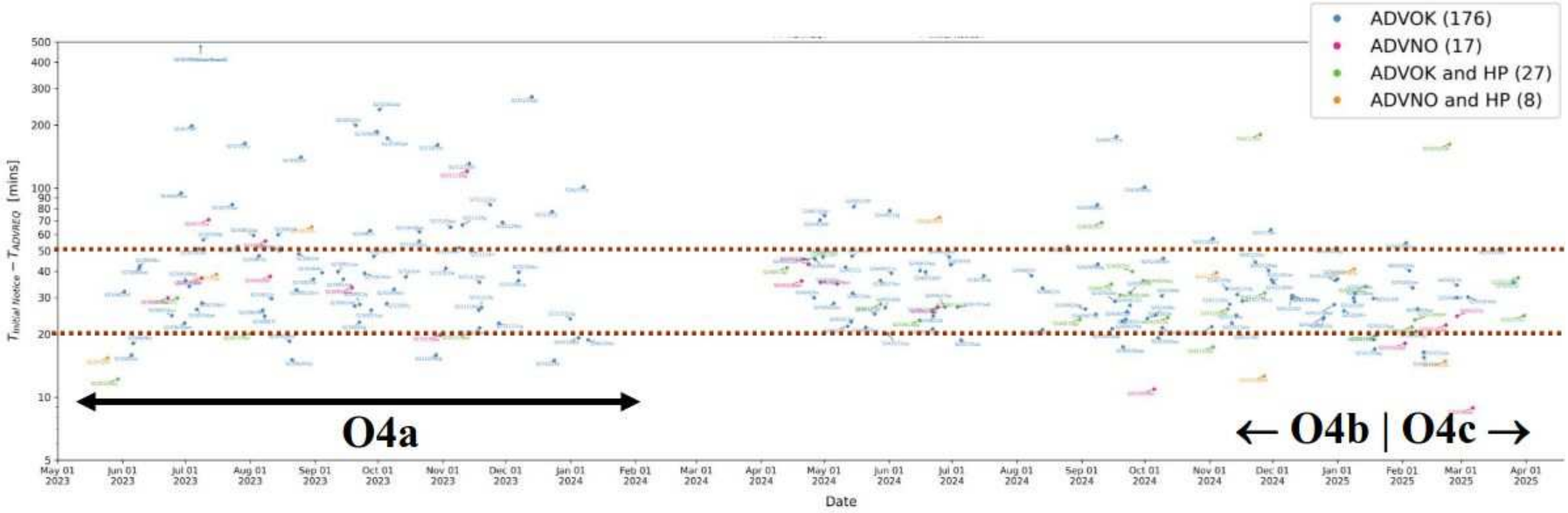

© Takahiro Sawada & Keita Kawabe

20

Mesure de linéarité des sphères au LAPP